

UNIVERSITY OF OKLAHOMA
GRADUATE COLLEGE

DYNAMIC PROPERTIES OF HUMAN MIDDLE EAR TISSUES

A DISSERTATION
SUBMITTED TO THE GRADUATE FACULTY
in partial fulfillment of the requirements for the
Degree of
DOCTOR OF PHILOSOPHY

By
XIANGMING ZHANG
Norman, Oklahoma
2013

DYNAMIC PROPERTIES OF HUMAN MIDDLE EAR TISSUES

A DISSERTATION APPROVED FOR THE
DEPARTMENT OF BIOENGINEERING

BY

Dr. Rong Z. Gan, Chair

Dr. Harold L. Stalford

Dr. Edgar A. O'Rear III

Dr. Binil Starley

Dr. Takumi Hawa

ACKNOWLEDGMENTS

First, I would like to thank my supervisor, Dr. Rong Z. Gan, director of the Biomedical Engineering Laboratory at the University of Oklahoma. Thank her for giving me the opportunity to work in her outstanding research team. Thank her for the guidance, advice and support during my study and research. The experience of the last three years in her lab will definitely benefit me for the future career.

Thanks to Dr. Hongbing Lu, professor at the University of Texas at Dallas, for his helpful advices and kind helps in my research.

Many thanks also go to my colleagues in the lab. Thanks to Don Nakmali and Xiyang Guan, who helped me in preparing the middle ear tissue samples and setting up the experimental equipments. Thanks to Fan Yang, a former graduate student in our lab, for the discussions and helps.

Finally, I would like to give my special thanks to my wife, Xiaotang Wang for her love and support in these years.

This research is supported by NIH R01DC006632 and R01DC011585.

TABLE OF CONTENTS

ACKNOWLEDGEMENTS	iv
TABLE OF CONTENTS	v
LIST OF TABLES	vii
LIST OF FIGURES	viii
ABSTRACT	xii

CHAPTER 1. INTRODUCTION AND BACKGROUND

1.1 Structure and Function of Human Ear	1
1.1.1 Outer ear.....	2
1.1.2 Middle ear.....	2
1.1.3 Inner ear.....	7
1.2 Mechanical properties of middle ear tissues.....	8
1.3 Objectives.....	13

CHAPTER 2. DYNAMIC PROPERTIES OF HUMAN TYMPANIC MEMBRANE

2.1 Dynamic properties measured by acoustic driving.....	15
2.1.1 Methods.....	16
2.1.2 Results.....	28
2.1.3 Discussion.....	34
2.2 Dynamic properties measured by dynamic mechanical analyzer.....	38
2.2.1 Methods.....	40
2.2.2 Results.....	45
2.2.3 Discussion.....	52
2.3 Conclusion.....	59

CHAPTER 3. DYNAMIC PROPERTIES OF HUMAN ROUND WINDOW MEMBRANE

3.1 Methods.....	61
3.2 Results.....	67
3.3 Discussion.....	74
3.4 Conclusion	81

CHAPTER 4. DYNAMIC PROPERTIES OF HUMAN STAPEDIAL ANNULAR LIGAMENT

4.1 Methods.....	83
4.2 Results.....	88
4.3 Discussion.....	96
4.4 Conclusion	98
CHAPTER 5. SUMMARY AND FUTURE STUDY	
5.1 Summary.....	99
5.2 Future Study.....	100
REFERENCES.....	102
APPENDIX.....	110

LIST OF TABLES

Table	Page
2.1 The geometric dimensions and resonance frequency of the TM specimens	17
2.2 The viscoelastic parameters of TM specimens obtained by acoustic driving.....	32
2.3 The dimensions of striped human TM samples used in DMA measurement (number unit in mm)	41
2.4 The shift factors, activation energies, and maximum frequency of human TM samples.....	46
2.5 The viscoelastic parameters of TM specimens obtained in DMA.....	52
3.1 The dimensions, resonance frequency f_n and vibration amplification ratio R of RWM specimens.....	63
3.2 The viscoelastic parameters of RWM specimens determined by the inverse-problem solving method.....	69
3.3 List of the viscoelastic parameters of a RWM specimen (RWM-6) determined under various changes in specimen geometry, sound pressure distribution and moisture (fluid) level.....	77
4.1 The dimensions of human SAL samples.....	86
4.2 The shift factors, activation energies, and maximum frequency of human SAL specimens.....	92
4.3 The viscoelastic parameters of human SAL samples.....	93

LIST OF FIGURES

Figure	Page
1.1 Anatomy of the human ear.....	1
2.1 (A): The TM sample with malleus and tympanic annulus attached. (B): The TM specimen fixed at metal mounting fixture along the longitudinal direction. A ruler was attached to the metal fixture at the load cell side as dimension measurements refer.....	16
2.2 Schematic of experiment setup for dynamic test on TM specimens..	18
2.3 Finite element model of the experiment setup with TM specimen for acoustic-structure coupled analysis. (A): The lateral view of the TM specimen; (B): The location of input sound source and the acoustic elements surrounding the TM.....	20
2.4 Generalized linear solid model for viscoelastic soft tissue.....	23
2.5 Schematic flowchart of the inverse-problem solving method to determine the complex modulus of TM sample.....	27
2.6 Vibration amplitude of silicone rubber film in frequency domain obtained by dynamic experiment (solid line) and FE modeling (dash line).....	28
2.7 Vibration amplitude measured from experiments on eight TM specimens over frequency range of 200-8000 Hz.....	30
2.8 The FE modeling results obtained from two TM models in comparison with the experimental curves. (A): Specimen TM-1; (B): Specimen TM-2.....	31
2.9 Complex modulus for eight TM specimens over the frequency range of 200-8000 Hz. (A): The storage modulus; (B): The Loss modulus; (C): Loss factor.....	33
2.10 Comparison of the storage modulus (A) and loss modulus (B) obtained from the present study (thick solid line) with Luo et al.'s results (2009b) in radial direction (dash line) and circumferential direction (thin solid line).....	36
2.11 Comparison of mean relaxation modulus in time domain obtained in this study (thick solid line) with the results reported by Luo et	

al.' s (2009b).....	38
2.12 The complex modulus curves obtained at the different temperatures (5°C, 25°C and 37°C) from two TM samples: (A) sample TM-1 and (B) sample TM-4.....	46
2.13 The master curves of the complex modulus at 37oC obtained from two TM sample: (A) sample TM-1 and (B) sample TM-4.....	47
2.14 The fitting of Arrhenius equation (solid lines) to the experimental natural logarithmic shift factor $\ln \alpha_T$ -absolute temperature (in Kelvin degree) curves obtained from samples TM-1 and TM-4.....	49
2.15 The master curves of the storage modulus and the loss modulus at 37°C from all 11 TM samples and the mean master curves of the storage modulus and the loss modulus.....	50
2.16 The theoretical fitting of generalized linear solid model to the experimental complex modulus for (A): sample TM-7 and (B) the mean experimental complex modulus.....	51
2.17 Comparison of the storage modulus and the loss modulus obtained from this study to the published data by Luo et al. (2009b) and Zhang and Gan (2010).....	54
2.18 (A): Damping of the TM calculated using Rayleigh type coefficient with $\beta=0.000075$; (B) damping of the TM calculated from the linear viscoelastic model determined from the dynamic test in this study.....	58
3.1 (A) The RWM specimen with the incus and stapes harvested from a human temporal bone. (B) Enlarged RWM specimen image with 1mm reference bas. (a) is the short axis of RWM, and (b) is the long axis of RWM	62
3.2 The schematic of the experiment setup for the dynamic test on the RWM specimen.....	64
3.3 The FE model of the dynamic experiment on the RWM specimen (RWM-1). (A) The plane view of the RWM model from the middle ear side. The edge was fully clamped. (B) The side view of the RWM model with sound pressure applied onto the RWM from cochlear side.....	66
3.4 The vibration amplitude-frequency curves measured from the	

dynamic experiments on eight RWM specimens.....	67
3.5 The FE modeling results (dash line) obtained from two RWM models in comparison with the corresponding experimental curves (solid line). (A) Specimen RWM-4; (B) Specimen RWM-8.....	68
3.6 The complex modulus determined from the FE modeling analysis for eight RWM specimens over the frequency range of 200-8000 Hz. (A) Storage modulus; (B) Loss modulus; (C) Loss factor	70
3.7 The mean complex modulus of the eight RWM specimens with standard deviations (S.D.). (A) Storage modulus; (B) Loss modulus; (C) Loss factor	72
3.8 The relaxation modulus in the time domain obtained from the complex modulus in frequency domain. (A) Individual relaxation modulus-relaxation time curves for the eight RWM specimens. (B) Mean relaxation modulus-relaxation time curve with S.D. for the eight RWM specimens.....	73
3.9 The effect of the specimen thickness variations on the complex modulus determined from the FE modeling analysis for the specimen RWM-6.....	75
3.10 The complex modulus determined from the FE modeling analysis for specimen RWM-6 with different fluid layers added.....	79
4.1 (A) The schematic of the experiment setup for the dynamic test of the SAL specimen in DMA. (B) The enlarged image for the fixation of stapes head to the mounting fixture. The SAL was hiding behind the bony structures	84
4.2 Images of the stapes footplate (A) and oval window (B) and stapes (C) obtained after experiments on one temporal bone specimen for measuring the dimensions of SAL	85
4.3 The complex shear modulus-frequency curves obtained at 5°C, 25°C and 37°C from two SAL specimens: (A) SAL-1 and (B) SAL-6.....	89
4.4 The master curves of the complex shear modulus at 37°C obtained from two SAL sample: (A) sample SAL-1 and (B) sample SAL-6.....	90

4.5	The master curves of the storage modulus and the loss modulus at 37°C from seven SAL samples and the mean master curves of the storage modulus and the loss modulus.....	93
4.6	The theoretical fitting of generalized linear solid model to the experimental complex modulus for (A): sample TM-7 and (B) the mean experimental complex modulus.....	95

ABSTRACT

Middle ear tissues, including the tympanic membrane (TM), round window membrane (RWM) and stapedial annular ligament (SAL), play important roles in acoustic transmission function in the middle ear. Changes of mechanical properties of ear tissues caused by diseases may induce the conductive hearing loss. It is critical to measure the mechanical properties of these tissues for understanding the middle ear transfer function and the mechanism of hearing loss. However, there are limited reports about mechanical properties of middle ear tissues in the literature because of the extreme small size and complicated geometry of these tissues. Moreover, most of published studies focused on mechanical properties under the static or quasi-static condition. As the middle ear tissues undergo vibration in the auditory frequency range, the dynamic properties or complex moduli of the tissues may have more realistic value than the static properties. The dynamic properties of middle ear tissues will provide the accurate data for modeling of human ear.

In this study, the dynamic properties of human TM, RWM and SAL specimens harvested from cadaver temporal bones were measured in the auditory frequency range. The generalized linear solid model was used to describe the viscoelastic behaviors of these tissues. Two different approaches were used to measure ear tissues. The first approach of using acoustic driving was developed for membrane tissues, such as TM and RWM. Vibration of the membrane specimens in response to acoustic driving load applied to the specimen was measured by laser Doppler vibrometer over the frequency range of 200-8000 Hz. The dynamic experiments were then simulated

in finite element models by acoustic-structure coupled analysis in ANSYS. Dynamic properties of the TM and RWM were derived by inverse-problem solving method.

The second approach was using dynamic mechanical analyzer based on the frequency-temperature superposition principle. The dynamic tests were conducted for the TM and SAL specimens at the frequencies from 1 Hz to 40 Hz at three different temperatures: 5°, 25° and 37°C. The frequency-temperature superposition principle was applied to expand the test frequency range to a much higher level (at least 3760 Hz). The viscoelastic parameters and the complex moduli in the frequency domain were obtained and the results were comparable to the published data. The potential effects of the experimental condition and specimen dimension measurement on the results were estimated.

The methods and results reported in this study contribute to soft tissue biomechanics. The complex moduli of middle ear tissues can be applied into finite element model of human ear to improve the model accuracy.

CHAPTER 1.

INTRODUCTION AND BACKGROUND

1.1 Structure and Function of Human Ear

Human ear is the organ detecting and sensing the sound and it comprises three basic parts - the outer ear, middle ear, and inner ear (Figure 1.1). Each part has a specific function in detecting and transmitting the environmental sound into the brain. Sound wave enters the outer ear as the input and travels through the ear canal (auditory canal) to the tympanic membrane (TM). The middle ear transfers the acoustic pressure to the mechanical vibrations of the ossicles and cochlear fluid. The organ of Corti in the inner ear transmits the cochlea fluid vibration into the electric signal which passes through the auditory nervous and reaches the perception of sound in the brain.

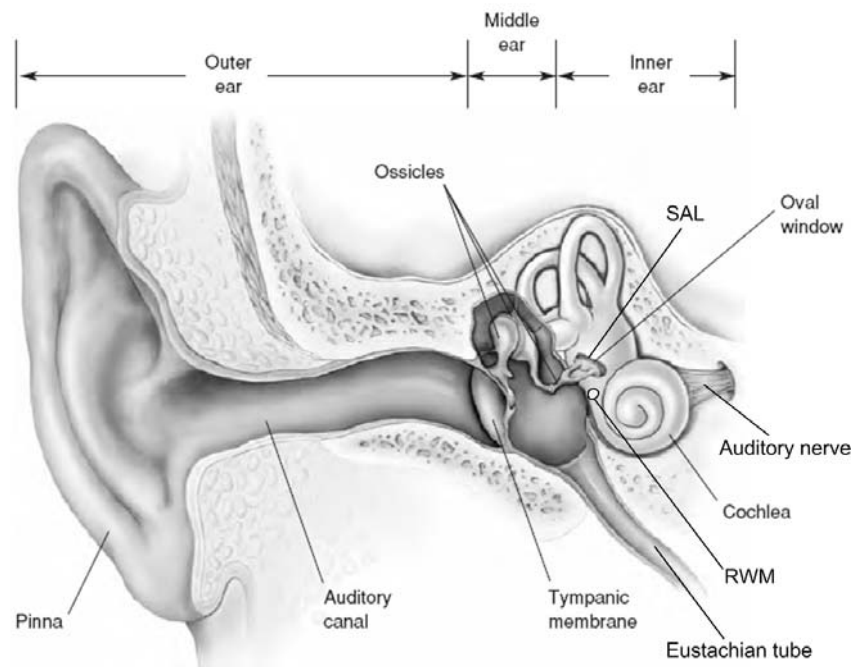


Figure 1.1 Anatomy of the human ear. (Keefe and Feeney, 2009)

1.1.1 Outer ear

The outer ear is composed of two major components: the pinna (also called auricle) and the ear canal. The pinna is a visible part of the ear which resides outside of the head. The function of the pinna is collecting, amplifying the incoming sound and directing it into the ear canal. It also plays a role in the vertical localization of the sound by human ear (Middlebrooks and Green, 1991). The ear canal is a long and narrow tube running from the pinna to the TM, which is also known as the eardrum. The size and shape of the ear canal vary among individuals. The ear canal is approximately 2.5 cm in length and 0.7 cm in diameter (Faddis, 2008). The function of the ear canal is to prevent the debris coming into the sound pathway and to guide sound pressure propagation. The ear canal also has the function of amplifying the sound from canal entrance to the TM by 5 to 20 dB over the frequency range from about 1.5 to 6 kHz (Shaw, 1974).

1.1.2 Middle ear

The middle ear consists of the TM, ossicular chain, round window membrane (RWM), stapedial annular ligament (SAL), Eustachian tube, and a small (about 0.6 ml) air-filled cavity called middle ear cavity or tympanic cavity. The major function of the middle ear is to transfer the acoustic pressure wave in the ear canal into the mechanical vibrations of the ossicular chain and ultimately transmit the vibrations into fluid in the cochlea. The following sections give more detailed introductions

about the structure and function of the ossicular chain and three middle ear soft tissues: TM, RWM, and SAL, which were studied in this dissertation.

Ossicular chain

The ossicular chain comprises three small bones (malleus, incus and stapes), two synovial joints (incudomalleolar joint and incudostapedial joint). It connects the TM at the manubrium as one end and the cochlea oval window at the footplate of stapes as another end. The footplate of stapes is surrounded by SAL, which seals the gap between the footplate of stapes and the bony wall of oval window. The ossicular chain is suspended by four ligaments (superior malleolar ligaments, lateral malleolar ligament, posterior incudal ligament and anterior malleolar ligament) in the middle ear cavity. There are two muscle tendons attached to the ossicular chain: the tensor tympani muscle tendon and stapedial muscle tendon. The tensor tympani muscle tendon is attached to the medial side of the malleus and innervated by the trigeminal nerve. The stapedial muscle tendon is attached to the posterior side of the head of stapes and innervated by the facial nerve. When elicited by the excessive sound in the ear canal, the muscles can contract to stiffen the ossicular chain and reduce the energy transmitted into the cochlea for protecting the inner ear (Borg and Counter, 1989). The basic function of ossicular chain is to transmit the TM vibration into the stapes footplate vibration which drives the lymphatic fluid in cochlea. The ossicular chain acts like a lever system to amplify the sound pressure on the TM to the driving

force on the footplate of stapes. The lever ratio depends on the frequency and may vary from 1.9 to 6 (Gyo et al., 1987).

Tympanic membrane (TM)

The TM is a concave thin membrane which separates the outer ear canal and middle ear cavity. The diameter of the adult TM is about 8 - 10 mm and the height of the cone is about 2.0 mm (Wever and Lawrence, 1982). The TM is attached to the malleus at the manubrium. At the end of the manubrium and in the center of the TM is the umbo. The TM consists of two parts: the pars tensa and pars flaccida. The pars tensa is the major part with the tympanic annulus around the circumference and the malleus manubrium attached to the pars tensa, while the pars flaccida is the small part superior to the manubrium. The pars tensa has multi-layer structure consisting of the epidermal, collagen fibrous and mucosal layers from the lateral to medial side. The collagen fibers are organized into the matrix of ground substance primarily along radial and circumferential directions (Lim, 1970; 1995). The collagen fibers provide the major mechanical support for the TM. The epithelial layer and the mucosa layer are contiguous with the lining the external skin and middle ear mucosa respectively. The thickness of the TM is not evenly distributed through the whole surface and varies between 40-120 μm (Kuyper et al., 2006; Vollandri et al., 2011). It is thicker around the boundaries of tympanic annular ligament and the manubrium, while thinner at the middle region between the boundaries. The TM plays an

important role in acoustic-mechanical transmission by converting the acoustic waves into vibrations of the ossicular chain. The mechanical properties of TM significantly affect the acoustic transfer function of middle ear.

Round window membrane (RWM)

Round window is one of the two openings into the cochlea from the middle ear. The RWM is the tissue which covers the round window. RWM consists of three layers from the middle ear to cochlear side: the outer epithelium, core of connective tissue layer and inner epithelium (Goycoolea and Lundman, 1997; Carpenter et al., 1989). The core of connective tissue contains collagen fibers, fibroblast and other elastic fibers and provides the main structural support for RWM. Adult human RWM is usually thicker at the edge than at the center, and its average thickness is about 70 μm (Goycoolea and Lundman, 1997; Carpenter et al., 1989). RWM vibrates with an opposite phase to the mechanical vibrations entering the cochlea through the stapes at the oval window. The RWM serves as a barrier between the middle ear cavity and cochlea and a pressure release window for cochlea fluid. RWM also plays an important role in middle ear and cochlear mechanics (Paparella et al., 1983; Nomura, 1984; Hellstrom et al., 1997). Mechanical properties of RWM directly affect cochlear fluid motion and thus the movement of the basilar membrane.

Stapedial annular ligament (SAL)

SAL lies in the gap between the stapes footplate and the margin of the oval window (Brunner, 1954; Bolz and Lim, 1972). The SAL provides a sealed but mobile boundary for the stapes and cochlea fluid vibration (Wolff and Bellucci, 1956; Whyte et al., 2002). Histology and scanning or transmission electron microscopy studies on the SAL show a lattice-like structure consisting of the peripheral mantle of microfibrils and transverse thick fibers cross the SAL (Ohashi et al., 2006).

The motion of the stapes footplate has been identified as the piston and hinge-like motions by von Békésy (1960) and Gyo et al. (1987) measured on human temporal bone (TB). The piston-like and rotational forms of stapes motion induce shear deformation of the SAL and the mechanical properties of SAL directly affect the acoustic-mechanical transmission from the middle ear to cochlea. It is well known that otosclerosis of the stapes footplate and abnormal ossification of the SAL reduce the movement of the stapes and cause the conductive hearing loss (Schuknecht et al., 1985; Merchant et al., 2001). The studies on effect of middle ear static pressure or inner ear pressure on umbo and stapes vibration conducted by Murakami et al. (1997; 1998) and Gan et al. (2006a) in TB indicated that one mechanism behind those effects on sound transmission through the middle ear was due to the stiffness changes of the SAL. Researches on middle ear influence on otoacoustic emission by Büki et al. (1996; 2000) suggested that evoked otoacoustic

emission changes might be caused by an increase in the stiffness of the SAL and the stiffness of SAL was expected to reflect hydrostatic intracranial pressure changes as well. Moreover, since the transmission of sound energy from the middle ear to the cochlear fluid is largely dependent on the SAL mechanical behavior, the properties of SAL have affected the outcomes of stapedotomy or stapesplasty surgical approaches with different prostheses or SAL grafts (Causse et al., 1991; Lopez A, et al., 1992; Hüttenbrink, 2003). Therefore, understanding of the mechanical properties of the SAL is one of the important research subjects in middle ear biomechanics.

1.1.3 Inner ear

The inner ear is the innermost part of the human ear, which is responsible for the sound detecting and balance (Torres and Giráldez. 1998). It can be divided in to two different sections: the cochlea and the vestibular system, which are dedicated for the hearing and balance, respectively. The human cochlea has a coiled and snail-like shape and about two and half turns. The fluid-filled inside space of the cochlea is divided into three channels: the scala tympani, scala media and scala vestibule, by two membranes: the Reissner's membrane and the basilar membrane (Hoffman and Bobbin, 1986). The scala tympani connects with the scala vestibuli at the apex of the cochlea, which is called helicotrema. There are two windows on the outer wall of cochlea: the oval window on the scala vestibule sealed by the stapes footplate and SAL, and the round window on the scala tympani covered by the RWM.

The function of the cochlea is to convert the mechanical vibration of cochlea fluid transmitted from the middle ear into the electrochemical nerve impulses which are passed on to the brain via the auditory nerve (Bess and Humes 2008). When the mechanical vibration of the stapes is transferred into the cochlea via the oval window, the vibration wave propagates through the cochlea fluid from scala vestibule to scala tympani. The inner hair cells of the organ of Corti on the basilar membrane can detect the fluid motion and generate the electrical signal to the auditory nerve. The hair cells at the base turn of the cochlea respond to the high-frequency sound, while those at the apex turn respond to the low-frequency sound (Schnupp et al., 2011; Olson et al., 2012).

1.2 Mechanical Properties of middle ear tissues

The middle ear has total eleven soft tissues including the TM, incudomalleal joint, incudostapedial joint, SAL, RWM, four suspensory ligaments and two muscle tendons. The mechanical properties of these tissues affect the middle ear transfer function (Feng and Gan, 2004) and energy transmission through the middle ear. Changes in the mechanical properties of these tissues caused by middle ear diseases may induce the conductive hearing loss. As an example, for the patients with otosclerosis, the extremely stiff SAL restricts the vibration of the stapes and reduces the hearing level significantly (Souza and Glasscock, 2004). Another example is otitis media, in which the negative middle ear pressure increases the stiffness of TM and other tissues. As a consequence, the mobility of the TM and ossicular chain

(Gan et al., 2011b) and the middle ear energy absorbance are reduced (Zhang and Gan, 2013c).

To measure the mechanical properties of middle ear tissues is critical and have significant impact on the researches of middle ear biomechanics for: 1) understanding the basic mechanism of acoustic transfer function of middle ear and the conductive hearing loss induced by the mechanical changes of middle ear tissues; 2) providing the material data for the middle ear artificial components, such as artificial TM, total ossicular replacement prosthesis, and partial ossicular replacement prosthesis, and middle ear surgical operations, such as tympanoplasty (Chu, and Jackler, 2003) and stapedectomy (de Souza and Glasscock 2004); 3) providing the necessary input information for the physical model, circuit model or finite element (FE) model of the human ear.

Despite the importance, there are only a few reports about the mechanical properties of middle ear tissues in the literature, because of their extreme small sizes and complicated geometry. Our research group reported experimental measurements and modeling analysis on the mechanical properties of stapedial muscle tendon, tensor tympani muscle tendon, anterior malleolar ligament and incudostapedial joint (Cheng and Gan, 2007, 2008a, 2008b; Zhang and Gan, 2011b). All those measurements were conducted by the quasi-static uniaxial tensile tests and the nonlinear elastic moduli of those tissues were obtained. The following paragraphs give the detailed introduction about the current research status and applications of

the mechanical properties of TM, RWM, and SAL, which were the three tissues measured by the dynamic tests in this study.

The TM is the largest and most studied one among the middle ear tissues. The static or quasi-static mechanical properties of TM have been reported in the literature, but the dynamic properties of TM over the auditory frequency range are very limited. Mechanical properties of the human TM as Young's modulus of 20 MPa was first reported by von Békésy in 1960 using a bending test on a rectangular cadaver TM strip (von Békésy, 1960). The TM sample was assumed as a homogeneous and isotropic material. In 1980, Decraemer et al. (1980) performed uniaxial tensile tests on human TM and reported the Young's modulus of 23 MPa at a relatively large strain. In 2005, Fay et al. (2005) discussed three approaches to derive the Young's modulus of the TM: constitutive modeling, re-interpretation of published data and correlation of dynamic measurement with composite shell model. They reported the Young's modulus of 30 - 90 MPa for an isotropic model and 100-400 MPa for an orthotropic model of the TM. Recently, Cheng et al. (2007) studied the viscoelastic properties of human TM using uniaxial tension tests and digital image correlation method, and reported TM Young's modulus varying from 0.4 - 22 MPa over the stress range from zero to 1 MPa. Huang et al. (2008) and Daphalapurkara et al. (2009) measured the linear viscoelastic properties of the TM using nanoindentation techniques. The steady-state values of the in-plane modulus of the TM was 17.4 MPa and 19.0 MPa for posterior and anterior portion, respectively, and the through-thickness or out-plane modulus was 6.0 MPa for both

posterior and anterior portions. There are some studies on the mechanical properties of animal TMs as well, such as those of cat (Buunen and Vlaming 1981; Decraemer et al. 1989), and gerbil (von Unge et al., 1993). All those mechanical properties reported in the literature were obtained under quasi-static loading conditions. The pioneering work on TM dynamic properties was reported by Kirkae (1960) based on tension test of a TM strip at 890 Hz. Since then, there was no data published on dynamic properties of the TM until the most recent work by Luo et al. (2009a; 2009b). Luo et al. investigated the relaxation modulus of the human TM at high strain rates using a miniature split Hopkinson tension bar (SHTB). The Young's modulus of 45.2 - 58.9 MPa in the radial direction and 34.1 - 56.8 MPa in the circumferential direction of the TM under strain rates of 150-2500 s⁻¹ (corresponding to the frequency range of 150 - 2500 Hz) were reported by Luo et al. (2009a; 2009b). However, Young's modulus at frequency higher than 2500 Hz is still not available because of the limitation of SHTB. New technology needs to be developed to measure the dynamic properties of TM at higher frequency range.

There is no report about the mechanical properties of human RWM yet in the literature. To better understand the role of RWM in normal, diseased, and implanted ears, the FE models of the human ear, including the middle ear cavity, RWM, and cochlea, in addition to the ossicles and TM, have been reported by Bohnke and Arnold (1999), Gan et al. (2007), and Zhang and Gan (2011a). However, the mechanical properties of RWM were assumed in these FE models because there were no mechanical properties of RWM available in the literature. Bohnke and

Arnold used 9.8 MPa as Young's modulus of RWM, Gan et al. used 0.35 MPa, and Zhang and Gan used 0.7 MPa for RWM. Noticeable differences of the RWM elastic modulus were observed among these studies. Recently, it has been reported that the vibration transducer of middle ear implantable hearing device has been attached on the RWM to stimulate cochlear fluid for restoring hearing level (Colletti et al., 2005, 2006; Tringali et al., 2009). The studies on RWM using implantable transducers indicate that the attachment method and the RWM mechanical properties directly affect the efficiency of vibration stimulation into the cochlea. The accurate measurement on the mechanical properties of RWM is needed for improving the FE modeling analysis of the human ear.

Mechanical properties of the SAL have only been reported once in the literature by Gan et al. (2011a). They measured the shear modulus of the SAL through the quasi-static pulling test. Their results show that the SAL has typical nonlinear mechanical behavior and the shear modulus varies from 3.6 to 220 kPa when the shear stress increases from 2 to 140 kPa. The deficiency of the dynamic properties of SAL affects fully understanding sound transmission from the middle ear to cochlea and the development of an accurate FE model of ear. Most FE models of the human ear, mechanical properties of the SAL were assumed through the cross-calibration process and a constant elastic modulus varying from 0.065 to 5.5 MPa was used for the FE models such as published by Gan et al. (2006b; 2007) and Wada et al (1992). There is an urgent need to measure SAL dynamic properties under auditory frequency range.

In summary, most of the published studies focused on the mechanical properties of middle ear tissues under the static or quasi-static conditions. The highest frequency of the dynamic measurement was limited to 2500 Hz for the TM sample. As the ear tissues work under the auditory frequency range from 20 to 20000 Hz, it is more important and valuable to measure the viscoelastic or dynamic properties in high frequency range compared with the static properties under slow strain rate. Most of the published FE models of ear used the linear static elastic properties plus Rayleigh damping coefficient for the middle ear tissues (Zhao et al., 2009) in the harmonic analysis. This kind of material model may induce unreasonable high damping for the middle ear tissues at high frequency range (> 4000 Hz). The middle ear tissues are typical viscoelastic materials, whose complex modulus and damping vary depending on the strain rate or the frequency. The lack of the dynamic properties of middle ear tissues affects the accuracy of the FE model of human ear. The experimental measurement on the dynamic properties of middle ear soft tissues will have significant impact on the research of middle ear biomechanics.

1.3 Objectives

The objectives of this study include:

- 1) To develop and validate new technologies and methods for expanding the frequency range of the dynamic tests on the middle ear tissues to a higher level (comparing 2500 Hz using SHTB). One major restriction for the dynamic tests

of ear tissues is that the standard materials testing system (MTS) or dynamic mechanical analyzer (DMA) cannot directly reach the test frequency to thousands Hz. To overcome this, two new approaches were established in this study. The first approach is the acoustic driving measurement using laser Doppler vibrometer (LDV) with the assistance of FE modeling analysis. This approach was employed to measure the dynamic properties of membrane tissues, such as TM and RWM. The second approach uses DMA based on the frequency-temperature superposition (FTS) principle, which can be applied to shift the complex modulus obtained at lower temperature to much higher frequency at higher temperature. The method developed in this aim can be applied to measure the dynamic properties of other human soft tissues and may have impact on the experimental biomechanics

- 2) To measure the dynamic properties of normal human TM, RWM and SAL in the auditory frequency range using the technologies and approaches established in Objective 1. The major outcomes of this aim are the complex modulus and loss factor (damping) of these tissues in frequency domain. The results provide the new data for the biomechanics of middle ear and can be applied to the FE model of human ear for improving the accuracy of the models.

CHAPTER 2.

DYNAMIC PROPERTIES OF HUMAN TYMPANIC MEMBRANE

In this chapter, two different approaches were used to measure the dynamic properties of human TM in the auditory frequency range: 1) measurement by acoustic driving with the assistance of FE modeling analysis; 2) measurement by the DMA based on the FTS principle. The detailed descriptions about these methods and results are presented in the following sections.

2.1 Dynamic properties measured by acoustic driving

The content of this section has been published in International Journal of Experimental and Computational Biomechanics by Zhang and Gan (2010).

Laser Doppler vibrometry has been broadly used for measuring the vibrations of TM in response to sound stimuli in the ear canal in cadaver ear or TB (Gan and Dai, et al., 2006; Dai et al., 2007). An experimental setup on a MTS for measuring the vibration of TM specimen using a LDV was developed in our lab. The experiment on the TM specimen was simulated in FE model with acoustic-structure coupled analysis. The generalized linear solid viscoelastic model was used as the constitutive law for the TM, and the dynamic properties of the TM was derived by inverse problem solving method.

2.1.1 Methods

I. TM specimen preparation

The TM samples were harvested from fresh or fresh frozen human TB through the Willed Body Program at the University of Oklahoma Health Sciences Center. The tympanic annulus of the TM was first separated from the bony ear canal, and then taken out with the malleus attached and placed in a normal saline solution (Fig. 2.1A). A rectangular strip was cut from the posterior or anterior part of the TM. The specimen had the tympanic annulus intact at both top and bottom sides to maintain the integrity of the membrane. The specimen was treated as a flat rectangular strip for the experiment and the curvature of the TM was neglected in this study.

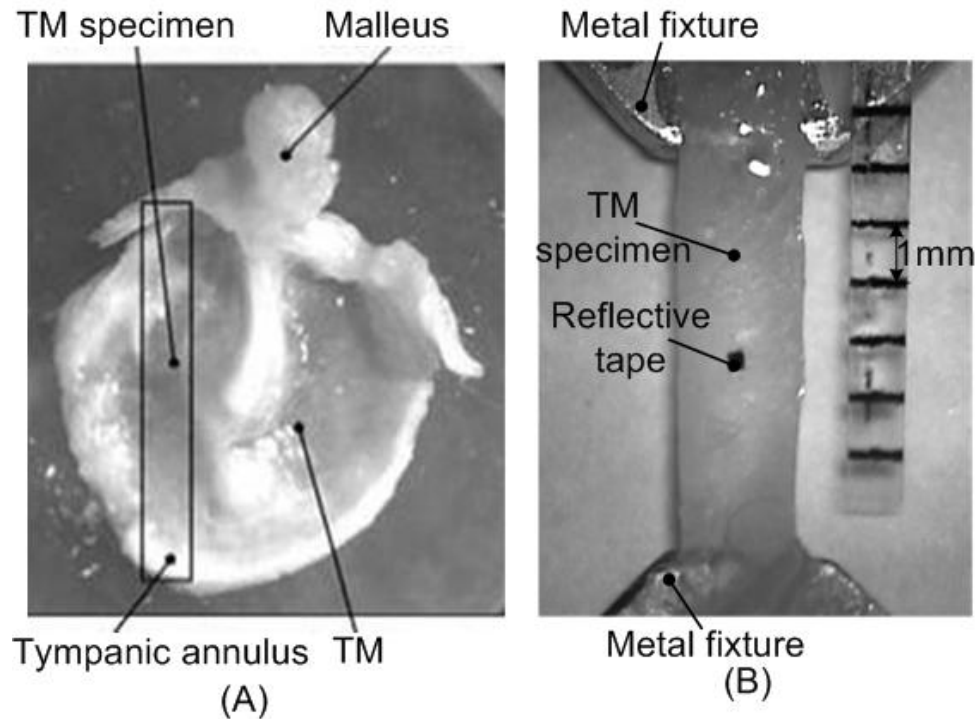


Figure 2.1 (A): The TM sample with malleus and tympanic annulus attached. (B): The TM specimen fixed at metal mounting fixture along the longitudinal direction. A ruler was attached to the metal fixture at the load cell side as dimension measurements refer.

The specimen was then laid on the base of a microscope (Olympus SZX12) and fixed to the soft tissue mounting fixtures at both annulus sides using cyanoacrylate gel glue (Loctite). Two plastic adapters were attached to the metal fixtures for holding the specimen along the longitudinal direction and stabilizing the whole structure as a unit. These adapters were used to avoid any damage on the TM specimen during the mounting process in MTS (TestResource, MN). A laser reflective tape, 0.5 mm², weighting 0.04 mg (3M Co., St. Paul, MN), was placed on the center of the specimen in the medial side of the TM. A ruler was attached to the top metal fixture or at the load cell side of the MTS for measuring dimensions. After the specimen was lined up with grips in MTS, the plastic adapters were removed and the initial state was set up as shown in Fig. 2.1B. The dimensions of the specimen were measured using image analysis tools (Adobe Photoshop 7.0). We completed the experiments on 8 specimens from 5 individual TMs (the mean age of donors was 67.5 years old). The length, width, and thickness of TM are listed in Table 2.1.

Table 2.1 The geometric dimensions and resonance frequency of the TM specimens.

TM Specimen	TM sites	Length (mm)	Width (mm)	Thickness (mm)	Resonance frequency (Hz)	Amplitude ratio <i>R</i>
TM-1	P	6.0	2.0	0.10	2400	11.5
TM-2	A	5.4	2.0	0.10	3000	18.7
TM-3	P	4.8	2.2	0.12	4350	12.5
TM-4	P	6.0	1.7	0.10	2850	8.4
TM-5	A	6.4	1.7	0.10	2400	10.3
TM-6	P	6.0	2.4	0.09	2200	9.9
TM-7	P	6.0	2.3	0.09	2200	13.6
TM-8	A	6.7	2.4	0.09	2050	10.4

Notes: TM sites: P: Posterior portion of eardrum; A: Anterior portion of eardrum.

II. Experimental setup and protocol

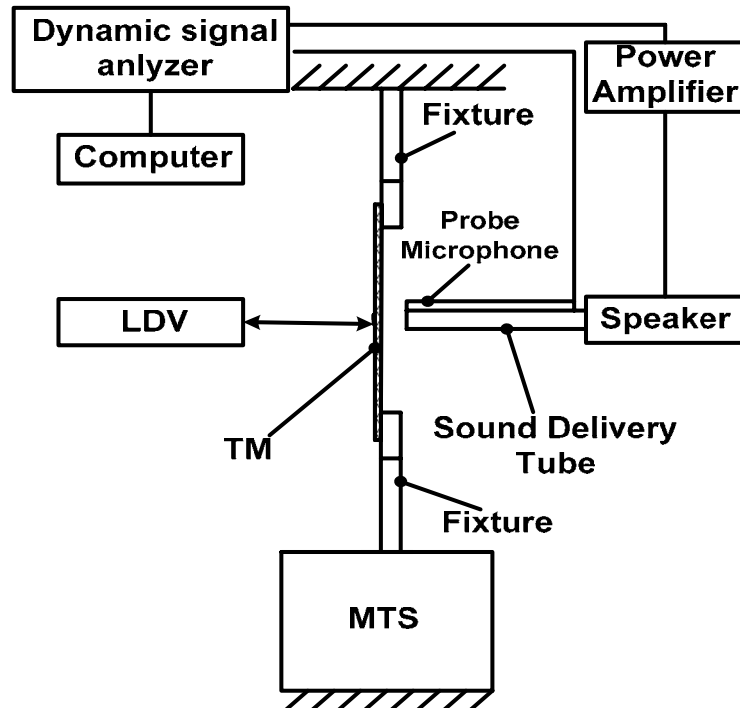


Figure 2.2 Schematic of experiment setup for dynamic test on TM specimens.

Figure 2.2 is the schematic diagram of experimental setup with LDV to measure dynamic properties of the TM specimen. The MTS with the SMT1 load cell (10-N capacity, Interface Inc.) was used to hold the specimen, conduct preconditioning and adjust the initial state of the specimen. A constant pure tone sound at 80 dB SPL across the frequency range of 200-8000 Hz were delivered to the lateral side of the TM specimen at its center from a speaker connected to dynamic signal analyzer (HP 35670A, CA) and power amplifier (2718, Brüel & Kjær, Norcross, GA). The inner diameter of sound delivery tube was 1 mm and the distance between the tube end and the specimen was set at 1 mm. A probe microphone (ER-7C, Etymotic Research, IL) attached on the sound delivery tube was used for monitoring the input sound

pressure level. The LDV (HLV-1000, Polytech PI, Tustin, CA) was used to measure the vibration of the TM by focusing the beam on the laser target. The velocity of the specimen (amplitude and phase) was acquired by the DSA and recorded on a personal computer (PC) for further analysis. The peak-to-peak displacement (dp-p) of the TM specimen was directly calculated from the voltage output of the laser vibrometer velocity decoder by a formula: $dp-p = k (A_{\text{volt}} / 2\pi f)$, where A_{volt} is voltage amplitude in mv, f is frequency in kHz, k is a constant related to selected scale and calibration factor in unit of $\mu\text{m}/\text{mv}/\text{s}$ (Gan et al., 2001).

It is well known that the stabilized state of biological soft tissue is only reached after preconditioning, a process that stress-strain curves are gradually stabilized during repeated load-unload cycles on the specimen (Fung, 1993). In this study the MTS machine was programmed to perform five-cycles of uniaxial preconditioning at stretch rate of 0.05 mm/sec and stretch ratio of 10% for each specimen. A threshold of 0.002 N was applied to the specimen through the load cell to set as the zero load or initial state. After preconditioning, 80 dB SPL acoustic load across 200-8000 Hz was applied to the center of the TM specimen and the vibration of the specimen was recorded. Note that the TM specimen was maintained in its physiological condition by spraying saline solution to its lateral side.

III. FE modeling of dynamic test

Building the FE model of dynamic test

Dynamic tests of TM specimens were simulated in FE models in ANSYS

(ANSYS Inc, Canonsburg, PA) using acoustic-structure coupled analysis as shown in Fig. 2.3. Figure 2.3A shows the lateral view of a TM specimen model with input sound pressure applied at the center of the TM (1 mm of diameter). The top and bottom edges were clamped while the left and right edges were free. Figure 2.3B shows the location of input sound source and the acoustic elements surrounding the TM specimen. The length, width and thickness of each FE model were based on the dimensions of each specimen measured during the experiments as listed in Table 2.1.

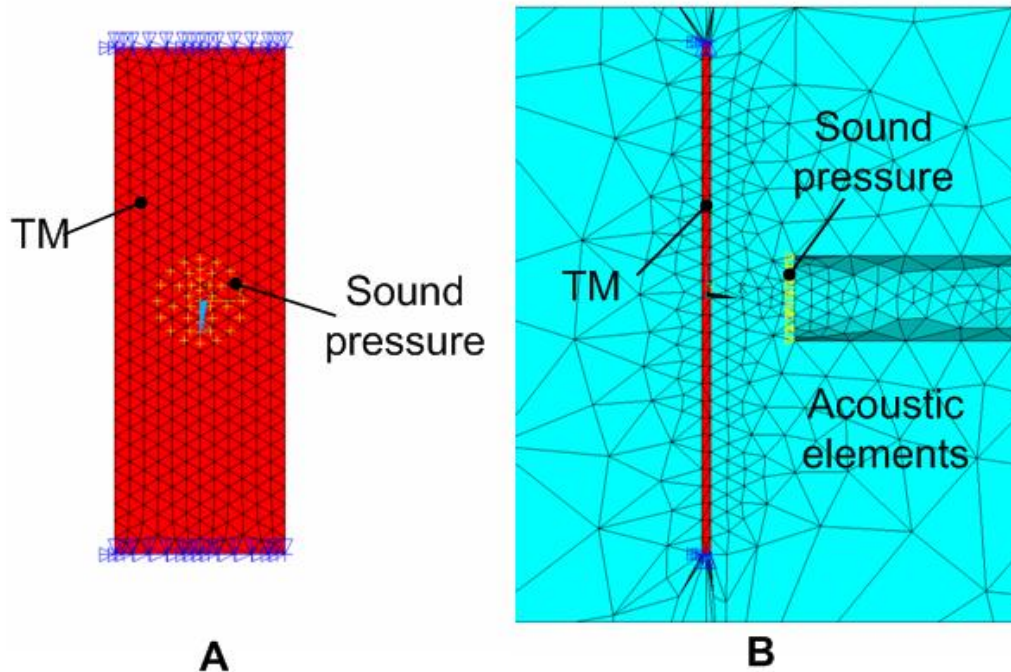


Figure 2.3 FE model of the experiment setup with TM specimen for acoustic-structure coupled analysis. (A): The lateral view of the TM specimen; (B): The location of input sound source and the acoustic elements surrounding the TM.

Following the common rule of thumb that at least six elements per shortest acoustic wavelength are adopted for acoustic scattering (Ihlenbury, 1998), the

maximum element edge size of 0.0071 m was estimated at 8000 Hz, i.e., $1/6(c/f) = 1/6(343\text{m/s}/8000/\text{s}) = 0.0071$ m, where c is the sound speed in air and f is the frequency. In fact, the maximum element size in the model is smaller than 0.007 m and the mesh is fine enough. The FE model of each specimen was meshed by four-node tetrahedral solid elements (Solid 185) with a total of 2,316 elements. The specimen was assumed as a homogenous isotropic material with the density of 1200 kg/m^3 and the Poisson's ratio of 0.3 (Gan and Sun et al., 2006; Gan et al., 2007; Wang et al., 2007). The air surrounding the TM was meshed by four-node tetrahedral acoustic elements (Fluid 30) with a total of 173,688 elements within a sphere of diameter 0.2 m. The density of air was assumed as 1.21 kg/m^3 and the boundary admittance coefficient was 0.007. To simulate the sound absorbance effect in the infinite open field, 3,232 two-dimensional three-node triangular elements (Fluid 130) were created covering the boundary surfaces of all air elements. For 2D acoustic elements, there was no need to add the boundary admittance coefficient.

The surface of acoustic elements (air) next to the TM solid structure was defined as fluid-structural interface (FSI) where the acoustic pressure distribution was coupled into structural analysis as the force input in ANSYS. The TM model has six FSIs on all of its side surfaces.

Sound pressure of 80 dB across the frequency range of 200-8000 Hz was applied at 1 mm away from the center of the TM with a circular area of diameter 1 mm to stimulate the experiment. Vibrations of the TM induced by sound pressure were calculated from the FE model based on material properties assigned to the TM.

The modeling results were compared with the measurements from the experiments.

The detailed calculation is described in the following two sections.

Viscoelastic model of TM specimen

The generalized linear solid model or (Machiraju, et al., 2006, Mclaughlin et al, 2011) composed by springs and dashpots as shown in Figure 2.4 was used to describe the viscoelastic behavior of the TM. Based on this model, the relaxation modulus of the TM can be presented as:

$$E(t) = E_0 + \sum_{i=1}^n E_i \exp\left(-\frac{t}{\tau_i}\right) \quad (2.1)$$

where E_i ($i=0,1,\dots, n$) is the relaxation modulus of the i th spring, τ_i is the relaxation time of the i th dashpot. For harmonic analysis, $E(t)$ in time domain can be converted into complex modulus in frequency domain as:

$$E^*(\omega) = E'(\omega) + iE''(\omega) \quad (2.2)$$

where $E'(\omega)$ is the storage modulus, $E''(\omega)$ is the loss modulus, ω is the angular frequency, and $E'(\omega)$ and $E''(\omega)$ are also expressed as:

$$E'(\omega) = E_0 + \sum_{i=1}^n E_i \tau_i^2 \omega^2 / (1 + \tau_i^2 \omega^2) \quad (2.3)$$

$$E''(\omega) = \sum_{i=1}^n E_i \tau_i \omega / (1 + \tau_i^2 \omega^2) \quad (2.4)$$

$$\eta(\omega) = \tan \delta = E''(\omega) / E'(\omega) \quad (2.5)$$

where δ is the phase angle of the complex modulus, $\eta(\omega)$ is the loss factor, defined as the ratio of storage modulus to the loss storage modulus. In this study, we

selected three spring-dashpot elements ($n=3$, giving 7 parameters $E_0, E_1, E_2, E_3, \tau_1, \tau_2$ and τ_3) to model the viscoelastic behavior of the TM. An inverse-problem solving approach was used in which the 7 parameters are adjusted to allow FE modeling results to agree with the experimental measurements on both the resonance frequency and displacement peak amplitude. The 7 parameters were then substituted into Eq. (2.3) and Eq. (2.4) to determine the complex modulus as a function of frequency.

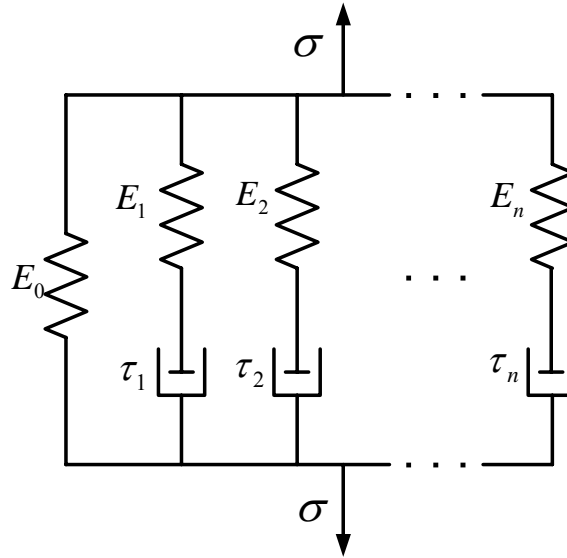


Figure 2.4 Generalized linear solid model for viscoelastic soft tissue.

Vibration analysis

Classic vibration theory (Szilard, 1974) of the thin membrane was used to analyze the motion of the TM. Forced vibration of the TM induced by acoustic load or input sound pressure is governed by:

$$\nabla^2 w + \frac{\bar{m}}{\alpha E^* h} \frac{\partial^2 w}{\partial t^2} = P \quad (2.6)$$

where E^* is the complex modulus which can be expressed as a real part and an imaginary part, ∇^2 is the Laplacian operator, w is the transverse displacement or flexibility, \bar{m} is the mass per unit area, P is the pressure applied onto the TM, h is the thickness of TM, and α is a coefficient related to the TM dimension. For harmonic vibration, sound pressure P and displacement w can be expressed in a Cartesian coordinate system as

$$P = P(t) = P_0 e^{i\omega t}, w = w(x, y, t) = W(x)\Phi(y)e^{i(\omega t - \delta)} \quad (2.7)$$

where x and y are the coordinates, respectively, $W(x)$ and $\Phi(y)$ must satisfy the fixed boundary condition of the TM and δ is the phase angle between the pressure and displacement. Substitute Eqs. (2.2 - 2.4) and Eq. (2.7) into Eq. (2.6), and the problem can be converted into a Bessel-type differential equation. Using Bessel functions, the first order (1,0) resonance frequency ω_n has an expression of

$$\omega_n = \sqrt{\frac{\beta E'(\omega_n)}{\bar{m}}} \quad (2.8)$$

where β is a coefficient related to the TM dimension and Poisson's ratio. Eq. (2.8) shows that the first order resonance frequency of the TM ω_n is proportional to the square root of its storage modulus E' . This provides the theoretical proof that the mechanical properties of the RWM can be determined by measuring the vibration resonance.

Under the first mode, the central (when $r=0$) displacement amplitude of the TM, $w_0 = w(0, \varphi, t)$, resolved from Eq. (2.6) can be expressed as

$$w_0(\omega) = \frac{P_0}{\alpha E'(\omega)} \frac{1}{\sqrt{\left(1 - \frac{\omega^2}{\omega_n^2}\right)^2 + \left[\frac{E''(\omega)\omega}{E'(\omega)\omega_n}\right]^2}} \quad (2.9)$$

When $\omega = 0$ (static deformation state),

$$w_0(0) = \frac{P_0}{\alpha E'(0)} = \frac{P_0}{\alpha E_0} \quad (2.10)$$

When $\omega = \omega_n$ (resonance),

$$w_0(\omega_n) = \frac{P_0}{\alpha E'(\omega_n)} \frac{E'(\omega_n)}{E''(\omega_n)} = \frac{P_0}{\alpha E'(\omega_n)} \frac{1}{\eta(\omega_n)} \quad (2.11)$$

Displacement amplification ratio R defined as the displacement at resonance frequency (when $\omega = \omega_n$) over the displacement at static state (when $\omega = 0$) is then expressed as:

$$R = \frac{w_0(\omega_n)}{w_0(0)} = \frac{E_0}{E'(\omega_n)\eta(\omega_n)} \quad (2.12)$$

Equations (2.8), (2.10), and (2.12) show that the resonance frequency ω_n , displacement amplitude at static state (approximately using the amplitude at 200 Hz) $w_0(0)$, and displacement amplification ratio R are all related to frequency-dependent storage modulus E' and the loss factor η of the TM, and finally determined by the viscoelastic parameters, $E_0, E_1, E_2, E_3, \tau_1, \tau_2$ and τ_3 . However, it was still very difficult to derive a theoretical solution. Thus, the FE modeling and inverse-problem solving method were used to determine these parameters and the complex modulus E^* .

Inverse-problem solving method

The inverse-problem solving approach was used to determine the viscoelastic parameters, $E_0, E_1, E_2, E_3, \tau_1, \tau_2$ and τ_3 , and finally to obtain the complex modulus of the TM. The FE model of each TM sample was used to verify these parameters as well as the complex modulus by comparing the FE model-derived displacement-frequency curve with the experimental measurement curve. Fig. 2.5 shows the schematic flowchart for the inverse-problem solving method. Briefly, the optimization process includes four steps: 1) the initial values of viscoelastic parameters were given as: $E_0 = 40MPa$, $E_1 = 10MPa$, $E_2 = 4MPa$, $E_3 = 1MPa$, $\tau_1 = 2 \times 10^{-5} s$, $\tau_2 = 2 \times 10^{-4} s$ and $\tau_3 = 2 \times 10^{-3} s$; 2) The storage modulus $E'(\omega)$ calculated by Eq. (2.3) and loss factor $\eta(\omega)$ by Eq. (2.5) were input into the FE model; 3) Harmonic analysis of the FE model was then conducted from 200 to 8000 Hz with an interval of 50 Hz. Vibrations of the central node of the TM induced by sound pressure of 80 dB SPL were calculated from the FE model; 4) The model-derived displacement-frequency curve was compared with the experimental curve for each sample. The correlation coefficient between the two sets of data was calculated. If the coefficient met the set value, the process was ended and the viscoelastic parameters were determined. If the correlation coefficient did not meet the set value, the viscoelastic parameters were adjusted based on Eqs. (2.3 - 2.5), (2.8), (2.10), and (2.12), and the iteration process was repeated from step 2). Through this process, the values of viscoelastic parameters were optimized and determined. Finally, they were substituted into Eqs. (2.3 - 2.5) to obtain the complex modulus and loss factor of the RWM as functions of frequency.

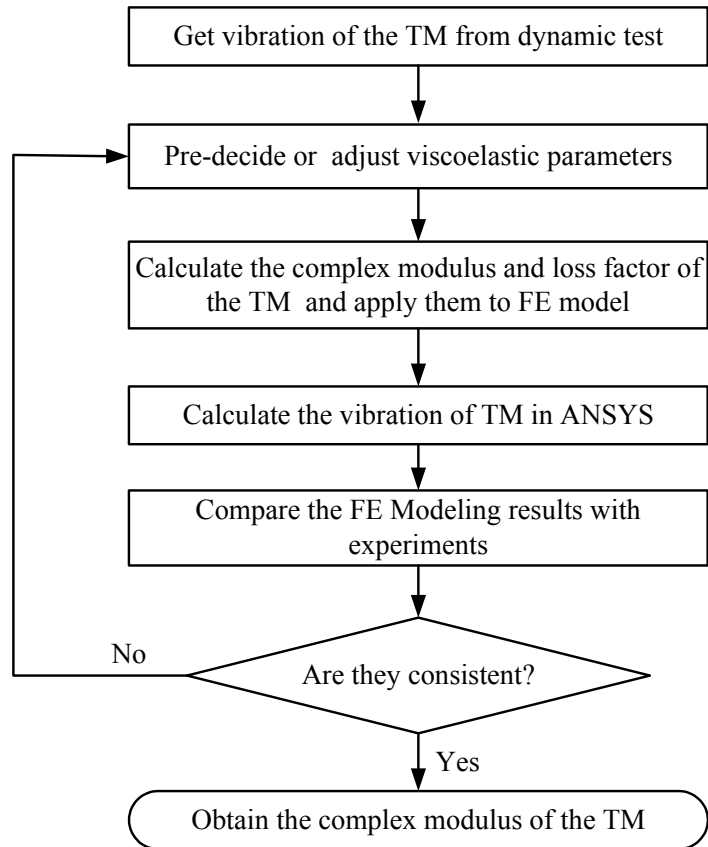


Figure 2.5 Schematic flowchart of the inverse-problem solving method to determine the complex modulus of TM sample.

It is noted that the complex modulus calculated from the model is sensitive to the geometry of TM specimen (coefficient a) or indirectly to the resonance frequency ω_n as shown in Eq. (2.9). To assess the influence of geometry variation in experiments on complex modulus (E' and E''), we employed the classic shell plate vibration theory (Szilard, 1974). The relationship between the geometry coefficient a and the thickness of TM sample h can be expressed as $a \propto h^{3/2}$ and the storage modulus as $E' \propto (1/h^{3/2})$. The thickness of TM measured using image analysis method had a resolution level of 10 μm . Thus, for a TM sample with measured thickness of 100 μm , the real thickness could be 90 or 110 μm . The model-derived

storage modulus E' value would have a variation range of $\pm 15\%$ of calculated value. Similarly, the variation range for loss modulus E'' would be $\pm 15\%$ of calculated value.

2.1.2 Results

I. Validation of the method

To verify the inverse-problem solving method through the experimental measurement and the FE modeling, we used the silicone rubber film (SKU 87315K61, McMaster-Carr, CA), a standard material, to perform the dynamic experiment and FE modeling first. The length, width and thickness of the silicone film were prepared at 6, 2 and 0.127 mm, respectively, which were similar to the TM specimen. The experimental procedure was the same as that for the TM specimen with 80 dB sound pressure input across 100-4000 Hz. The FE model of the silicone film sample was created based on its dimensions.

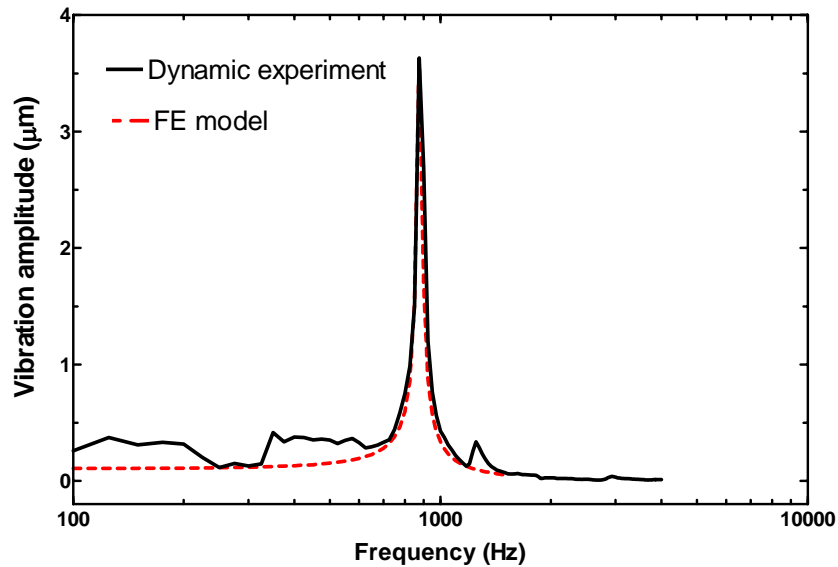


Figure 2.6 Vibration amplitude of silicone rubber film in frequency domain obtained by dynamic experiment (solid line) and FE modeling (dash line).

Considering there is no published viscoelastic properties of this specific material over frequency range of 0-4000 Hz, the silicone film sample was conducted the quasi-static tensile and stress relaxation tests in the MTS (TestResources, MN). The quasi-static elastic modulus was obtained as 2.8 MPa from tensile testing at strain rate of 0.0033 s^{-1} . The relaxation modulus range was 2.8 - 3.1 MPa obtained from relaxation testing at the initial strain rate of 25 s^{-1} and relaxation time of 100 s. The dynamic test was then conducted on the silicone film sample. Figure 2.6 shows the vibration amplitude curves of the silicone film measured from experiment (solid line) and calculated from the FE model (dash line). As can be seen in this figure, the displacement amplitude reaches the peak at 875 Hz or resonance frequency with the amplitude ratio R of 34.2 for both experiment and FE model. The material parameters of the silicone film were determined as: $E_0=2.63 \text{ MPa}$, $E_1=0.275 \text{ MPa}$, $E_2=0.11 \text{ MPa}$, $E_3=0.075 \text{ MPa}$, $\tau_1=1.0\text{E-}5\text{s}$, $\tau_2=1.0\text{E-}4\text{s}$ and $\tau_3=1.0\text{E-}3\text{s}$. Thus, the relaxation modulus $E(t)$ in MPa was obtained from Eq. (2.1):

$$E(t) = 2.63 + 0.275e^{-t/0.00001} + 0.11e^{-t/0.0001} + 0.075e^{-t/0.001} \quad (2.13)$$

The storage modulus E' was 2.63-2.82 MPa across the frequency up to 4000 Hz, which is within the range of 2.8 – 3.1 MPa obtained from the stress-relaxation test. The static Young's modulus was then calculated as 2.63 MPa which is very close to 2.80 MPa measured from the tensile test. This indicates that the inverse-problem solving method by optimizing 7 parameters with experimental measurements is a feasible approach to determine the material properties.

II. Dynamic properties of the TM

Dynamic experiments were conducted on eight TM specimens with the length ranging from 4.8 mm to 6.7 mm with a mean of 5.91 mm. The width ranging from 1.7 mm to 2.4 mm with a mean of 2.09 mm; and the mean thickness of 0.1 mm as listed in Table. 2.1, Figure 2.7 shows the displacement amplitude-frequency curves of eight TM specimens recorded from experiments. The displacement amplitudes of TM specimens at low frequency (under 1500 Hz) are about 0.02 - 0.03 μm with a few spikes. Each TM specimen shows the peak amplitude at resonance frequency between 2000 Hz and 3000 Hz except specimen TM-3 with a resonance frequency of 4350 Hz. Specimen TM-3 also shows small amplitude compared with other specimens. The resonance frequency and amplitude ratio R of each TM specimen are listed in Table 1. TM-3 had the smallest length and largest thickness among all specimens, and thus resulted in the highest resonance frequency and smallest displacement. The amplitude ratio R of specimen is between 8.4 and 18.7 with a mean of 11.91. Note that some small peaks shown in Fig. 2.6 were not included.

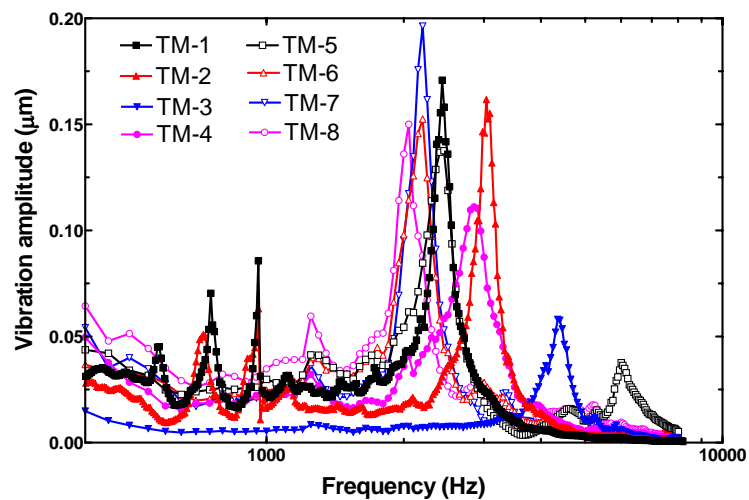


Figure 2.7 Vibration amplitude measured from experiments on eight TM specimens over frequency range of 200-8000 Hz.

Eight FE models were created to simulate the dynamic experiments of the TM specimens. As an example, Fig. 2.8 shows the results from two specimens: the vibration amplitude-frequency curves derived from FE modeling, as well as the experimental measurements. Fig. 2.8A is obtained from specimen TM-1 and Fig. 2.8B from TM-2. The FE modeling results matched well with the experimental data across the frequency range of 200-8000 Hz, particularly at the resonance frequency. Some small peaks at lower frequency were not considered during modeling.

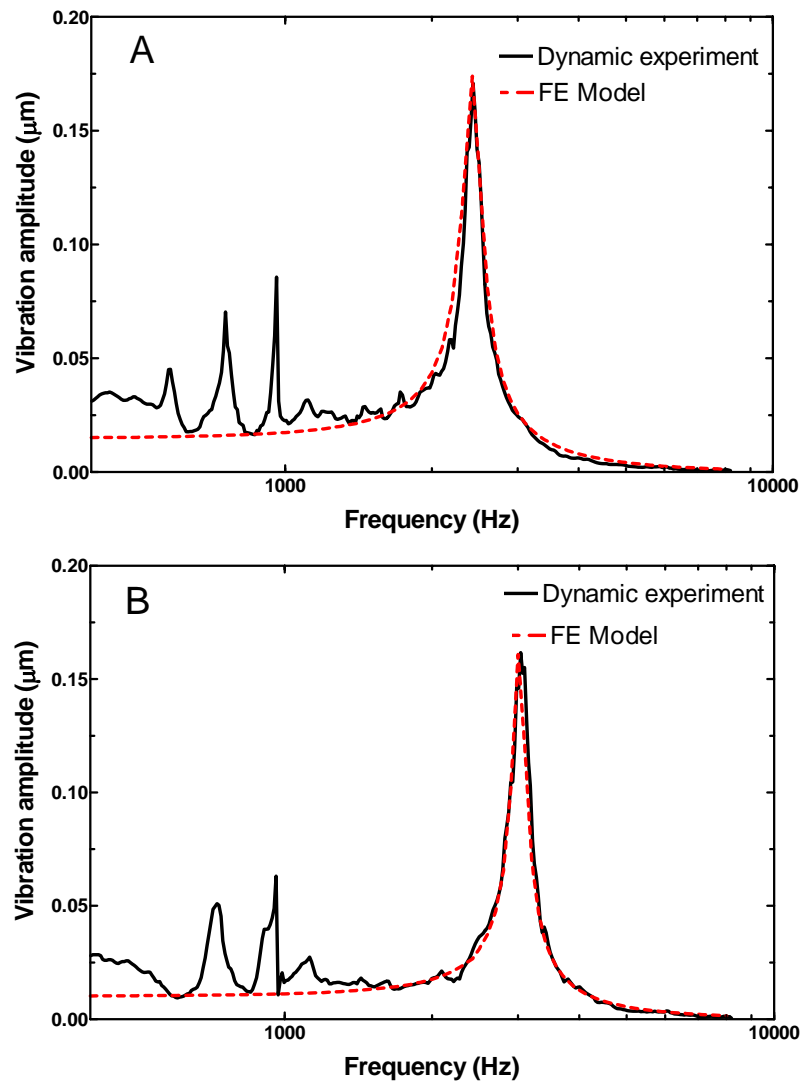


Figure 2.8 The FE modeling results obtained from two TM models in comparison with the experimental curves. (A): Specimen TM-1; (B): Specimen TM-2.

Table 2.2 The viscoelastic parameters of TM specimens obtained in acoustic driving.

TM Specimen	E_0 (MPa)	E_1 (MPa)	E_2 (MPa)	E_3 (MPa)	τ_1 (s)	τ_2 (s)	τ_3 (s)
TM-1	49.0	12.0	3.00	1.00	2.0E-5	2.0E-4	2.0E-3
TM-2	60.0	10.0	2.00	1.00	2.0E-5	2.0E-4	2.0E-3
TM-3	65.2	11.8	3.80	1.20	2.2E-5	2.2E-4	2.2E-3
TM-4	61.8	17.5	5.00	1.20	3.5E-5	3.5E-4	3.5E-3
TM-5	46.0	12.0	4.80	1.50	2.5E-5	2.5E-4	2.5E-3
TM-6	39.0	10.2	4.16	1.04	3.0E-5	3.0E-4	3.0E-3
TM-7	41.2	9.20	3.05	1.00	2.0E-5	2.0E-4	2.0E-3
TM-8	60.6	15.4	5.60	1.45	3.2E-5	3.2E-4	3.2E-4

The seven parameters of generalized linear solid model for each TM specimen obtained by inverse –problem solving method are listed in Table 2. There are some differences between individual specimens for each parameter which reflect the individual variation between the TM samples and experimental set up. Based on these parameters, the storage modulus E' , loss modulus E'' and loss factor η were calculated and displayed in Fig. 2.9 across the frequency range of 200 Hz to 8000 Hz. Figure 2.9A shows that the storage modulus increases with frequency and the largest storage modulus is 66.50 MPa at 200 Hz and 81.20 MPa at 8000 Hz. The smallest storage modulus is 40.50 MPa at 200 Hz and 51.30MPa at 8000 Hz. Loss modulus is shown in Fig. 2.9B. The largest loss modulus is 2.87 MPa at 200 Hz and 7.81 MPa at 8000 Hz and the smallest is 1.07 MPa at 200 Hz and 5.21 MPa at 8000 Hz. Loss modulus has a peak value between 4000-6000 Hz. The loss modulus of each TM specimen is much smaller than the storage modulus, which indicates that the TM may mainly show elastic properties. Fig. 2.9C shows the loss factor across the frequency range of 200-8000 Hz obtained from 8 TM specimens. Change of loss

factor with frequency is similar to that of loss modulus: increasing rapidly at frequency below 4000 Hz, and then reaching the maximum value around 4000-6000 Hz.

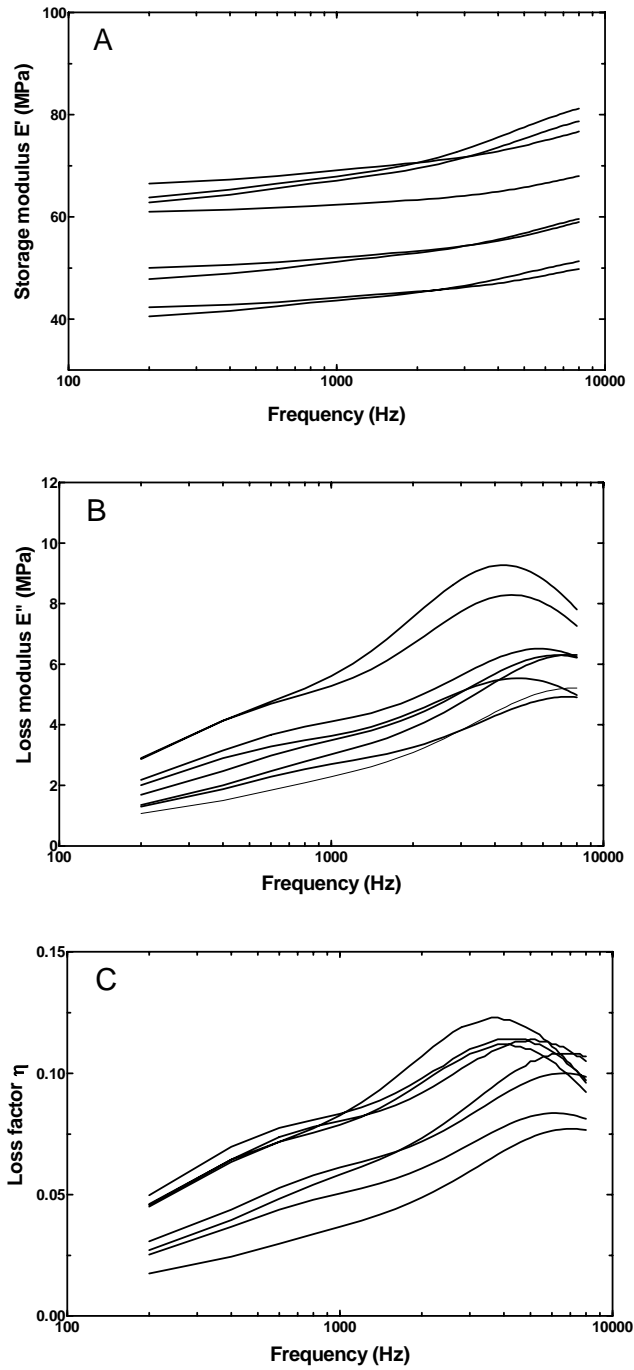


Figure 2.9 Complex modulus for eight TM specimens over the frequency range of 200-8000 Hz. (A): The storage modulus; (B): The Loss modulus; (C): Loss factor.

2.1.3 Discussion

I. Comparison with published results

Most published Young's moduli of the human TM are obtained from static or quasi-static tests. There are very few results of dynamic tests on the TM over auditory frequency range reported in the literature. Recently, Luo et al. published the relaxation moduli of the human TM specimens along the radial and circumferential directions for normal and diseased tissues using the miniature SHTB (2009a; 2009b). The high strain rate was reached at 150-2500 s⁻¹, corresponding to 150-2500 Hz in frequency. Figure 2.10 shows comparisons of the storage modulus (Fig. 2.10A) and loss modulus (Fig. 2.10B) of the present results (thick solid lines with square solid symbols) with Luo's data (dash lines with solid circular symbols for radial direction and thin solid lines with open triangular symbols for circumferential direction). The results are presented as mean values with standard derivations (S.D.). In both the present study and Luo et al.'s (2009b), the TM specimens were normal tissue and assumed as a homogeneous material. In the present study, the mean storage modulus of eight TM specimens is 54.34 MPa at 200 Hz and 65.54 MPa at 8000 Hz with a S.D. about 10 MPa at 200 Hz and 12 MPa at 8000 Hz. The mean loss modulus E'' is 1.92 MPa at 200 Hz and 6.12 MPa at 8000 Hz with a S.D. of 0.70 MPa at 200 Hz and 1.06 MPa at 8000 Hz. Luo et al. (2009b) reported $E_0=41.52$ MPa, $E_1= 25.44$ MPa and $\tau_1=50.7$ μ s for radial direction and $E_0=30.04$ MPa, $E_1= 69.08$ MPa and $\tau_1=25.3$ μ s for circumferential direction. The standard derivation of their results was

25% of the mean value. Compared with Luo et al.'s data which are limited below 2500 Hz, the storage moduli E' obtained from this study are generally consistent with their results (Fig. 2.10A). The storage modulus from this study overlapped with the modulus along radial direction measured by Luo et al. (2009b). The values of loss modulus obtained from this study are consistent with Luo (2009b) data at $f < 500$ Hz (Fig. 2.10B). As frequency increases over 500 Hz, the loss modulus is not increasing as much as observed from Luo et al.'s data. It is speculated that viscous effect of the TM specimen in Luo et al.'s experiments may be higher than the tissues used for the present study.

The difference of loss modulus measured in this study from that reported by Luo et al. may be related to individual variation of the human TM specimens and different experimental setups. In Luo et al.'s study, the preconditioning process was completed using the incident and reflected elastic waves generated by SHTB. In the present study, a standard and accurately controlled preconditioning for soft tissues (Fung, 1993) was conducted. The measurement of resonance frequency and amplitude using acoustic load is sensitive to additional mass on the specimen, such as the saline solution which added to the TM. In Luo et al.'s study, the saline solution was sprayed directly to the TM specimen and the measurement was completed within a few seconds, thus more water was maintained on the TM than that in this study. The physiological condition of the tissue during experiment influences the viscous properties of soft tissue. This may explain the difference of loss modulus between this study and Luo et al.'s results. In our experiments, the

initial tension set on the specimen and the sound pressure level applied over the frequency range of 200-8000 Hz may have some effects on the results of viscoelastic modulus, in particular, the loss modulus. However, further study of the effect of those parameters on measurement and modeling results is necessary.

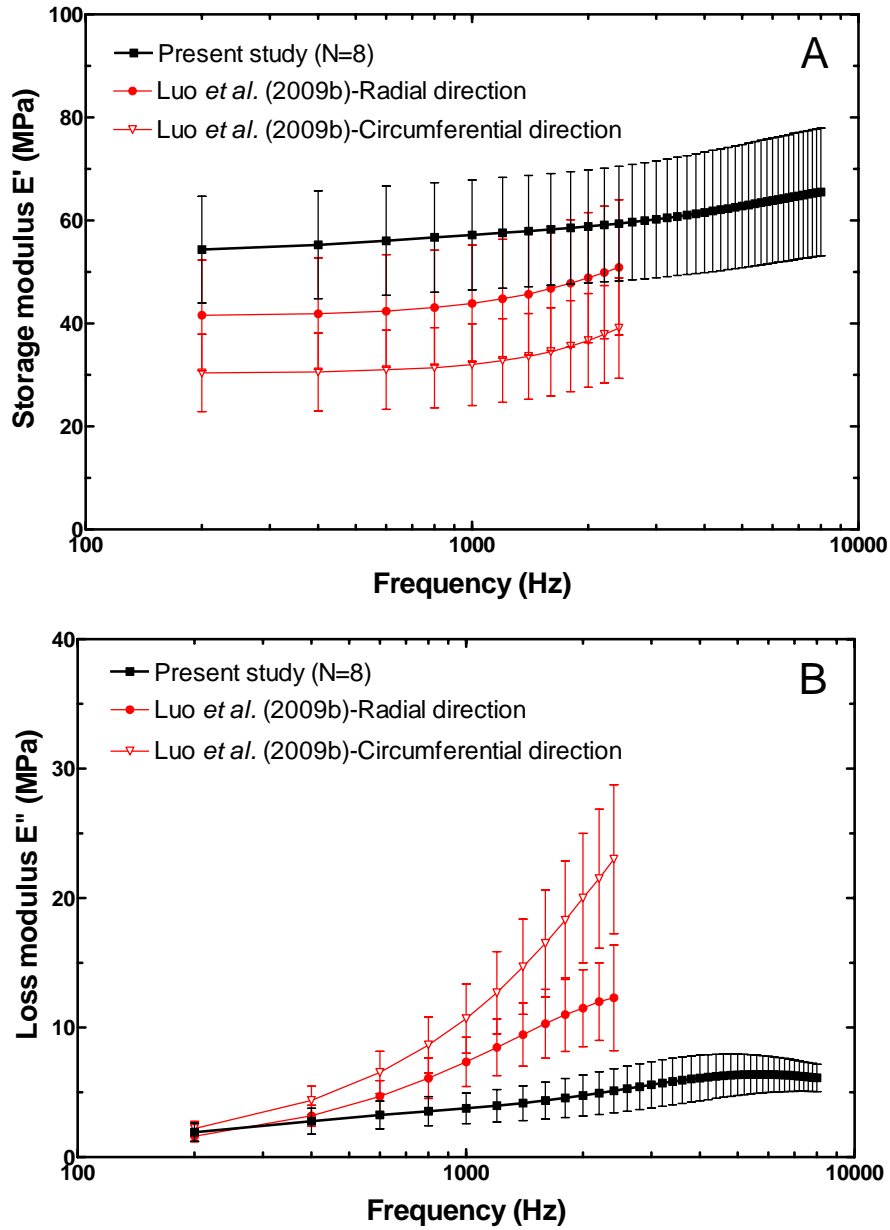


Figure 2.10 Comparison of the storage modulus (A) and loss modulus (B) obtained from the present study (thick solid line) with Luo et al.'s results (2009b) in radial direction (dash line) and circumferential direction (thin solid line).

One of the advantages of the method developed in this study comparing with previous published works is that the dynamic measurement of ear soft tissue can be archived much higher frequencies by using acoustic load stimulation. The resonance analysis can provide accurate mechanical properties of the structure or material over a broad range of frequency. However a disadvantage of this study is that mechanical properties of the specimen depend on both the experimental measurements and FE modeling analysis.

II. Relaxation modulus in time-domain

In addition to viscoelastic modulus derived in frequency domain, we used the parameters listed in Table 2 to calculate the relaxation modulus in time domain using Eq. (2.1). Figure 2.11 shows the mean relaxation modulus from the present study (thick solid lines with square solid symbols) compared with that of Luo et al.'s measurements in radial and circumferential directions. The mean initial modulus (at time $t=0$) observed from eight TM specimens in present study is 70.21 MPa, larger than 67 MPa, along the radial direction and smaller than 99.12 MPa, along the circumferential direction reported by Luo et al.'s (2009b). The mean static modulus (at time tending to ∞) is 54.76 MPa from the present study which is larger than the results obtained by Luo et al. in both radial and circumferential directions. It took about 0.1 ms to reach the stabilized state for the TM specimens in this study and about 0.2 ms for radial specimens and 0.12 ms for circumferential specimens in Luo et al.'s study. The results indicate that the TM specimens in this study reach their

stable state more quickly comparing with that in Luo et al.'s study. This is consistent with the results that the specimens in Luo et al.'s study had more viscous effects.

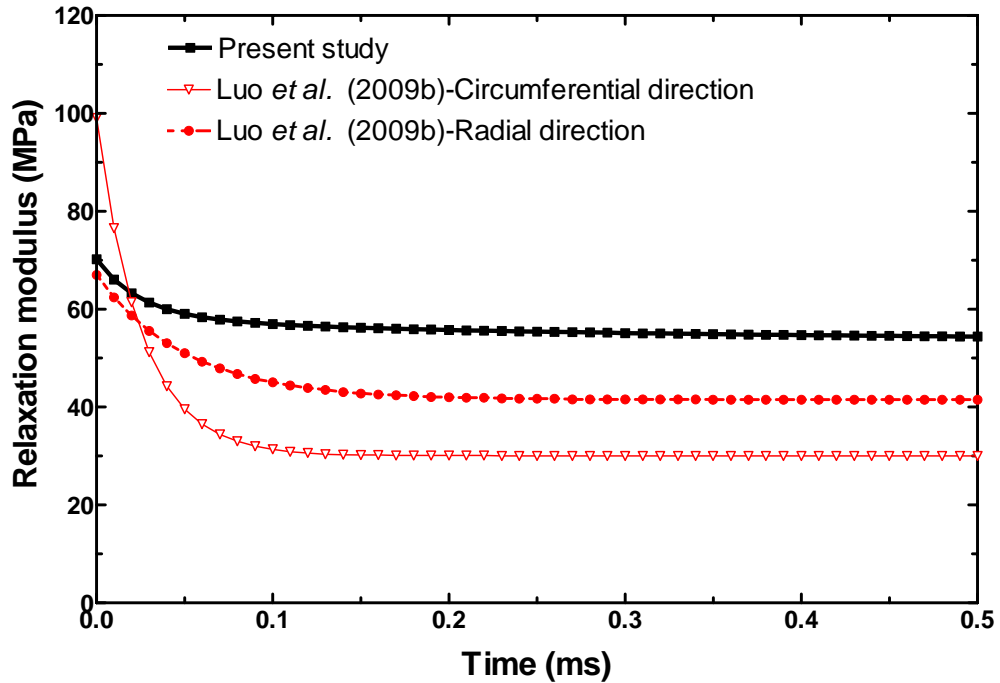


Figure 2.11 Comparison of mean relaxation modulus in time domain obtained in this study (thick solid line) with the results reported by Luo et al.'s (2009b).

2.2 Dynamic properties measured by DMA

The content of this section has been published in Ann. Biomed. Engi. by Zhang and Gan (2013a).

DMA is widely used to measure the complex modulus of materials in the frequency domain. However, the current commercial DMA has limited higher frequency access which cannot reach the human auditory frequency range. An approach called FTS principle using the DMA may be a possible method for

measuring the TM dynamic properties over the auditory frequency range. The FTS is an empirical method used to expand the effective frequency scale for viscoelastic measurements on polymers and fibrous composites (Ferry, 1980; Nielsen and Landel, 1994). The basic theory of FTS considers the viscoelastic behavior of some materials as a function of two principle variables: frequency and temperature. The effect of temperature changes on the viscoelastic properties of the material is equivalent to that of frequency changing (Ferry, 1980).

The FTS was originally developed for amorphous polymers and is applicable to a variety of polymer systems (Radebaugh and Simonelli, 1983; Tajvidi et al., 2005). Recently, researchers have applied the FTS principle to biological tissues. Peters et al. (1997) measured the shear modulus, loss factor and relaxation modulus of bovine brain tissues at 7 - 37°C over the frequency range of 0.16 to 16 Hz and extrapolated the dynamic shear modulus for much higher frequencies (up to 1.6 MHz). Chan (2001) measured the viscoelastic properties of the vocal-fold tissue at 5 - 37°C over the frequency range of 0.01 to 15 Hz and expanded the equivalent frequency up to about 500 Hz using FTS.

In this study, the dynamic properties of human TM were measured using a DMA based on the FTS principle. The test was conducted at the frequency range from 1 Hz to 40 Hz at three different temperatures: 5°, 25° and 37°C. The FTS principle was applied to extend the testing frequency range to a much higher level (at least 3800 Hz). The generalized linear solid model was used as the constitutive law for the TM, and the complex modulus of the TM was obtained. The methods

and data reported here contribute to the biomechanics of the middle ear and improve the accuracy of FE model for the human ear.

2.2.1 Methods

I. TM specimen preparation

A total of 11 TM specimens from six individual donors (five female and one male, age ranged from 64 to 74 with a mean value of 68.8) were employed in this study. A similar process was conducted to prepare the rectangular TM samples, as described in Section 2.1.1. The TM sample was cut from the posterior or anterior portion of the TM (Fig. 2.1). The length (gap between two fixture adapters) and width of the specimen were measured and listed in Table 2.3. The length of all 11 TM samples ranges from 5.6 to 7.6 mm with a mean of 6.5 mm and S.D. of 0.7 mm. The width ranges from 1.7 to 2.5 mm with a mean of 2.1 mm and S.D. of 0.3 mm. The side image of the specimen was also taken by the CCD camera to measure the thickness of the specimen. The thickness of all samples was measured around 0.06 mm at the central (middle) region of the sample with a resolution of 0.01 mm. Kuyper et al. (2006) reported that the thickness of human TM was not uniform and the mean thickness of 0.04 - 0.12 mm was observed in the central region between the umbo and annulus from three TM specimens. In this study, the non-uniformity of the thickness was not taken into account and the thickness of central region of the sample was used.

Table 2.3 The dimensions of striped human TM samples used in DMA measurement (number unit in mm).

Sample	TM -1	TM -2	TM -3	TM -4	TM -5	TM -6	TM -7	TM -8	TM -9	TM -10	TM -11	Mean \pm S.D.
Length	7.6	7.4	6.0	5.6	6.4	7.0	7.1	7.4	5.6	6.0	5.6	6.5 \pm 0.7
Width	2.1	2.5	2.4	2.2	2.0	1.8	1.7	1.8	2.1	2.3	2.2	2.1 \pm 0.3

II. Viscoelastic model of TM specimen

As the first step to study the dynamic properties of TM using FTS, the sample was considered as an isotropic and homogeneous material in this study. The generalized linear solid model was used in this study. The relaxation modulus and the complex modulus of the TM are represented by Eqs. (2.1 – 2.5) in Section 2.1.1.

In this study, we selected two spring-dashpot elements ($n=2$, giving 5 parameters $E_0, E_1, E_2, \tau_1,$ and τ_2) to represent the viscoelastic behavior of the TM. The five parameters will be determined by fitting the generalized linear solid model with the master curve of the complex modulus obtained through the FTS.

III. Dynamic test on TM specimen

In this study, the complex modulus including the storage modulus and the loss modulus of the human TM specimen at three temperatures ($5^\circ, 25^\circ,$ and 37°C) were measured in the DMA (Bose ElectroForce 3200, Eden Prairie, MN). The TM sample was placed inside the temperature-control chamber in the DMA. A thermocouple was placed at 2 cm behind the sample to measure the temperature in the chamber. There was a negative feedback circuit to control temperature stably. The precision of

temperature controlling was $\pm 1^\circ\text{C}$. In the temperature range of 5 - 37°C, there is no phase change (freezing) of fluid in tissue cells, and there is no denature of proteins. Thus, the structure of the soft tissue in this temperature range should not change (Peter et al., 1997; Chan, 2001). The temperature of 37°C was chosen as the reference temperature. The TM samples were subjected to the sinusoidal vibrations with small amplitudes at different frequencies. At each frequency f , the displacement d and force F were recorded as the function of time t :

$$d = d_0 e^{i2\pi ft} \quad (2.14)$$

$$F = F_0 e^{i(2\pi ft + \delta)} \quad (2.15)$$

where σ_0 and E_0 were stress and strain amplitude, respectively. The complex modulus at this frequency f was calculated as:

$$|E^*| = \frac{\sigma_0}{E_0} = \frac{F_0/wh}{d_0/l} \quad (2.16)$$

$$E' = |E^*| \cos \delta \quad (2.17)$$

$$E'' = |E^*| \sin \delta \quad (2.18)$$

where w , h , and l were the width, thickness and length of the TM specimen, respectively. The test protocol for each TM specimen is described below.

Preconditioning test

In this study the DMA was programmed to perform five cycles of uniaxial preconditioning at a frequency of 0.1 Hz and stretch displacement of 1.0 mm for each specimen before the dynamic test. For all TM samples, their stress-stretch

curves were almost identical after 5 loading-unloading cycles, which indicated the mechanical properties of TM were stabilized.

Dynamic test

After preconditioning, the dynamic test was conducted at 5°, 25°, and 37°C in sequence. At each temperature, the TM sample was tested at 1, 2, 5, 10, 20, and 40 Hz with the displacement amplitude of 0.2 mm. The sample took a rest for at least 2 minutes for recovering after each run. Note that the sample was kept in physiological moisture by adding saline solution onto its surface between each test. To keep sample in the same moisture condition, the accurate amount of saline solution was controlled by a syringe.

IV. Frequency-temperature superposition (FTS) principle

The FTS principle was first reported in the 1950s (Ferry, 1950; Williams et al., 1955), and has become a useful extrapolation technique as applied to polymers, plastics, and composites. The later theories of FTS address a simple relationship between the temperature and frequency (or time) effects on the molecular behaviors of polymers and thus the viscoelastic properties of these materials (Ferry, 1980). The curves of the complex modulus E^* obtained at a relatively low temperature T can be shifted along the frequency axis by a shift factor α_T to a higher temperature T_0 (served as reference temperature). This concept can be expressed by the equation:

$$E^*(T_0, f) = E^*(T, f / \alpha_T) \quad (2.19)$$

where f is the frequency. The shift factor α_T quantifies the temperature's effect on the material's complex modulus. It is temperature-dependent and needs to obey the Arrhenius equation (Radebaugh and Simonelli, 1983):

$$\ln \alpha_T = \frac{E_a}{R} \left(\frac{1}{T} - \frac{1}{T_0} \right) \quad (2.20)$$

where T and T_0 are the absolute temperature in Kelvin, E_a is the activation energy for the material, and R is the universal gas constant equal to 8.314 J/mol.K.

Another widely used empirical equation for the FTS principle is the WLF equation, which was first introduced by Williams, Landel and Ferry (1955):

$$\log \alpha_T = \frac{c_1(T - T_g)}{c_2 + T - T_g} \quad (2.21)$$

where c_1 and c_2 are empirical constants and T_g is the glass transition temperature. The glass temperature is the temperature below which the polymer chain backbone configuration rearrangement stops (Nielsen and Landel, 1994). Combining the Eqs. (2.20) and (2.21) presents the relation between the activation energy E_a , c_1 and c_2 :

$$E_a = 2.303 R c_1 c_2 T^2 / (c_2 + T - T_g)^2 \quad (2.22)$$

The following procedure for the FTS principle was used to determine the dynamic properties of the TM samples at the higher frequencies: 1) the complex moduli (storage modulus E' and loss modulus E'') obtained at three different temperatures (5°, 25°, and 37°C) were plotted together as functions of the frequency in logarithmic scale; 2) the complex modulus curves at the lower temperatures were shifted horizontally to the higher frequencies; 3) when the curves were adjacent to

each other, the commonly called “master curve” at the reference temperature (37°C) was formed to predict the complex modulus at the higher frequency range; 4) the shift factor aT and the activation energy E_a were calculated from Eqs. (2.19) and (2.20). Moreover, there are three requirements for the FTS principle to hold (Ward, 1971): perfect matching of the curve shapes at adjacent regions, same shift factor value for all viscoelastic parameters, and the shift factor obeying the Arrhenius equation or the WLF equation. In this study, these requirements were checked and satisfied.

2.2.2 Results

Dynamic experiments were conducted on 11 TM specimens, and the storage modulus E' and the loss modulus E'' of these specimens were obtained over 1 to 40 Hz. Figure 2.12 shows the typical complex modulus-frequency curves at the different temperatures (5°, 25° and 37°C) obtained from two TM specimens (TM-1 and TM-4). Both the storage modulus and the loss modulus increased with the frequency increasing or temperature decreasing. Larger slopes were found at the lower frequency range for the loss modulus. Other TM samples had the complex modulus-frequency curves similar to that shown in Fig. 2.12. The inter-subject difference of the E' and E'' curves was observed due to the variation between the TM specimens and the possible error of the experimental measurements.

Table 2.4 The shift factors, activation energies E_a , and maximum frequency of human TM samples. (E_a unit in kJ/mol, frequency unit in Hz)

	TM -1	TM -2	TM -3	TM -4	TM -5	TM -6	TM -7	TM -8	TM -9	TM -10	TM -11	Mean \pm S.D.
α_{25}	6.7	6.0	5.4	5.0	5.0	7.2	5.5	5.8	4.8	7.0	6.4	5.9 \pm 0.8
α_5	153	126	108	98	90	196	118	137	95	191	165	134 \pm 38
$\ln\alpha_{25}$	1.90	1.79	1.69	1.61	1.61	1.97	1.70	1.76	1.57	1.95	1.86	1.76 \pm 0.14
$\ln\alpha_5$	5.03	4.84	4.68	4.58	4.50	5.28	4.77	4.92	4.55	5.25	5.11	4.86 \pm 0.28
E_a	113.6	109.0	105.2	102.6	101.0	119.1	107.0	110.4	101.7	118.3	114.9	109.3 \pm 6.5
Max. fre	6120	5040	4320	3920	3600	7840	4720	5480	3800	7640	6600	5371 \pm 1506

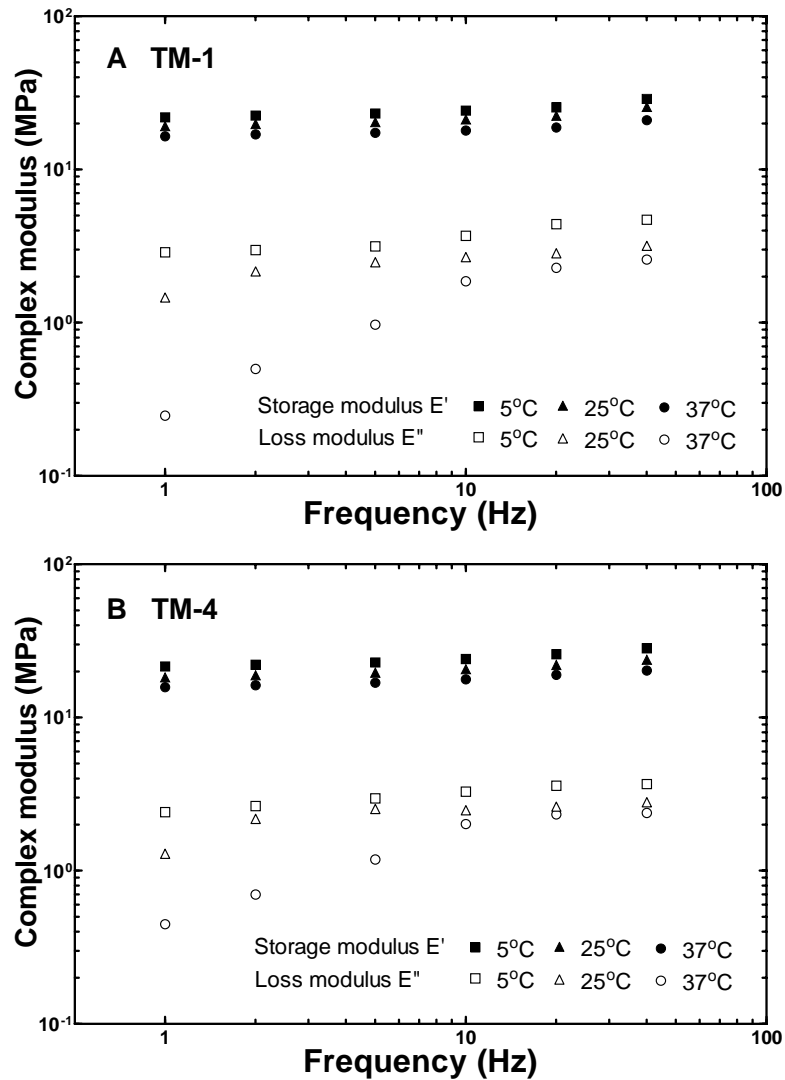


Figure 2.12 The complex modulus obtained at the different temperatures (5°C, 25°C and 37°C) from two TM samples: (A) sample TM-1 and (B) sample TM-4.

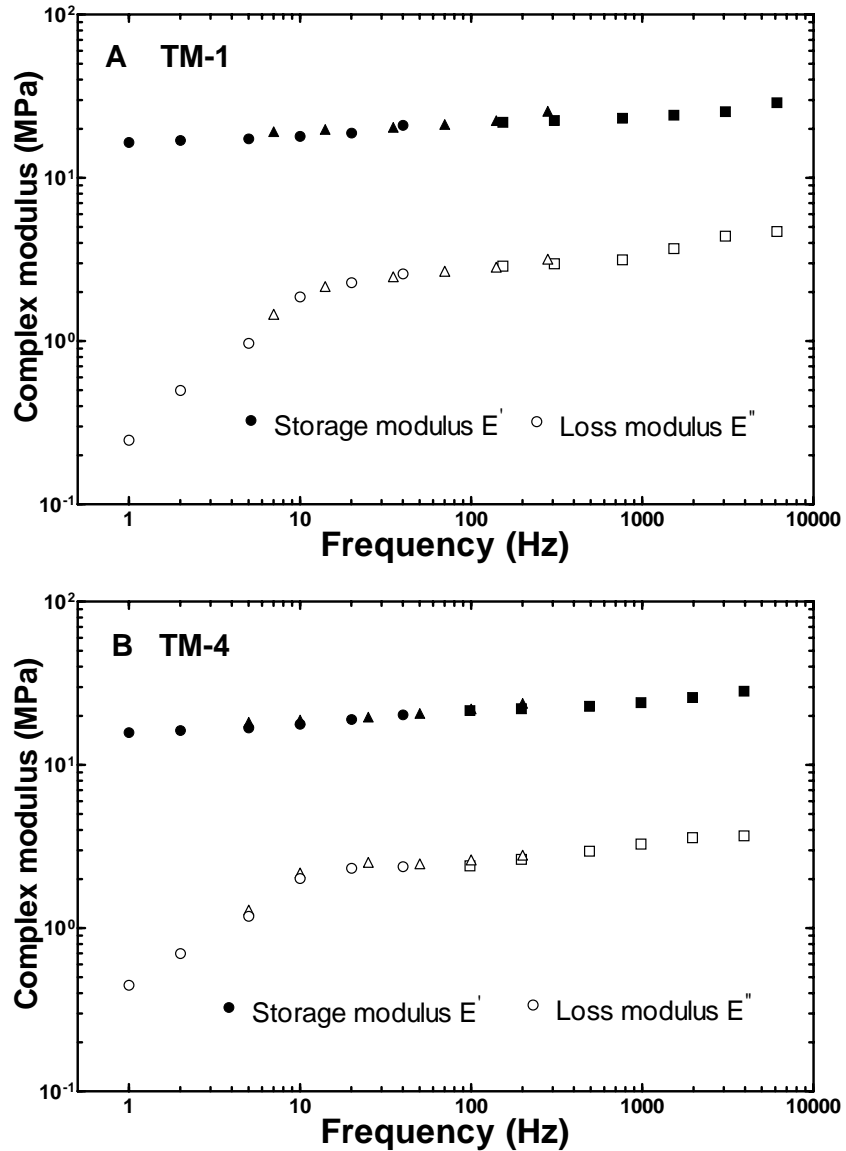


Figure 2.13 The master curves of the complex modulus at 37°C obtained from two TM sample: (A) sample TM-1 and (B) sample TM-4.

Following the procedure described in Section-IV of Methods, the complex modulus curves at the lower temperatures were shifted and the master curves created. Figure 2.13 shows the master curves of the complex modulus at the reference temperature 37°C for specimens TM-1 and TM-4. The complex modulus-frequency curves are generally well matched at the adjacent regions after the horizontal shifts.

Thus, the first requirement of the FTS principle is satisfied. The horizontal shift factors are the same for the storage modulus and loss modulus in each specimen, which meets the second requirement of the FTS principle. For specimen TM-1, the storage modulus is 16.5 MPa at 1 Hz and increases to 31.2 MPa at 6120 Hz, while the loss modulus is 0.25 MPa at 1 Hz and 4.7 MPa at 6120 Hz. For specimen TM-4, the storage modulus is 15.8 MPa at 1 Hz and increases to 28.3 MPa at 3920 Hz, while the loss modulus is 0.45 MPa at 1 Hz and 3.7 MPa at 3920 Hz. The shift factors and maximum frequency of the master curves for all 11 TM specimens are listed in Table 2.4. The mean value of the shift factors from 25° to 37°C is 5.9 ± 0.8 . The mean value of the shift factors from 5°C to 37°C is 134.2 ± 37.7 . The maximum frequency ranges were from 3800 to 7840 Hz with a mean value of 5371 ± 1506 Hz.

The temperature dependence of the shift factor was tested by fitting experimental data into the Arrhenius equation (Eq.(2.20)). The activation energy of the TM samples is calculated as the ratio between $R \cdot \ln \alpha_T$ and $(\frac{1}{T} - \frac{1}{T_0})$. As an example, Fig. 2.14 shows the natural logarithmic shift factor $\ln \alpha_T$ -temperature curves obtained from specimens TM-1 and TM-4. The relation between the shift factors and the temperature are well matched with the Arrhenius equation (the value of coefficient of determination r^2 was 0.997 for TM-1 and 0.999 for TM-4). The values of r^2 for all TM samples are not less than 0.997, thus the third requirement of the FTS principle was satisfied. The activation energy was obtained as 113.6 kJ/mol for TM-1 and 102.6 kJ/mol for TM-4. Table 2.4 lists the activation energy of all TM

samples, which ranges from 101.0 to 118.3 kJ/mol with a mean value of 109.3 ± 6.5 kJ/mol.

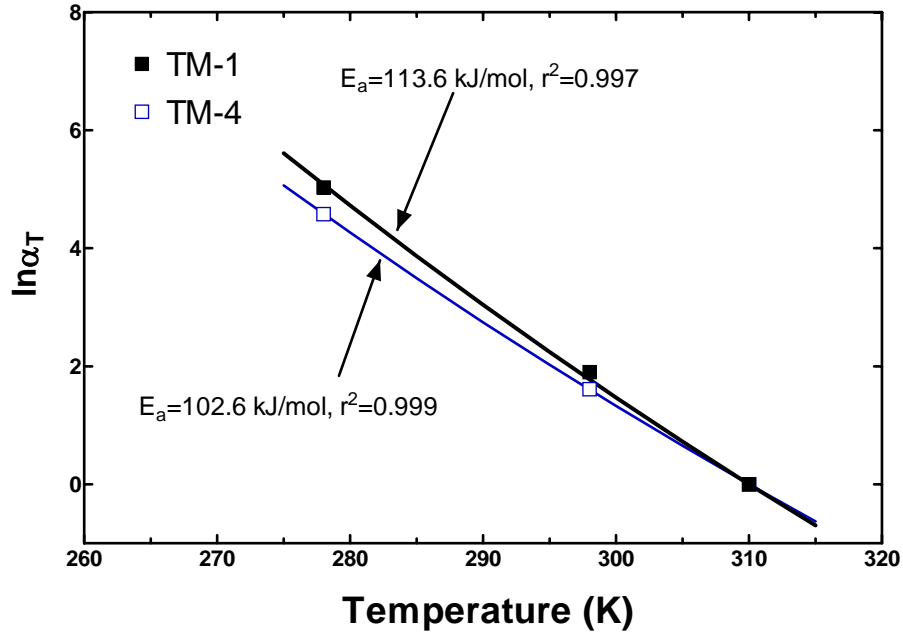


Figure 2.14 The fitting of Arrhenius equation (solid lines) to the experimental natural logarithmic shift factor $\ln \alpha_T$ -absolute temperature (in Kelvin degree) curves obtained from samples TM-1 and TM-4.

Figure 2.15 shows the master curves of the complex modulus for all 11 TM samples. The complex modulus generally increases with the frequency increasing except the loss modulus of some specimens decreases a little between 40 to 500 Hz. The storage modulus ranges from 10.3 to 20.9 MPa at 1 Hz. The loss modulus ranges from 0.18 to 0.45 MPa at 1 Hz. The maximum frequency of the master curves for the 11 TM samples was different and ranged from 3800 to 7840 Hz as listed in Table 2.4.

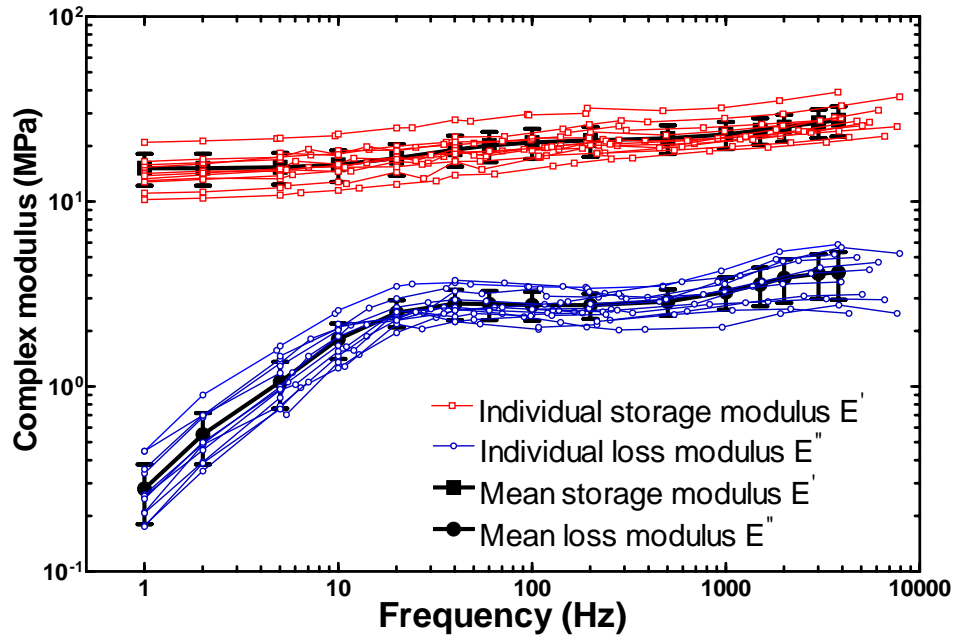


Figure 2.15 The master curves of the storage modulus and the loss modulus at 37°C from all 11 TM samples and the mean master curves of the storage modulus and the loss modulus.

The mean complex modulus was calculated over the common frequency range for the 11 samples (1-3800 Hz). The mean master curves of the storage modulus E' and the loss modulus E'' with S.D. in Fig. 2.15 were also plotted to 3800 Hz. Figure 2.15 also shows the mean master curves of the storage modulus E' and the loss modulus E'' with S.D., which were plotted up to 3800 Hz. The mean storage modulus was 15.1 ± 3.0 MPa at 1 Hz and 27.6 ± 5.1 MPa at 3800 Hz. The mean loss modulus was 0.28 ± 0.1 MPa at 1 Hz and 4.1 ± 1.2 MPa at 3800 Hz. The slope of the master curves of the loss modulus decreased to almost zero at 20-100 Hz and then increased at 300 Hz. The larger slope was observed at frequencies below 10 Hz and between 1000-3800 Hz as opposed to other frequency ranges. The change of the

slope at certain frequencies relates to the two parameters of relaxation time τ_1 and τ_2 .

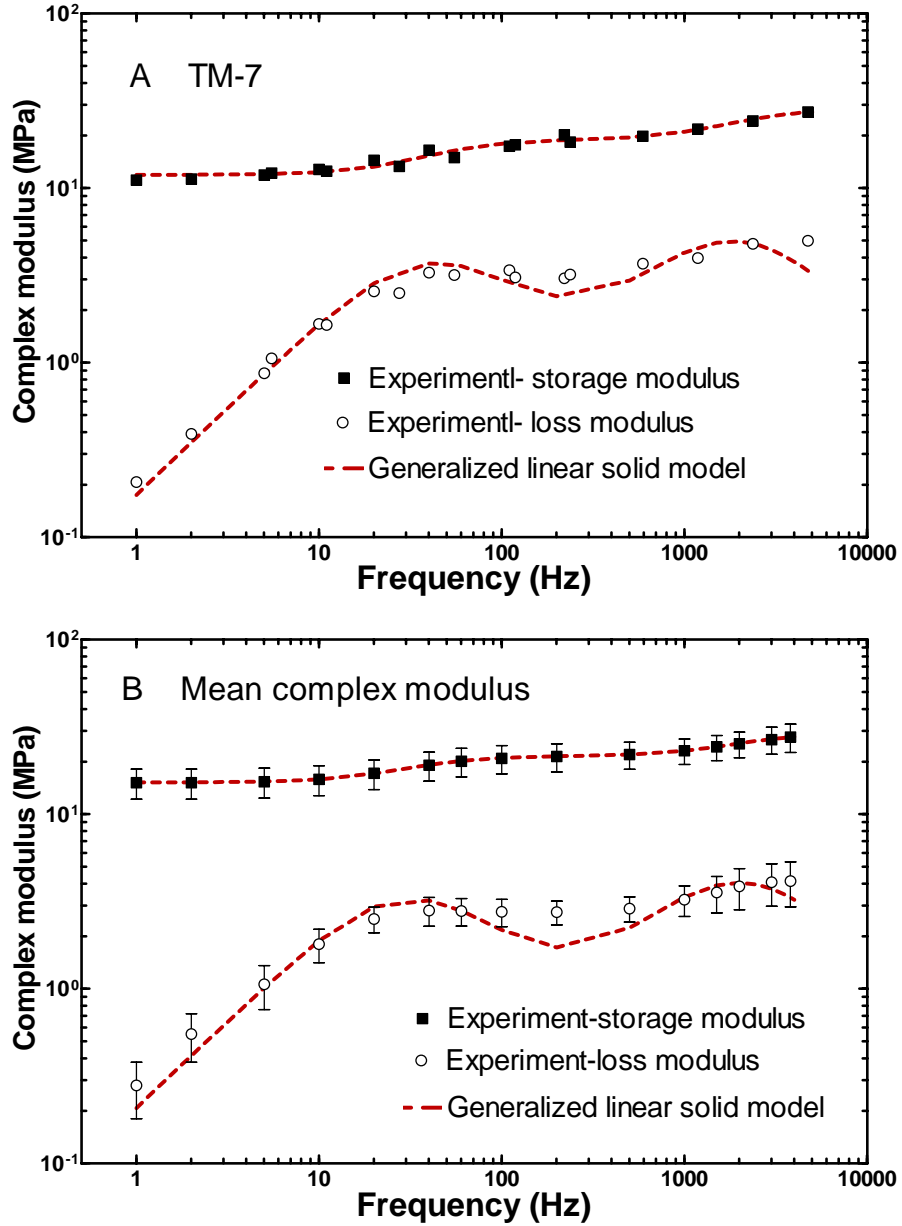


Figure 2.16 The theoretical fitting of generalized linear solid model to the experimental complex modulus for (A): sample TM-7 and (B) the mean experimental complex modulus.

The generalized linear solid model was used to describe the viscoelastic behavior of the TM samples. As the storage modulus has all five viscoelastic

parameters (E_0, E_1, E_2, τ_1 , and τ_2) while the loss modulus only has four of them, the experimental data of the storage modulus were first used to fit the theoretical storage modulus-frequency relation (Eq.(2.3)) to determine the five parameters. The theoretical loss modulus was then calculated from Eq. (2.4) by substituting the values of the parameters, and the results were compared with the experimental data. As an example, the five parameters for TM-7 were determined as $E_0=11.9$ MPa, $E_1=7.0$ MPa, $E_2=9.6$ MPa, $\tau_1=3.85$ ms and $\tau_2=84.3$ μ s. Figure 2.16A shows the storage modulus of specimen TM-7 derived from the generalized linear solid model in comparison with the experimental results. Table 2.5 lists the viscoelastic parameters determined from all 11 TM samples with the mean values and S.D. The mean experimental complex modulus curves shown in Figure 2.15 were also fitted by the generalized linear solid model with the five parameters determined as $E_0=15.2$ MPa, $E_1=6.3$ MPa, $E_2=7.9$ MPa, $\tau_1=5.14$ ms and $\tau_2=78.6$ μ s. The results are shown in Fig. 2.16B where the theoretical complex modulus curves were compared with the mean experimental data.

Table 2.5 The viscoelastic parameters of TM samples obtained in DMA. (E_0, E_1 , and E_2 unit in MPa).

	TM -1	TM -2	TM -3	TM -4	TM -5	TM -6	TM -7	TM -8	TM -9	TM -10	TM -11	Mean \pm S.D.
E_0	17.7	15.0	13.6	16.7	14.0	17.0	11.9	13.3	21.6	14.8	10.8	15.1 \pm 3.0
E_1	6.3	5.2	4.1	5.1	5.4	9.6	7.0	6.4	8.6	6.1	5.8	6.3 \pm 1.6
E_2	9.1	5.7	4.4	7.3	11.5	12.0	9.6	9.1	11.8	4.7	5.6	8.3 \pm 2.9
τ_1 (ms)	3.66	6.37	7.36	7.53	9.47	3.98	3.85	6.36	5.95	4.59	3.83	5.72 \pm 1.91
τ_2 (μ s)	41.7	104.5	152.4	99.8	83.7	47.4	84.3	54.7	74.5	67.3	126.6	85.1 \pm 33.9

2.2.3 Discussion

I. Comparison with published data

To date, the published mechanical properties of the human TM were obtained mostly from the static or quasi-static test. In this study, the complex moduli of the human TM samples were obtained over the frequency range of 1 to 3800 Hz. The storage modulus obtained at the low frequencies, such as 1 Hz, can be considered comparable to the elastic modulus obtained from the quasi-static test. The mean storage modulus of the 11 TM samples at 1 Hz was 15.1 ± 3.0 MPa from this study. This value is close to or in the range of that reported in the literature: 20 MPa reported by von Békésy (1960), 23 MPa by Decraemer et al. (1980), 0.4 - 22 MPa by Cheng et al. (2007), and 17.4 MPa for the posterior portion and 19.0 MPa for the anterior portion reported by Huang et al. (2008). Aernouts et al. (2012) recently reported the Young's modulus of the human TM from three samples as 2.1, 2.3 and 4.4 MPa, respectively. The storage modulus at 1 Hz obtained in this study is about 5 times larger than the value reported by Aernouts et al. Fay et al. (2005) reported the Young's modulus of 30-90 MPa for an isotropic model and 100-400 MPa for an orthotropic model of the human TM, which are much larger than the values reported in this study.

Kirikae (1960) measured the Young's modulus of the human TM sample at a single frequency of 890 Hz and reported the value of 40 MPa. In this study, the mean storage modulus at 890 Hz was 22.6 ± 3.9 MPa, which is about half of the value reported by Kirikae. To our best knowledge, there are two other dynamic tests of the

human TM over the auditory frequency range reported in the literature by Luo et al. (2009) and Zhang and Gan (2010). Figure 2.17 shows the comparisons of the storage modulus and loss modulus obtained in this study (solid lines with square symbols) with Luo et al.'s data (solid lines with triangles) and Zhang and Gan's data (solid line with circles). The results are presented as the mean values with S.D. The TM specimens were normal tissues and assumed as a homogeneous material in all three studies. The common frequency range over 200 Hz in this study was chosen to compare the results from the published studies.

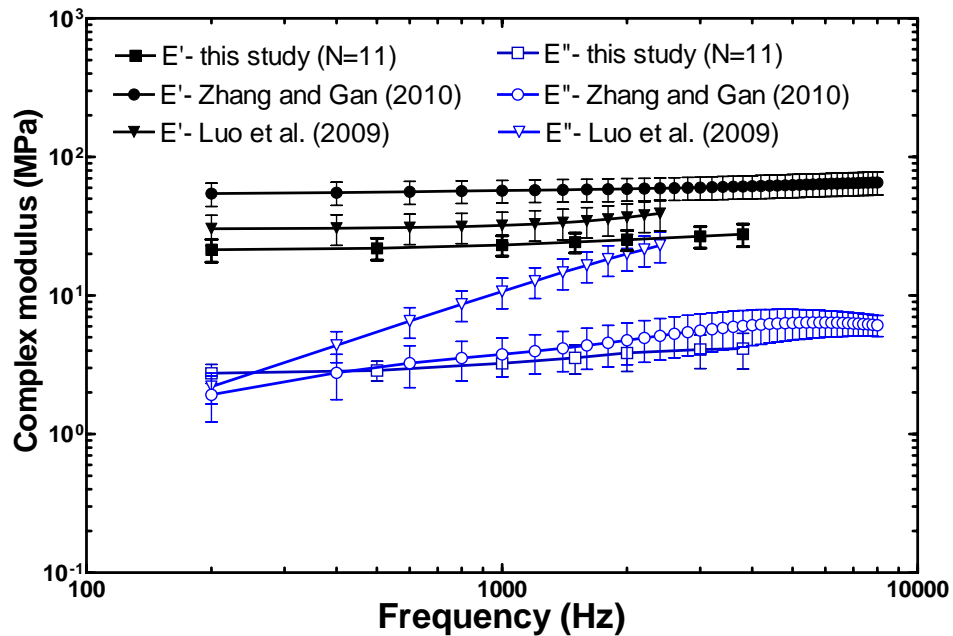


Figure 2.17 Comparison of the storage modulus and the loss modulus obtained from this study to the published data by Luo et al. (2009b) and Zhang and Gan (2010).

As shown in Fig. 2.17, the mean storage modulus of the 11 TM samples obtained from this study is lower than that from the other two studies, particularly as

being lower than Zhang and Gan's results. The loss modulus shows the different results, and the curve obtained from this study is very close to that of Zhang and Gan's data over the entire frequency range but lower than that from Luo et al.'s study above 400 Hz. The slopes of the storage modulus-frequency curves from the three studies are close to each other over 200-3800 Hz range. However, the slope of the loss modulus-frequency curve in this study is smaller than that in the two published studies. The rationale for the difference in the slope of loss modulus is still not very clear. One possible cause for the difference between this study and the published studies is the different test temperatures. As shown in Fig. 2.12, the loss modulus has a larger slope at a lower temperature.

The difference of this study from the published studies is probably caused by: 1) the individual variation of the human TM specimens. The human TM samples in the different studies were obtained from donors with different ages, genders and health conditions. The TM samples from the different portions or fiber directions of the TM might have created different mechanical properties. In this study, the TM sample strip was cut along the superior-inferior direction. 2) The physiological condition or moisture level of the TM sample. In this study, we tried to keep the moisture levels to be consistent for all TM samples as we did in the studies using the acoustic driving and laser measurement and that used by Luo et al. in the split Hopkinson tension bar test 18. However, it is not easy to control the moisture level to be similar in different experimental setups. 3) The testing temperature. The temperature had obvious effect on the mechanical properties of the TM as shown in

this study. The complex modulus was obtained at the reference temperature of 37°C in this study, while the experiments were conducted at room temperature in other studies. The storage modulus at 37°C is about 15% lower than that at 25°C. 4) Other differences in experimental methods between this study and the published studies.

The human TM is a multi-layer membrane consisting of the epidermal, collagen fibrous and mucosal layers from the lateral to medial side. The collagen fibers are organized into the matrix of ground substance primarily along the radial and circumferential directions (Lim, 1995). The radial fibers are thicker and stronger than the circumferential fibers. The arrangement of collagen fibers in two layers with different directions makes the TM inhomogeneous and orthotropic. In this study, as the first step in measuring the dynamic properties of the human TM was to use the DMA, the TM was assumed as a homogeneous, isotropic and linear viscoelastic material. This simplification makes the results reported here different from the actual mechanical properties of either the radial or the circumferential fibers in the TM.

In this study, the TM sample was cut along the superior-inferior axis, which included both the radial and circumferential fibers. The longitudinal axis of the TM sample strip was along neither the radial nor the circumferential direction of the TM, but more closely to the circumferential direction. The circular fibers provide less stiffness than the radial fibers as reported by Fay et al. (2005). Moreover, the pre-stress existing in the intact TM was released when the sample was cut and the stiffness of the TM sample was reduced. Thus, the storage modulus of the TM

reported in this study was lower than that of the intact TM as estimated by Fay et al.

II. Feasibility of FTS on ear soft tissues

The results obtained in this study show that the complex modulus-frequency curves of the human TM samples satisfy all three requirements commented by Ward (1971). Thus, the FTS principle is feasible to measure the dynamic properties of the TM at higher auditory frequencies. This method also has the potential to test other middle ear soft tissues, such as the SAL and the RWM. These soft tissues are mainly composed by collagen fibers and can be considered as homogenous materials as well.

Compared to published dynamic testing methods, the advantages of the method developed in this study includes: 1) measurement in the frequency domain with no need of conversion from the time domain or the help of FE analysis; 2) no limitation on the tissue sample shape and geometry, unlike the acoustic driving method (Zhang and Gan, 2010) which is only applicable to a thin membrane; 3) the ability to reach higher frequency levels (higher than 3800 Hz) compared to the method using the Hopkinson tension bar.

III. Application of the complex modulus and future studies

The complex modulus of the human TM obtained in this study can be applied into the FE model of the human ear and help improve the accuracy of the model. In

almost all published FE models of the human middle ear, a Rayleigh type damping was applied for the soft tissues including the TM (Zhao et al., 2009). As an example, a value of 0.000075 was used for the β coefficient of Rayleigh damping in Gan et al.'s FE models (Gan et al., 2004; 2007). A constant elastic modulus and Rayleigh type damping in the FE models make the loss modulus or damping of the TM proportional to the frequency, which makes the damping too high at the higher frequencies (Fig. 2.18A). Recently, Zhang and Gan (2011a) reported a FE model of the human ear with viscoelastic properties for the middle ear soft tissues. The damping or loss modulus was not proportional to the frequency but calculated by equations such as Eqs. (2.4) and (2.5) in this study. The damping reaches its maximum value around 4-6 kHz and then decreases (Fig. 2.18B). The application of the viscoelastic properties for the middle ear soft tissues has improved the results at the higher frequencies as shown in Zhang and Gan's model when compared with the previous model (Gan et al., 2007).

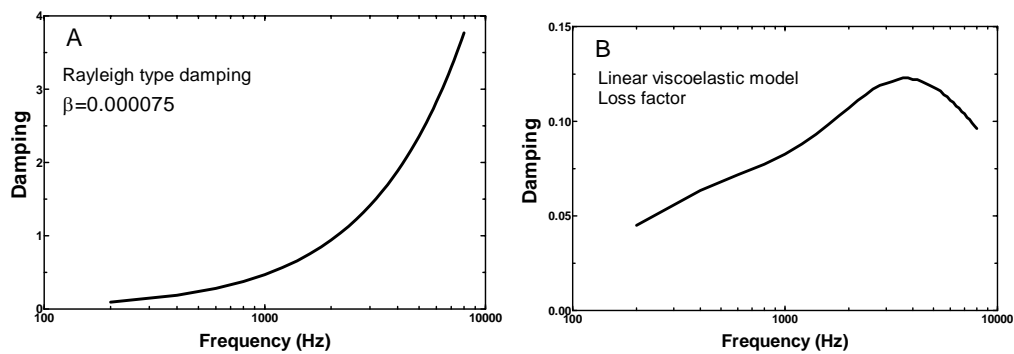


Figure 2.18 (A): Damping of the TM calculated using Rayleigh type coefficient with $\beta=0.000075$; (B) damping of the TM calculated from the linear viscoelastic model determined from the dynamic test in this study.

Future studies will be conducted to measure the dynamic properties of TM samples in diseased conditions, such as otitis media, which is the most common middle ear disease in children, and to measure the dynamic properties of other ear tissues. The relationship between the macro mechanical properties of the human TM sample and the micro fibrous structure will also be studied through experiments or the FE modeling analysis.

2.3 Conclusion

In this study, two new approaches were developed to measure the dynamic properties of human TM specimens in auditory frequency range. In the first approach using acoustic driving, the vibrations of the TM specimen in response to acoustic stimuli applied to the center of the TM specimen were measured by LDV over the frequency range of 200-8000 Hz. The dynamic experiments on TM specimens were simulated in FE models for acoustic-structure coupled analysis in ANSYS. Both the experimental and FE modeling methods were first validated using a standard silicone-film material. A good agreement between the experimental measurements and FE modeling was observed in all TM specimens. The dynamic properties of the TM were derived by inverse-problem solving method and presented as complex modulus in frequency-domain and the relaxation modulus in time-domain. In the second approach using DMA based on the FTS principle, the dynamic tests were conducted at frequencies from 1 Hz to 40 Hz at three different temperatures: 5°, 25° and 37°C. The FTS principle was applied to expand the

frequency range to a much higher level (at least 3,800 Hz). The feasibility of the FTS principle was assessed and verified. The viscoelastic parameters were determined by fitting the model to the experimental results. The results obtained from this study were compared with the data reported by Luo et al (2009b), using a SHTB. A general consistency between these three techniques was demonstrated with some differences, particularly, in loss modulus variation at higher frequencies. The dynamic properties of the human TM obtained in this study provide a better description of the damping behavior of ear tissues, which can be applied into the FE model of the human ear to replace the Rayleigh type damping. The data reported here contribute to the biomechanics of the middle ear and improve the accuracy of the FE model for the human ear.

CHAPTER 3.
DYNAMIC PROPERTIES OF HUMAN ROUND WINDOW
MEMBRANE

The contents of this chapter have been published in Medical Engineering & Physics by Zhang and Gan (2013b). In this chapter, the dynamic properties of human RWM were measured using the experimental set up with acoustic driving and LDV. The complex modulus of RWM was finally determined by the inverse-problem solving method the assistance of FE modeling analysis.

3.1 Methods

3.1.1 RWM specimen preparation

Eight RWM samples from fresh human cadaver TB (three left and five right) obtained through the Willied Body Program at the University of Oklahoma Health Sciences Center were used for this study. All donors had no history of ear diseases associated with the RWM and the average age of the donors was 70 (ranging from 59 to 82, 5 males and 3 females). To maintain soft tissue compliance and hydration within five days before the experiment, the bones were immersed in a 0.9% saline solution mixed with providine (i.e., 15% amount of providine in saline solution) at 5 °C until use. The TB was cut into a block ($2 \times 2 \times 2 \text{ cm}^3$) containing the middle ear cavity and cochlea. The middle ear cavity was then opened and the TM with malleus attached was carefully removed under microscope (Olympus SZX12). Incus and stapes remained intact in the specimen block, and the round window niche was

identified as well as the RWM (Fig. 3.1A). The cochlea was then removed and RWM was exposed from both the middle ear and cochlear sides. The specimen was examined under microscope to verify that the RWM was not damaged during the preparation. Subsequently, we place microbeads (30 μm in diameter, Mo-Sci Corp, Rolla, MO) onto the center of the cochlear side of RWM as the laser reflecting target. The mass of each bead is about 3.96×10^{-5} mg. Such a small mass should not affect the measurement. Figure 3.1B shows a RWM specimen image obtained by a CCD camera in this study. The RWM was in an elliptical shape with the short axis (a) and long axis (b). Table 3.1 lists the dimensions of (a) and (b) measured from each specimen using the image analysis tools (Adobe Photoshop 7.0) with the average long axis of 2.08 mm and short axis of 1.81 mm.

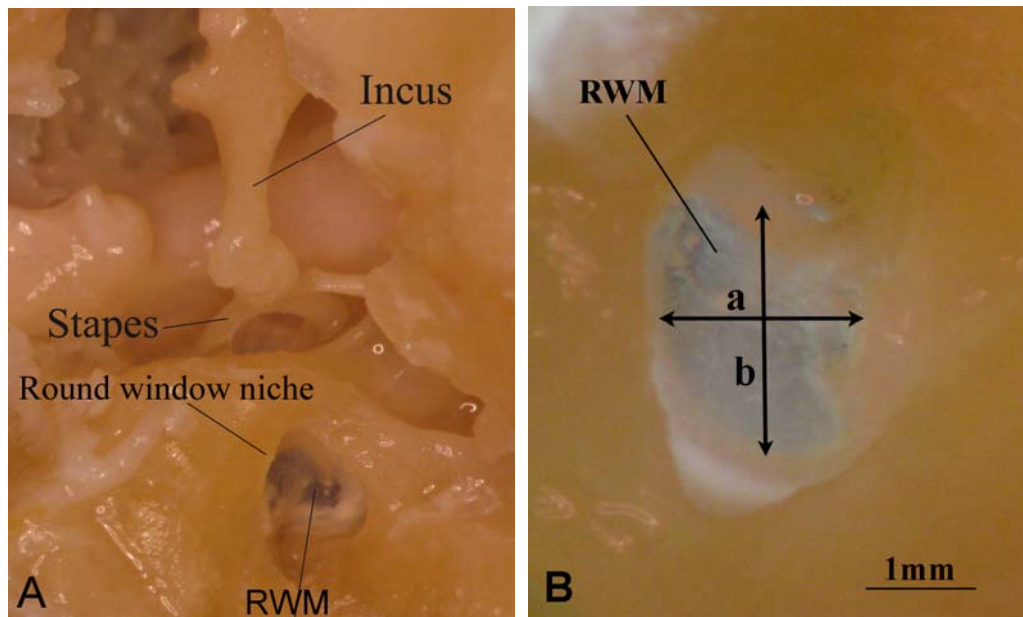


Figure 3.1 (A): The RWM specimen with the incus and stapes harvested from a human TB. (B): Enlarged RWM specimen image with 1mm reference bar. (a) is the short axis of RWM, and (b) is the long axis of RWM.

Table 3.1 The dimensions, resonance frequency f_n and vibration amplification ratio R of RWM specimens.

RWM Specimen	RWM -1	RWM -2	RWM -3	RWM -4	RWM -5	RWM -6	RWM -7	RWM -8	Mean \pm S.D
a (mm)	1.92	1.78	1.88	1.68	1.74	1.82	1.86	1.76	1.81 \pm 0.08
b (mm)	2.18	2.06	2.08	1.88	2.00	2.06	2.12	1.98	2.05 \pm 0.09
f_n (Hz)	1500	1665	1888	2132	1892	1886	1687	1896	1818 \pm 193
R	4.08	2.98	3.51	5.66	3.81	2.88	3.18	3.37	3.68 \pm 0.89

3.1.2 Experimental setup

The experimental setup was similar to that used to measure the dynamic properties of human TM by acoustic driving, which was described in Chapter 2, Section 2.1.1. Figure 3.2 is the schematic diagram of the experimental setup. Briefly, the RWM specimen with the bony wall was fixed in a micro-manipulator and placed on a vibration isolation table. 80 dB SPL pure tones across the frequency range of 200-8000 Hz were delivered to the middle ear side of the RWM by a sound delivery tube (inner diameter 1 mm) connected to the speaker. The sound signals were generated by the dynamic signal analyzer (DSA, HP 35670A, CA) and amplified by the power amplifier (B & K 2718, Norcross, GA). The distance between the tube end and the surface of RWM was set at 1 mm. A probe microphone (ER-7C, Etymotic Research, IL) attached to the sound delivery tube was used for monitoring the input sound pressure level. Because the round window niche formed a semi-closed chamber for sound approaching to the RWM and the distance between the sound delivery tube end and the RWM was small, the sound pressure was reasonably considered as evenly distributed onto the RWM surface.

The laser beam was focused on the microbeads, and the vibration at the center of RWM was acquired by DSA and recorded on a computer for further analysis. The vibration amplitude of the RWM was directly calculated from the voltage output of the laser vibrometer velocity decoder.

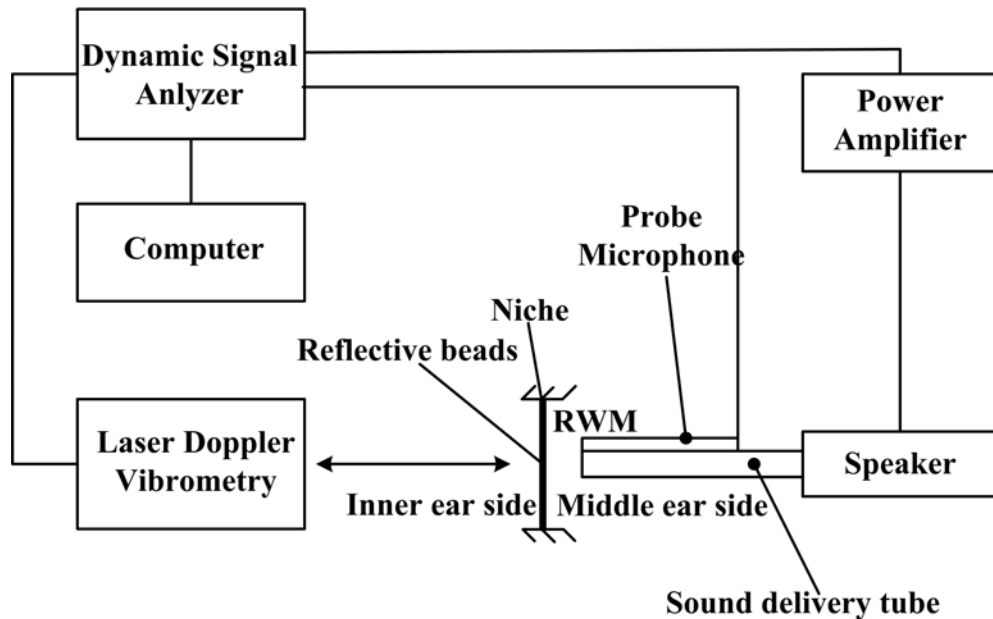


Figure 3.2 The schematic of the experiment setup for the dynamic test on the RWM specimen.

Because of the extremely small size and fixed bony boundary of the RWM specimen, it was impossible to carry out a standard preconditioning procedure in a mechanical testing system. Harmonic 80 dB SPL sound stimuli were actually applied to the sample during each measurement and could serve as preconditioning. To doubly ensure the preconditioning and stabilization of the mechanical properties of RWM samples, cyclic hydraulic pressure was loaded and unloaded onto the specimen surface by using saline solution in a 1 cc syringe. The peak pressure was

estimated around 10 Pa. The movement of RWM was observed under a surgical microscope. This process was repeated for 5 cycles to reach the stabilized state for the specimen. After preconditioning, an 80 dB SPL acoustic load across 200-8000 Hz was applied on the specimen, and the vibration was recorded. Note that the RWM specimen was maintained in moist conditions by spraying saline solution onto the middle ear side surface.

3.1.3 FE modeling Analysis

Dynamic tests of the RWM specimens were simulated as FE models in ANSYS (ANSYS Inc, Canonsburg, PA). Using the same FE model-based inverse-problem solving method, which is described in Chapter 2, Section 2.1.1, the dynamic properties of RWM was determined. The FE model analysis was also used to estimate the effects of specimen geometry and experimental conditions on the results of the RWM dynamic property measurement.

RWM in a normal ear is a thin, semitransparent and nearly circular membrane with a diameter of about 1.8 mm. The average thickness of a normal adult RWM was reported as 70 μm by Goycoolea et al. (1997) and Sahni et al. (1987). The smallest thickness of 56 μm at the RWM center was reported by Nomura (1984). In this study, each RWM specimen was modeled as an elliptical membrane with uniform thickness of 70 μm . The short axis a and long axis b were based on our real measurements listed in Table 3.1. Eight FE models of RWM samples were built, and Fig. 3.3A shows the plane view of one RWM model while Fig. 3.3B shows the

transverse view with sound pressure applied on the middle ear side of the RWM. The reflective microbeads attached on RWM for laser measurement were not simulated in FE model. The beads should not affect the RWM vibration due to the small size and mass (3.96×10^{-5} mg per bead, estimated as 0.0163% of the average mass of RWM specimen).

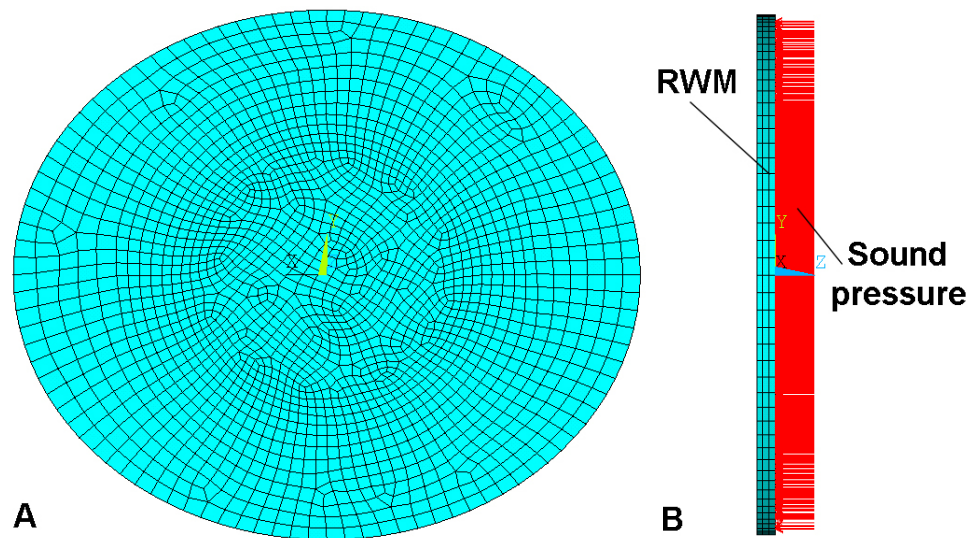


Figure 3.3 The FE model of the dynamic experiment on the RWM specimen (RWM-1). (A) The plane view of the RWM model from the middle ear side. The edge was fully clamped. (B) The side view of the RWM model with sound pressure applied onto the RWM from cochlear side.

The model was meshed by 5892 hexahedral elements (element type Solid 185), and convergence analysis showed this element number was adequate to reach accurate results. Density of the RWM was assumed as 1200 kg/m^3 , the same as that of TM. 80 dB SPL across the frequency range of 200-8000 Hz was applied onto the medial side of the RWM, similar to the experiment. The edge of the RWM was set as fully clamped without free displacement based on the observation on histology

sections in the literature (Toth et al., 2006; Li et al., 2007).

The RWM sample was considered as an isotropic and homogeneous material in this study. The generalized linear solid model was used in this study. The relaxation modulus and the complex modulus of the TM are represented by Eqs. (2.1 - 2.5) in Section 2.1.1. In this study, we selected one spring-dashpot elements ($n = 1$, giving 3 parameters E_0 , E_1 , and τ_1) to represent the viscoelastic behavior of the RWM. These parameters will be determined by the inverse-problem solving method. The detailed process was described in Chapter 2, Section 2.1.1.

3.2 Results

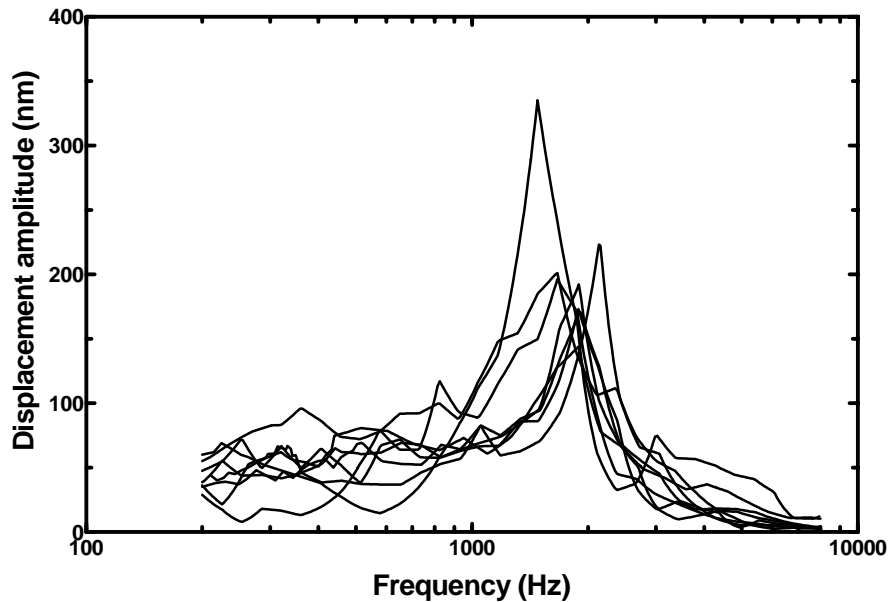


Figure 3.4 The vibration amplitude-frequency curves measured from the dynamic experiments on eight RWM specimens.

Figure 3.4 shows the displacement amplitude-frequency curves of eight RWM specimens recorded from experimental measurements. Each specimen has a

prominent displacement peak between 1500 and 2100 Hz. The displacement at low frequency (below 500 Hz) has a range between 34 and 68 nm. The resonance frequency $f_n = \omega_n / 2\pi$ and amplification ratio R of each RWM specimen are listed in Table 1. The mean resonance frequency was 1818 ± 193 Hz. The amplification ratio R was ranged between 2.88 and 5.66 with a mean value of 3.68 ± 0.89 .

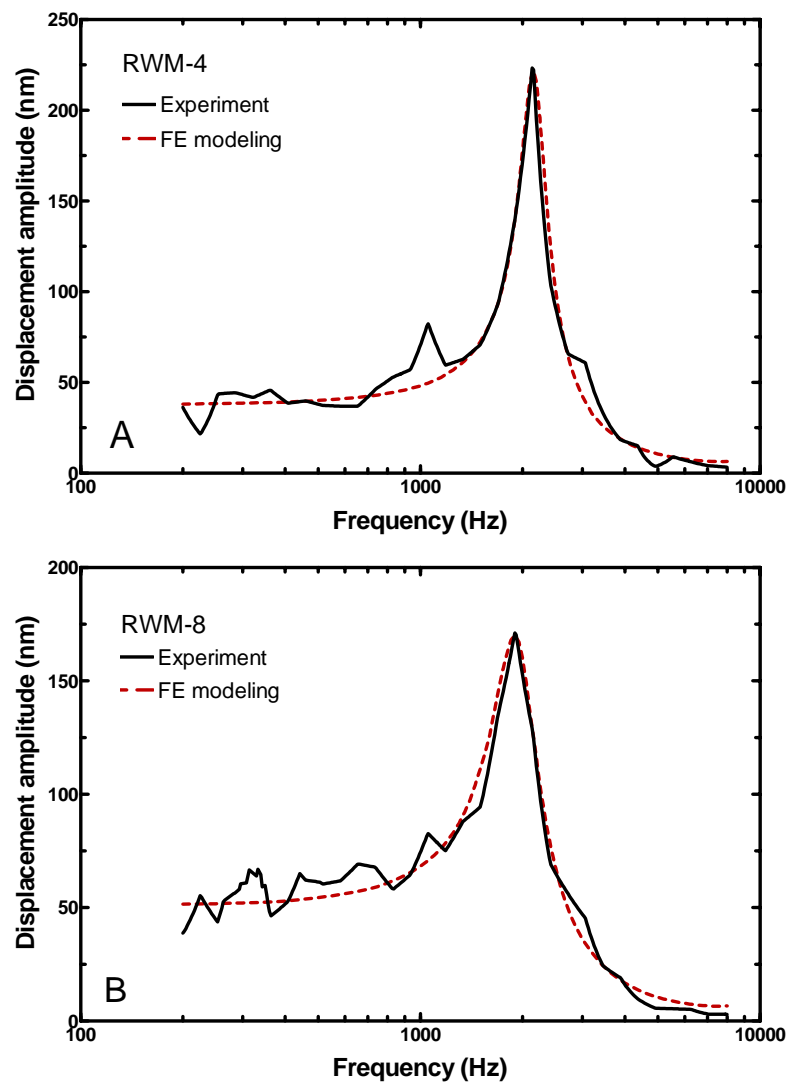


Figure 3.5 The FE modeling results (dash line) obtained from two RWM models in comparison with the corresponding experimental curves (solid line). (A) Specimen RWM-4; (B) Specimen RWM-8.

FE models were created to simulate the dynamic experiments of RWM specimens. As an example, Fig. 3.5 shows the results from two specimens: the vibration amplitude-frequency curves derived from the FE modeling (dash lines) and the experimental measurements (solid lines). Figure 3.5A was obtained from specimen RWM-4 with a resonance frequency of 2132 Hz from experiment and 2150 Hz from FE model. Figure 3.5B was obtained from specimen RWM-8 with a resonance frequency of 1896 Hz from experiment and 1900 Hz from FE model. In general, the FE modeling results agreed well with the experimental data over the entire frequency range, particularly near the resonance frequency. Some very small peaks at a lower frequency (for example, at 1 kHz of RWM-4) were not considered as the primary resonance peak. The curves from the FE model were obtained under ideal conditions and had no such artificial peaks. The potential resources of these peaks may come from the sound distortion or the experimental setup.

Table 3.2 The viscoelastic parameters of RWM specimens by the inverse-problem solving method. (E_0 and E_1 unit in MPa, τ_1 unit in μs).

	RWM-1	RWM-2	RWM-3	RWM-4	RWM-5	RWM-6	RWM-7	RWM-8
E_0	1.92	1.78	1.88	1.68	1.74	1.82	1.86	1.76
E_1	2.18	2.06	2.08	1.88	2.00	2.06	2.12	1.98
τ_1	4.08	2.98	3.51	5.66	3.81	2.88	3.18	3.37

Three parameters E_0 , E_1 , and τ_1 for each RWM specimen obtained through the inverse-problem solving with the FE model are listed in Table 3.2. The value of E_0 ranged from 1.86 to 2.80 MPa, E_1 ranged from 1.38 to 2.70 MPa, while τ_1 ranged from 27 to 36 μs . There are some differences between the specimens for each

parameter, which may be caused by individual variations between RWM specimens (physiological conditions, geometric dimensions) and the variations between experimental setups.

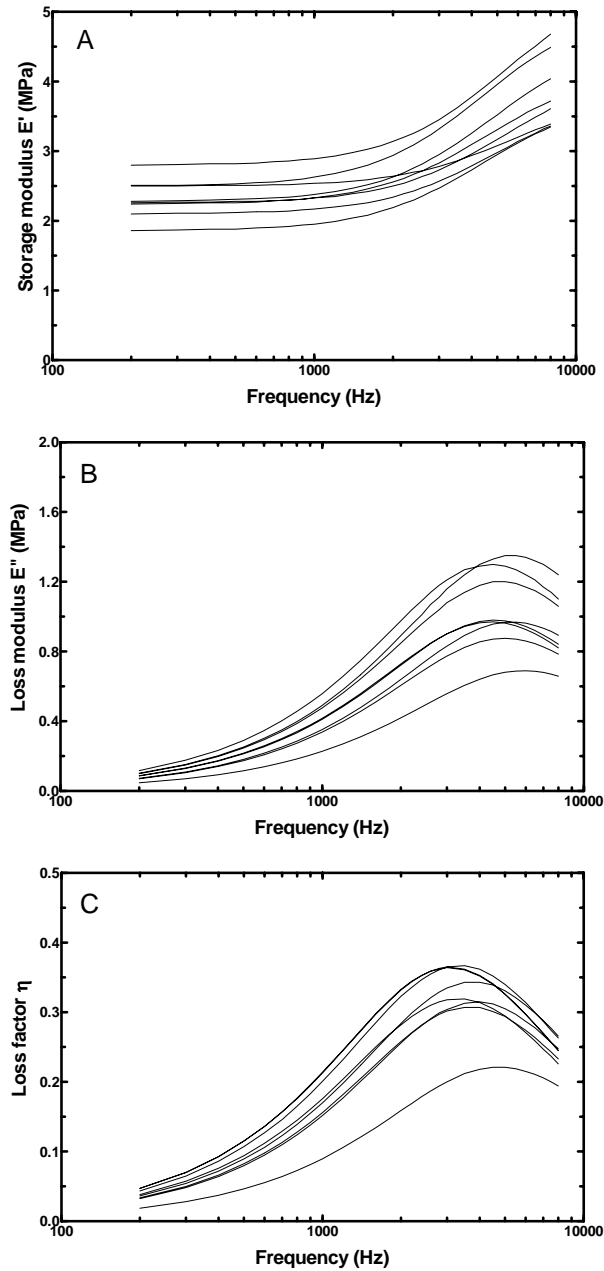


Figure 3.6 The complex modulus determined from the FE modeling analysis for eight RWM specimens over the frequency range of 200-8000 Hz. (A) Storage modulus; (B) Loss modulus; (C) Loss factor.

Based on the parameters listed in table 3.2, the storage modulus E' , loss modulus E'' , and loss factor η of all eight specimens were calculated and displayed in Fig. 3.6 across the frequency range of 200 to 8000 Hz. Figure 3.6A shows that the storage modulus increased with frequency for all specimens. The largest storage modulus values were 2.80 MPa at 200 Hz, and 4.68 MPa at 8000 Hz (RWM-3), and the smallest storage modulus values were 1.86 MPa at 200 Hz, and 3.35 MPa at 8000 Hz (RWM-2). As shown in Fig. 3.6B, the loss modulus increased with the increase of frequency and reached its maximum values around 4500-6000 Hz before decreasing. The largest loss modulus was 0.117 MPa at 200 Hz (RWM-6), and 1.24 MPa at 8000 Hz (RWM-3). The smallest loss modulus was 0.047 MPa at 200 Hz and 0.659 MPa at 8000 Hz (RWM-4). Figure 3.6C shows the loss factor obtained from the eight specimens. The change of the loss factor with frequency was similar to that of the loss modulus: increasing rapidly at frequencies below 4000 Hz, and then reaching the maximum values at around 4500-6000 Hz.

Mean values of the complex modulus and the loss factor with S.D. obtained from the eight specimens are shown in Fig. 3.7. Figure 3.7A shows the mean storage modulus was 2.32 ± 0.29 MPa at 200 Hz and 3.83 ± 0.52 MPa at 8000 Hz. The storage modulus increased slowly below 1000 Hz and increased rapidly over 1000 Hz. Figure 3.7B shows that the mean loss modulus was 0.085 ± 0.022 MPa at 200 Hz and 0.925 ± 0.192 MPa at 8000 Hz. The maximum loss modulus was 1.038 ± 0.225 MPa at 5000 Hz. The loss modulus is much smaller than the storage modulus. As shown in Fig. 3.7C, the mean loss factor was 0.037 ± 0.009 at 200 Hz and

0.240±0.023 at 8000 Hz. The maximum loss factor was 0.323±0.051 at 3500 Hz.

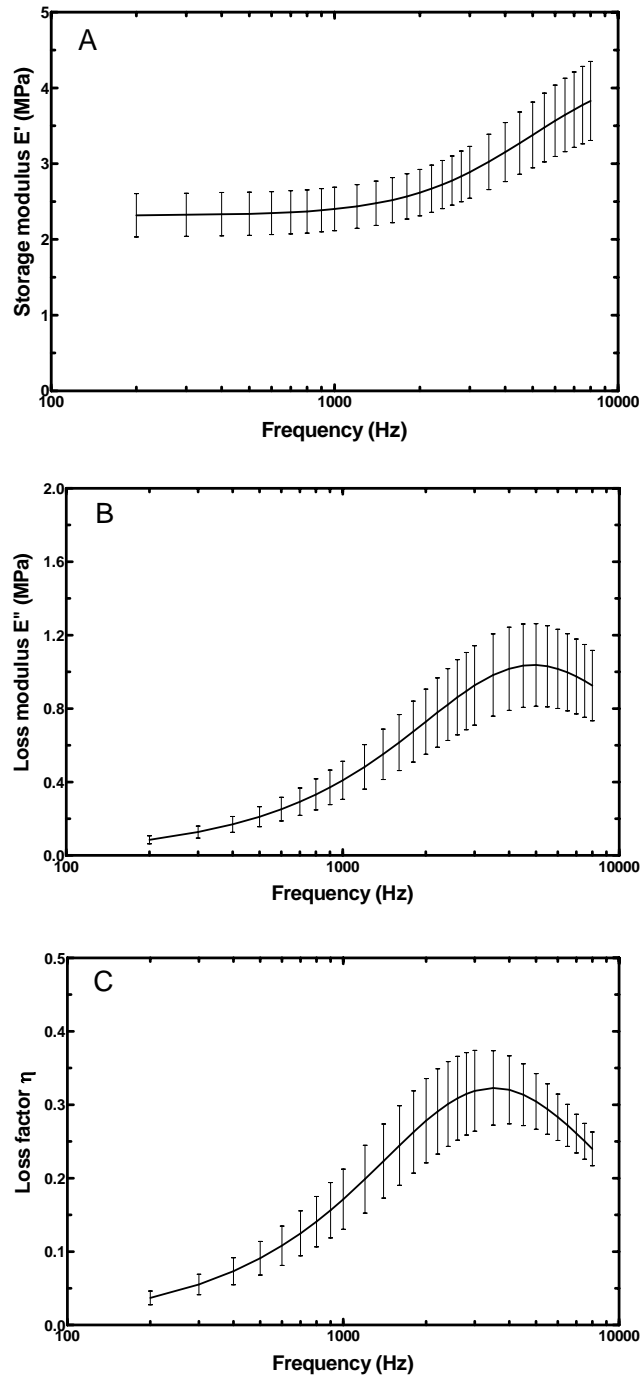


Figure 3.7 The mean complex modulus of the eight RWM specimens with standard deviations (S.D.). (A) Storage modulus; (B) Loss modulus; (C) Loss factor.

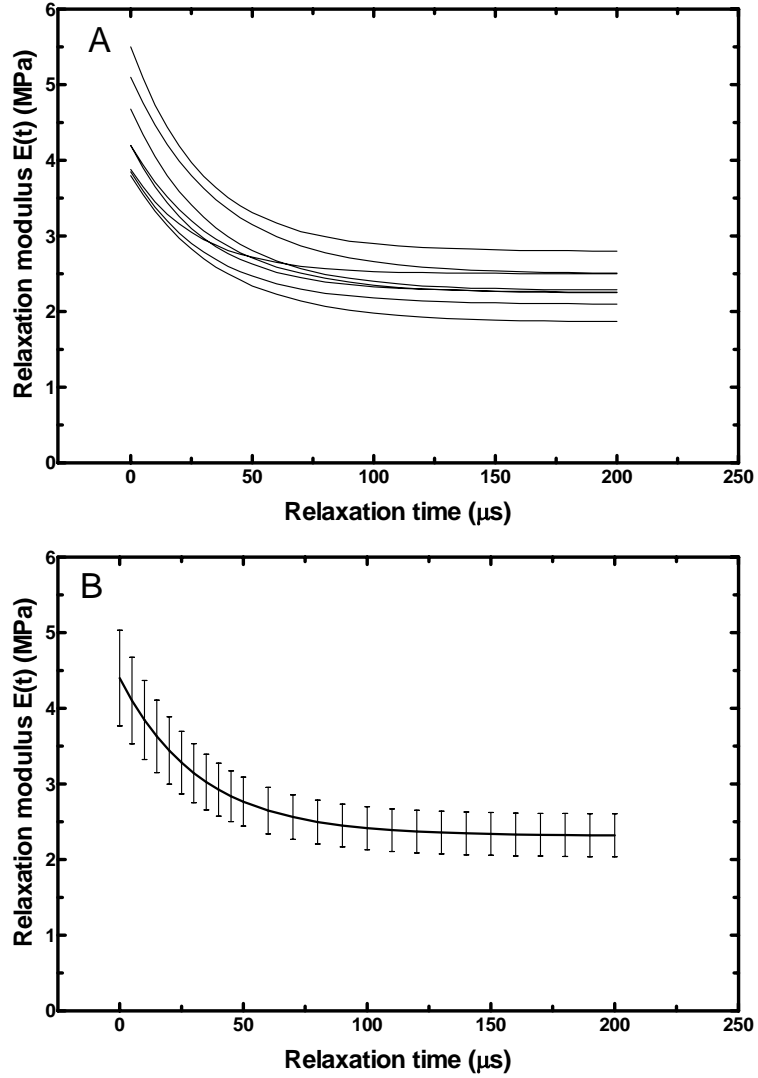


Figure 3.8 The relaxation modulus in the time domain obtained from the complex modulus in frequency domain. (A) Individual relaxation modulus-relaxation time curves for the eight RWM specimens. (B) Mean relaxation modulus-relaxation time curve with S.D. for the eight RWM specimens.

In addition to complex modulus in frequency domain, we used the parameters listed in Table 3.2 to calculate the relaxation modulus in time domain for RWM specimens using Eq. (2.1). Figure 3.8A shows the relaxation modulus of eight specimens. The initial modulus (at time $t=0$) ranged from 3.80 to 5.50 MPa, and the static modulus (at time $t=\infty$) ranged from 1.86 to 2.80 MPa. As shown in this figure,

RWM specimens reached the relaxation state at 200 μ s. Figure 3.8B shows the mean relaxation modulus changing with time. The mean initial modulus was 4.40 ± 0.63 MPa, and the mean static modulus was 2.32 ± 0.29 MPa.

3.3 Discussion

3.3.1 Effect of specimen shape and thickness variation on results

In this study, the RWM was simulated as a flat membrane structure in the FE model as the first step. However, the real human RWM has a slight convexity towards the cochlea (Carpenter et al., 1989; Goycoolea and Lundman, 1997). To estimate the effect of that assumption on results, a FE model with a curved surface was created based on specimen RWM-6. The dimensions of sample RWM-6 were close to the mean values of all specimens. A curvature was chosen as 0.1 mm^{-1} based on the published image observations (To' th et al., 2006; Li et al., 2007). The viscoelastic parameters E_0 , E_1 and τ_1 derived from the model with a curved surface were 2.31 MPa, 2.40 MPa, and 36 μ s, respectively. These values are slightly smaller than that derived from the model with a flat surface (See Table 3.2). The assumption of a flat RWM did not affect the results significantly.

FE model of the RWM was created using the actual long axis and short axis measured from each specimen (Table 3.1). However, the thickness of 70 μ m was used for all RWM specimens based on published data (Goycoolea and Lundman, 1997). The real thickness of RWM specimen varies with the samples, which may affect the complex modulus derived from the FE model. To assess the effect of

thickness variation on complex modulus of RWM, the FE models with different thicknesses were created based on specimen RWM-6. The thickness was changed from 70 μm (named as control) to 60 and 80 μm , and the other parameters were maintained as the same as the control (specimen RWM-6). The parameters E_0 , E_1 and τ_1 derived from the models with different thicknesses are listed in the first three rows of Table 3.3. The storage modulus and loss modulus from these models are shown in Fig. 3.9. These results show that the complex modulus values obtained from the model may change up to 38% compared with control results when RWM thickness changed 14% from the control value.

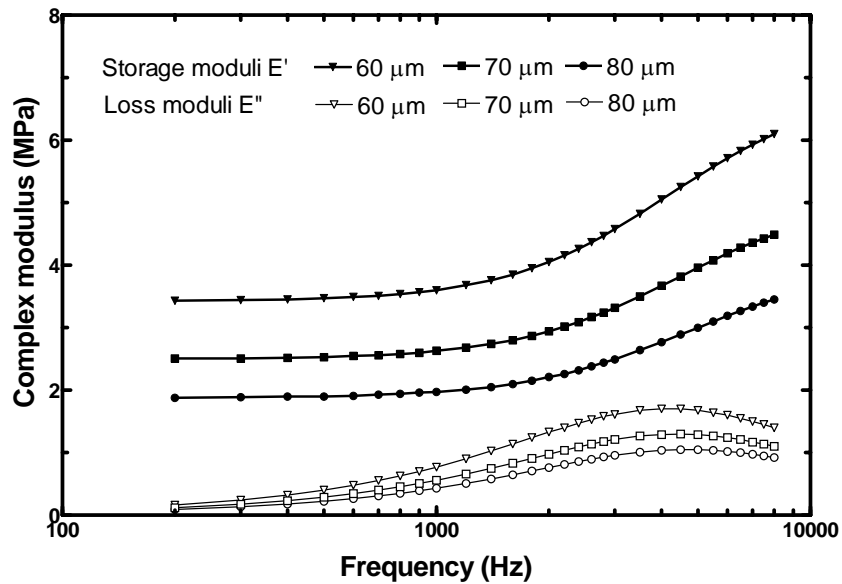


Figure 3.9 The effect of the specimen thickness variations on the complex modulus determined from the FE modeling analysis for the specimen RWM-6.

Human RWM is thicker at the edge and thinner toward the center (Goycoolea and Lundman, 1997; To'th et al., 2006; Li et al., 2007). The uneven thickness

distribution may also affect the resonance frequency and vibration mode of the RWM. To estimate this effect on the complex modulus, a FE model with thickness of 80 μm at the edge and 60 μm at the center was created based on specimen RWM-6. The parameters, E_0 , E_1 and τ_1 were determined as 2.25 MPa, 2.34 MPa, and 35 μs , respectively. The storage modulus was about 10% smaller than that derived from the FE model with uniform thickness of 70 μm .

3.3.2 Effect of experimental conditions on results

In all experiments, the sound pressure (80 dB SPL) was delivered at 1 mm away from the RWM through the tube with inner diameter of 1 mm. In modeling analysis, we assumed that the sound pressure was uniformly applied on the RWM surface because of the round window niche making a semi-closed chamber around the RWM. To estimate the effect of uneven sound pressure applied on the specimen for calculation results of the complex modulus, we modified the distribution of sound pressure on RWM with pressure at the edge lower than that at the center. The sound pressure distribution at 1 mm away from the sound source was calculated following the procedure described in Chapter 2, Section 2.1.1.

Briefly, an open air field with diameter of 0.2 m was built surrounding a circular plate with a diameter of 2 mm (simulating the RWM) and the sound delivery tube had diameter of 1 mm. The acoustic-structure interface was defined on the boundary between the air and the plate. The pressure distribution on the plate was first obtained through the acoustic-structure coupled analysis and then applied into the

FE model of the RWM. The sound pressure at the center of a circular area (1 mm diameter) was 80 dB SPL and gradually reduced to 75 dB at the edge. The calculated complex modulus parameters E_0 , E_1 and τ_1 of specimen RWM-6 from the FE model were 2.46 MPa, 2.70 MPa and 35 μ s, respectively, as listed in Table 3.3 (fourth row). These values are very close to those determined from the control model listed in the first row of Table 3.3. Thus, the acoustic load variation caused by the sound delivering tube may not have a noticeable effect on the results.

Table 3.3 List of the viscoelastic parameters of a RWM specimen (RWM-6) determined under various changes in specimen geometry, sound pressure distribution and moisture (fluid) level.

RWM model	E_0 (MPa)	E_1 (MPa)	τ_1 (μ s)
Control (RWM-6)	2.51	2.63	36
Thickness-60 μ m	3.42	3.41	38
Thickness-80 μ m	1.88	2.11	34
Uneven acoustic load	2.46	2.70	35
Fluid-5 μ m	2.61	2.93	34.5
Fluid-10 μ m	2.74	3.18	33

Another variation of the experiment conditions is the moisture content of the specimen during the experiment. It was reported that the moisture or hydration level may affect mechanical properties of the soft tissues and fibrous composites (Fraga et al., 2003; Johnson et al., 2010). The low moisture content or dehydration makes the tissue stiffer. The human RWM is a soft tissue with collagen fibers as the main supporting structure. The mechanical properties of the RWM specimen are naturally affected by moisture content. To maintain the specimen in an ideal physiological

condition, a saline solution was sprayed onto the specimen during the experiment. The amounts of saline and measurement time were controlled to ensure the results being consistent. In this study, the dynamic measurement was started 30 seconds after the saline was added onto the specimen. Each run of the measurement was finished within 6 seconds for frequency sweeping between 200 to 8000 Hz. The moisture content of the RWM specimen is not anticipated to have noticeable changes in such a short period of time.

Another potential effect of the moisture content on the measurement is the additional mass probably added to the specimen since the resonance frequency is sensitive to mass. To assess the effect of fluid mass on measurement, a water layer with thickness of 5 μm or 10 μm was added to the FE model in the middle ear side of the RWM. The complex modulus parameters E_0 , E_1 and τ_1 of specimen RWM-6 were determined and listed in the last two rows of Table 3.3. Figure 3.10 shows the storage modulus and loss modulus variations in response to water layer thickness or moisture content. These results show that additional water layer thickness affected the storage modulus up to 13% and the loss modulus up to 28%. The water layer affected the loss modulus more than the storage modulus and affected the storage modulus at higher frequencies more than that at lower frequencies. The results suggest that, if there was additional fluid on the RWM surface and it was not taken into account in FE model, the complex modulus obtained by the inverse-problem solving method should be smaller than the real values. In this study, the moisture content of the RWM specimens were maintained by spraying of saline solution on

the specimen, and the specimen was checked under the microscope before measurement to verify there was not much additional fluid on specimen surface. Although the fluid layer thickness could not be measured precisely, we estimated that the fluid layer in this study was less than 10 μm and that this thickness would not affect the RWM storage modulus measurement more than 13%.

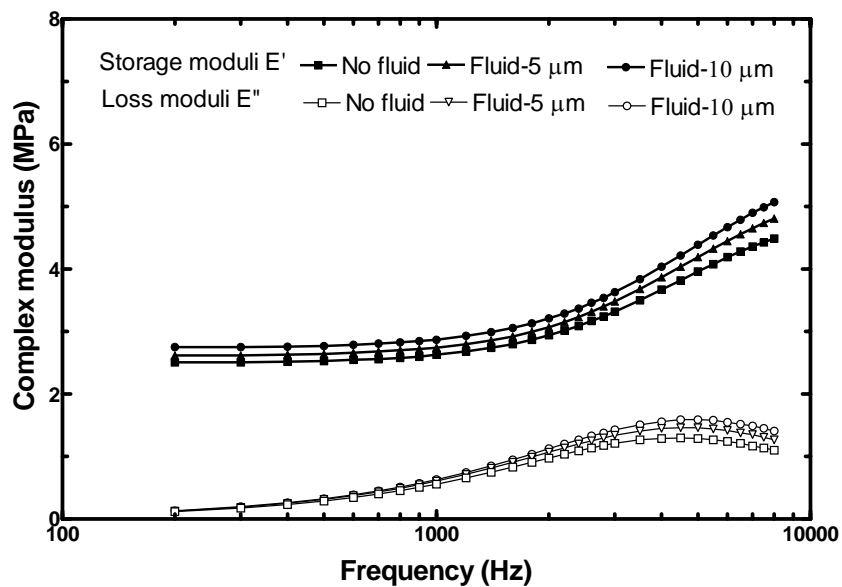


Figure 3.10 The complex modulus determined from the FE modeling analysis for specimen RWM-6 with different fluid layers added.

In this study, the displacement was obtained from the center point of the RWM sample in the experimental measurement. The information from the displacement at the center of the membrane is enough to obtain the mechanical properties of the RWM with the help of the FE model. However, the complex vibration modes do exist in the RWM sample as well as in the FE model. We are unable to measure the modes of the RWM in this study, but the FE model can be used to analyze the

complex patterns of the RWM. In this study, the primary displacement peak presented at (0, 0) mode (at the lowest resonance frequency) of the RWM. The displacement curves were not used to characterize these complex mode patterns, which is far beyond the scope of this study.

3.3.3 Contribution of this study and future work

Dynamic properties of the human RWM over the auditory frequency range were measured for the first time in this study. The results reported here added new knowledge to the biomechanics of human ear and can be applied into the FE modeling of middle ear transfer function as well as cochlea mechanics. In published FE models, a relatively large range of static elastic moduli from 0.35 to 9.8 MPa were assigned to RWM (Bohnke and Arnold, 1999; Gan et al., 2007; Zhang and Gan, 2011a). In this study, the mean static modulus was measured as 2.32 MPa, which was in the range chosen by these published FE models. Moreover, the stapes footplate displacement at high frequency (above 5000 Hz) derived from Gan et al.'s model is lower than the experimental value measured in the human temporal bones. Application of the frequency-dependent modulus obtained in this study into the FE model of human ear may enhance the model accuracy for prediction of middle ear function.

Future studies on the mechanical properties of RWM and their applications may be expanded in three directions:

- 1) Dynamic properties of the RWM in pathological ears, such as otitis media.

Otitis media may significantly change the thickness (Sahni et al., 1987) and permeability (Ikeda and Morizono, 1988) of the RWM. The morphological variations may also change the mechanical properties of the RWM. To understand the relationship between the morphology of the RWM and its physical and mechanical properties in diseased ears will assist clinical diagnosis and drug treatment of otitis media induced mixed hearing loss.

2) Application of dynamic properties of the RWM into FE model of the human ear. As one of two windows connecting the middle ear and cochlea, RWM plays an important role in the interaction between the cochlea and middle ear, particularly when fluid is filled in the middle ear cavity (i.e., otitis media).

3) Coupling between RWM and the implantable transducer for design and function evaluation of implantable hearing devices. The FE model of the human ear will be used to optimize the coupling location and method based on mechanical properties of the RWM.

3.4 Conclusion

In this study, an experimental setup to measure the dynamic properties of the human RWM specimens was developed. Vibrations of the RWM in response to acoustic driving were measured by laser Doppler vibrometry over the auditory frequency range of 200-8000 Hz. The dynamic experiments on RWM specimens were simulated in FE models, and generally good agreements between the

experimental measurements and FE modeling were observed in all RWM specimens. Dynamic properties of the RWM were derived by the inverse-problem solving method and presented as the complex modulus in frequency-domain and relaxation modulus in time-domain. The mean value of the storage modulus of eight RWM specimens was 2.32 ± 0.29 MPa at 200 Hz and 3.83 ± 0.52 MPa at 8000 Hz, while the mean loss modulus was 0.085 ± 0.022 MPa at 200 Hz and 0.925 ± 0.192 MPa at 8000 Hz. The effects of the specimen thickness variation and experimental conditions, including the sound pressure distribution and the moisture of the specimen, on the complex modulus measurements were discussed using the FE modeling analysis. The dynamic properties of the RWM reported in this study provide new knowledge on the RWM and middle ear and cochlea mechanics.

CHAPTER 4.

DYNAMIC PROPERTIES OF HUMAN STAPEDIAL ANNULAR LIGAMENT

In this chapter, the dynamic properties of human SAL were measured using DMA based on the FTS principle, following the same approach used to measure the dynamic properties of human TM which was described in Chapter 2 Section 2.2.

4.4 Methods

4.4.1 SAL specimen preparation

Seven fresh human temporal bones obtained through the Willed Body Program at the University of Oklahoma Health Sciences Center were used for this study. The average age of donors was 68.8 (ranging from 64 to 75 years, three male and four female). The preparation of the SAL sample was similar to that reported in Gan et al., (2011a), which measured the mechanical properties of SAL under static conditions. Briefly, The TB was immersed in 0.9% saline solution mixed with 15% providine at 5°C before the experiment to maintain SAL compliance and hydration. The TB was checked under the microscope for not having any abnormality before experiments. After opening the tegmen and removing the TM together with the malleus and incus, the TB was cut into a nearly 2 cm×2 cm×1.5 cm cube to expose the stapes with attached SAL and surrounding bony wall. The scala vestibuli wall near the oval window was open to release cochlear pressure and saline solution was added beneath the stapes footplate to maintain the physiological condition for the tissue.

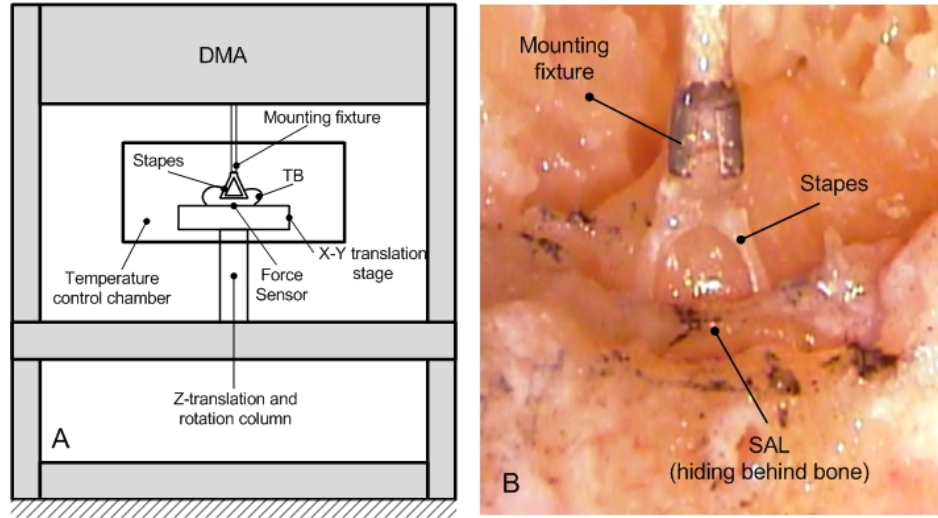


Figure 4.1 (A) The schematic of the experiment setup for the dynamic test of the SAL specimen in DMA. (B) The enlarged image for the fixation of stapes head to the mounting fixture. The SAL was hiding behind the bony structures.

Fig. 4.1A shows the schematic of the experimental setup for the dynamic tests of the SAL specimens. The bony part of the whole SAL sample block was fixed on a X-Y translational stage, which was placed in the temperature chamber of DMA (ElectroForce 3200, Bose, Eden Prairie, MN). The SAL sample was aligned in DMA by adjusting the X-Y translational stage and Z-translational column under microscope. A titanium partial ossicular-replacement prosthesis (PORP, Gyrus ENT, LLC, Memphis, TN) was used as a mounting fixture as shown in Fig. 4.1B. The stapes head was mounted to the metal cap of the PORP with a tiny drop of cyanoacrylate gel glue. Care was taken not to allow the glue to reach the SAL.

4.4.2 Measurement of SAL specimen dimensions

The dimensions of SAL specimens used in this study were measured following the method which was reported in Gan et al. (2011a). As the SAL specimens were

hiding between the stapes footplate and the cochlea bony wall, they were not visible during the tests. Their dimensions were measured after the dynamic test, when the stapes footplate was pulled out from the oval window. The still images of the stapes and oval window were captured using a digital CCD camera. Figure 4.2A shows the measurements of stapes footplate length $L1$ and width $L2$, and Fig. 4.2B shows the oval window length $L3$ and width $L4$. The length or width difference between the stapes footplate and oval window, $L3-L1$ and $L4-L2$, were calculated and the average value was used for the SAL thickness T , with the assumption that the SAL thickness were uniformly distributed along the perimeter of the footplate. The SAL height, which was considered to be the same as the stapes footplate height h was measured from the captured image of the specimen as shown in Fig. 4.2C. The perimeter of the SAL inner rim or footplate perimeter C was calculated from the transferred binary image of the stapes footplate. Table 4.1 lists the dimensions of SAL specimens ($N=7$) with the mean and standard deviation (S.D).

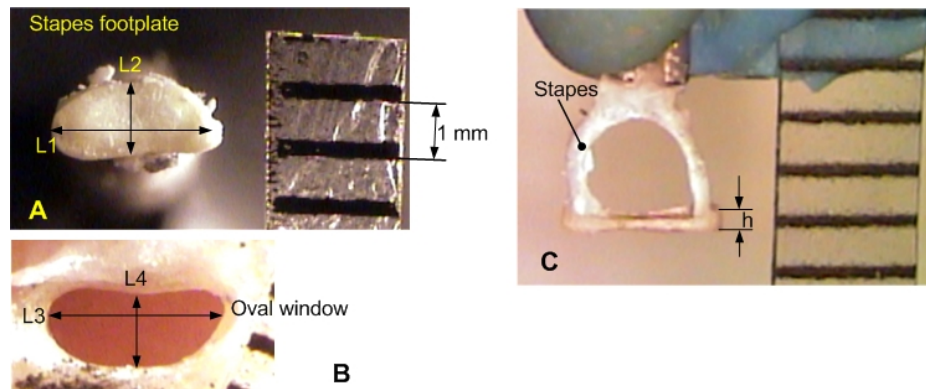


Figure 4.2 Images of the stapes footplate (A) and oval window (B) and stapes (C) obtained after experiments on one TB specimen for measuring the dimensions of SAL.

Table 4.1 The dimensions of human SAL samples (unit in mm).

SAL specimens	SAL-1	SAL-2	SAL-3	SAL-4	SAL-5	SAL-6	SAL-7	Mean±S.D.
FP length L1	2.90	2.82	2.78	2.58	2.32	2.68	2.12	2.60±0.28
FP width L2	1.20	1.22	1.18	1.14	1.08	1.12	1.04	1.14±0.07
OW length L3	3.12	3.00	2.96	2.76	2.54	2.84	2.30	2.79±0.29
OW width L4	1.32	1.36	1.30	1.28	1.24	1.24	1.18	1.27±0.06
Thickness T	0.09	0.08	0.08	0.08	0.10	0.07	0.08	0.08±0.01
Height h	0.29	0.26	0.27	0.24	0.23	0.25	0.20	0.25±0.03
Perimeter C	8.56	7.86	7.74	8.32	7.26	8.04	7.06	7.83±0.54

Note: FP denotes stapes footplate; OW denotes oval window.

4.4.3 Viscoelastic model of SAL specimen

The SAL specimens underwent the shear stress and strain during the tests, as analyzed in Gan et al. (2011a). The shear stress τ and shear strain γ can be calculated by:

$$\tau(t) = F / Ch = F_0 e^{i(2\pi ft + \delta)} / Ch \quad (4.1)$$

$$\gamma(t) = d / T = d_0 e^{i2\pi ft} / T \quad (4.2)$$

where t is time, f is the frequency, δ is the phase difference between the force and displacement, F_0 and d_0 are the force amplitude and displacement amplitude, respectively. The storage shear modulus G' and loss shear modulus G'' of the SAL are then calculated by:

$$|G^*| = \frac{F_0 / Ch}{d_0 / T} \quad (4.3)$$

$$G' = |G^*| \cos \delta \quad (4.4)$$

$$G'' = |G^*| \sin \delta \quad (4.5)$$

In this study, SAL was considered as an isotropic and homogeneous material and the generalized linear solid model was used. The complex shear modulus can be expressed as:

$$G'(\omega) = G_0 + \sum_{i=1}^n G_i \tau_i^2 \omega^2 / (1 + \tau_i^2 \omega^2) \quad (4.6)$$

$$G''(\omega) = \sum_{i=1}^n G_i \tau_i \omega / (1 + \tau_i^2 \omega^2) \quad (4.7)$$

$$\eta(\omega) = \tan \delta = G''(\omega) / G'(\omega) \quad (4.8)$$

Two spring-dashpot elements ($n = 2$, giving 5 parameters G_0, G_1, G_2, τ_1 , and τ_2) were selected to represent the viscoelastic behavior of SAL. Five parameters were determined through the theoretical fitting with the experimental data for each SAL specimen.

4.4.4 Dynamic test on TM specimen

Preconditioning test

The preconditioning tests were conducted in the DMA first to stabilize the mechanical properties of SAL specimens. Five cycles uniaxial vibration was performed at a frequency of 0.1 Hz and displacement amplitude of 0.1 mm for each specimen before the dynamic test.

Dynamic test

The general process of the dynamic test was the same as that in the dynamic tests on TM specimens. Briefly, after preconditioning, the dynamic test was

conducted at 5°, 25°, and 37°C in sequence. At each temperature, the TM sample was tested at 1, 2, 5, 10, 20, and 40 Hz with the displacement amplitude of 0.1 mm. The SAL specimen took a rest for at least 2 minutes for recovering after each run. Note that the SAL sample was kept in physiological moisture by adding saline solution through the opened hole on cochlea wall. To keep sample in the same moisture condition, the accurate amount of saline solution was controlled by a syringe.

4.5 Results

Dynamic experiments were conducted on seven SAL specimens. The storage shear modulus G' and the loss shear modulus G'' of these specimens were obtained over 1 to 40 Hz. Figure 4.3 shows the typical complex shear modulus-frequency curves at the three different temperatures (5°, 25° and 37°C) obtained from two SAL specimens (SAL-1 and SAL-6). The storage shear modulus increased with the frequency increasing or temperature decreasing. However, the loss shear modulus decreased above 20 Hz at 5°C. Larger slopes were found at the lower frequency range and lower temperatures for the loss modulus. Other SAL specimens had the similar complex shear modulus-frequency curves to that shown in Fig. 4.3, with some individual variations.

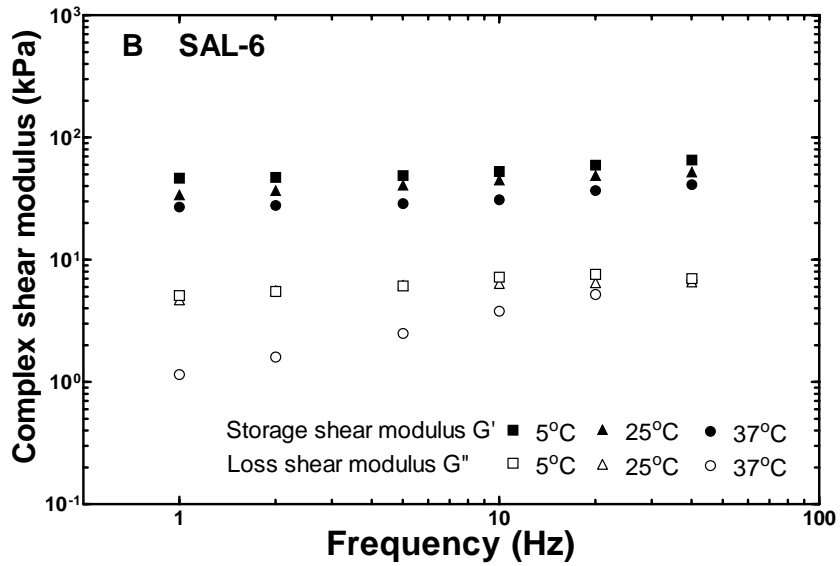
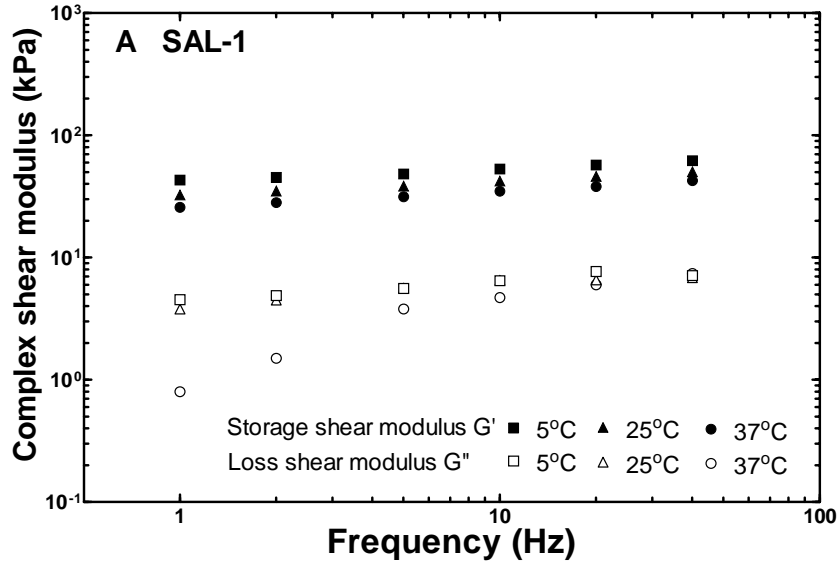


Figure 4.3 The complex shear modulus-frequency curves obtained at 5°C, 25°C and 37°C from two SAL specimens: (A) SAL-1 and (B) SAL-6.

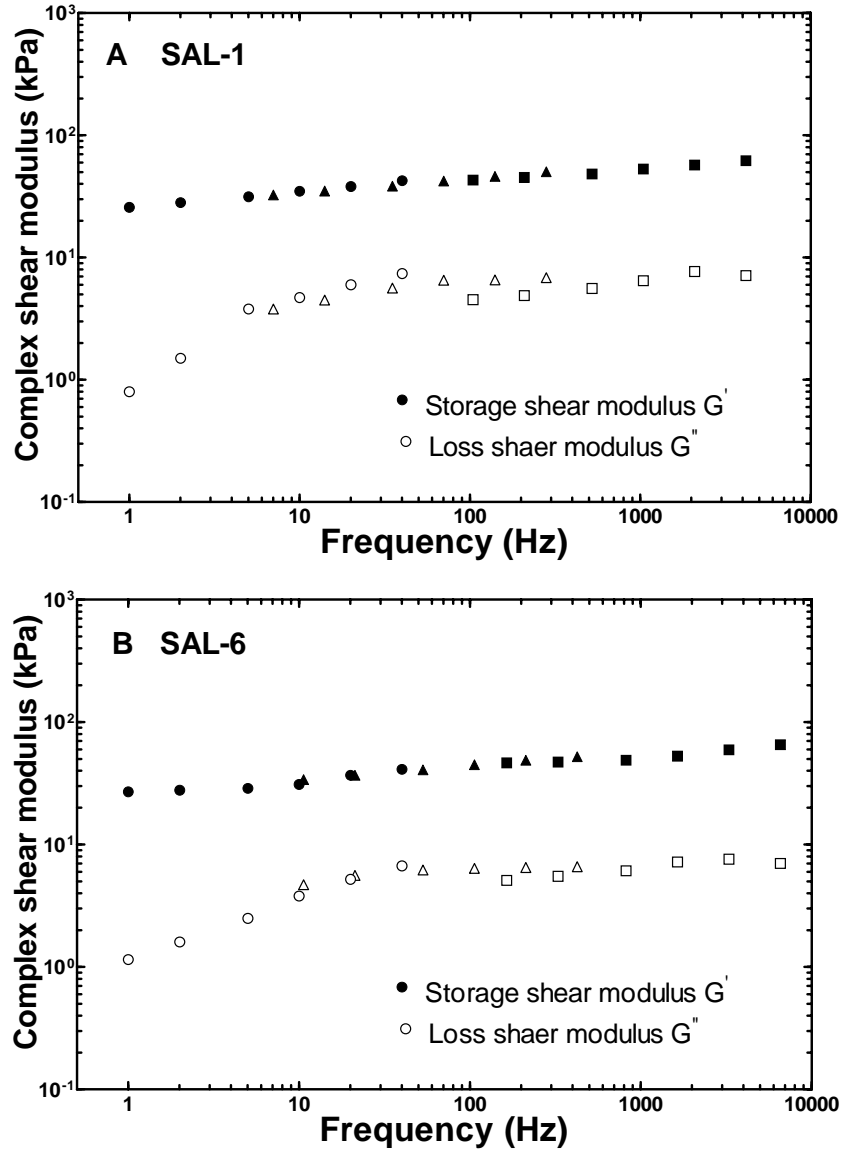


Figure 4.4 The master curves of the complex shear modulus at 37°C obtained from two SAL sample: (A) sample SAL-1 and (B) sample SAL-6.

Following the procedure described in Chapter 2, Section 2.2, the complex shear modulus curves at the lower temperatures were shifted and the master curves were created. Figure 4.4 shows the master curves of the complex shear modulus at the reference temperature 37°C for specimens SAL-1 and SAL-6. The same horizontal shift factors were used for the storage modulus and loss modulus in each specimen,

which meets the second requirement of the FTS principle. The complex shear modulus-frequency curves are generally well matched at the adjacent regions after the horizontal shifts. For specimen SAL-1, the storage shear modulus is 25.8 kPa at 1 Hz and increases to 62.1 kPa at 4160 Hz, while the loss shear modulus is 0.8 kPa at 1 Hz and 7.1 kPa at 4160 Hz. For specimen SAL-6, the storage shear modulus is 27.0 kPa at 1 Hz and increases to 65.5 kPa at 3760 Hz, while the loss shear modulus is 1.2 kPa at 1 Hz and 7.0 kPa at 3760 Hz. The shift factors and maximum frequency of the master curves for all seven SAL specimens are listed in Table 4.2. The mean value of the shift factors from 25° to 37°C (α_{25}) is 7.9 ± 1.4 . The mean value of the shift factors from 5°C to 37°C (α_5) is 123.3 ± 24.4 . The maximum frequency ranges were from 3760 to 6560 Hz with a mean value of 4931 ± 975 Hz.

The temperature dependence of the shift factor was tested by fitting experimental data into the Arrhenius equation (Eq.(2.20)). The activation energy of the TM samples is calculated as the ratio between $R \cdot \ln \alpha_T$ and $(\frac{1}{T} - \frac{1}{T_0})$. The relation between the shift factors and the temperature are well matched with the Arrhenius equation. The values of r^2 for all TM samples are not less than 0.984. The activation energies of all SAL specimens were obtained and listed in table 4.2, which range from 100.3 to 111.7 kJ/mol with a mean value of 105.8 ± 4.0 kJ/mol.

Table 4.2 The shift factors, activation energies, and maximum frequency of human SAL specimens. (E_a unit in kJ/mol, frequency unit in Hz)

	SAL-1	SAL -2	SAL -3	SAL -4	SAL -5	SAL -6	SAL -7	Mean±S.D.
α_{25}	7.0	6.7	8.5	8.1	7.9	10.6	6.8	7.9±1.4
α_5	104	94.0	142	119	132	164	108	123.3±24.4
$\ln\alpha_{25}$	1.94	1.90	2.14	2.09	2.07	2.36	1.92	2.06±0.16
$\ln\alpha_5$	4.64	4.54	4.96	4.78	4.88	5.10	4.68	4.80±0.20
E_a	102.5	100.3	109.3	105.2	107.7	111.7	103.6	105.8±4.0
Max. freq	4160	3760	5680	4760	5280	6560	4320	4931±975

The results obtained here show that the complex shear modulus-frequency curves of the human SAL specimens satisfied all three requirements for the FTS principle. Thus, the FTS principle is feasible to measure the dynamic properties of the SAL at the auditory frequency range.

Figure 4.5 shows the master curves of the complex shear modulus for all seven SAL specimens. The complex shear modulus generally increases with the frequency increasing except the loss shear modulus decreases a little between 60 to 200 Hz and above 3000 Hz. The storage shear modulus ranges from 23.8 to 41 kPa at 1 Hz. The loss shear modulus ranges from 0.18 to 0.45 MPa at 1 Hz.

The mean complex shear modulus was calculated over the common frequency range for the seven SAL samples (1-3760 Hz) and the mean master curves of the storage shear modulus G' and the loss shear modulus G'' with S.D. were plotted up to 3760 Hz in Fig. 4.5. The mean storage shear modulus was 31.7 kPa at 1 Hz and 61.9 kPa at 3760 Hz. The mean loss shear modulus was 1.1 kPa at 1 Hz and 6.5 kPa at 3760 Hz.

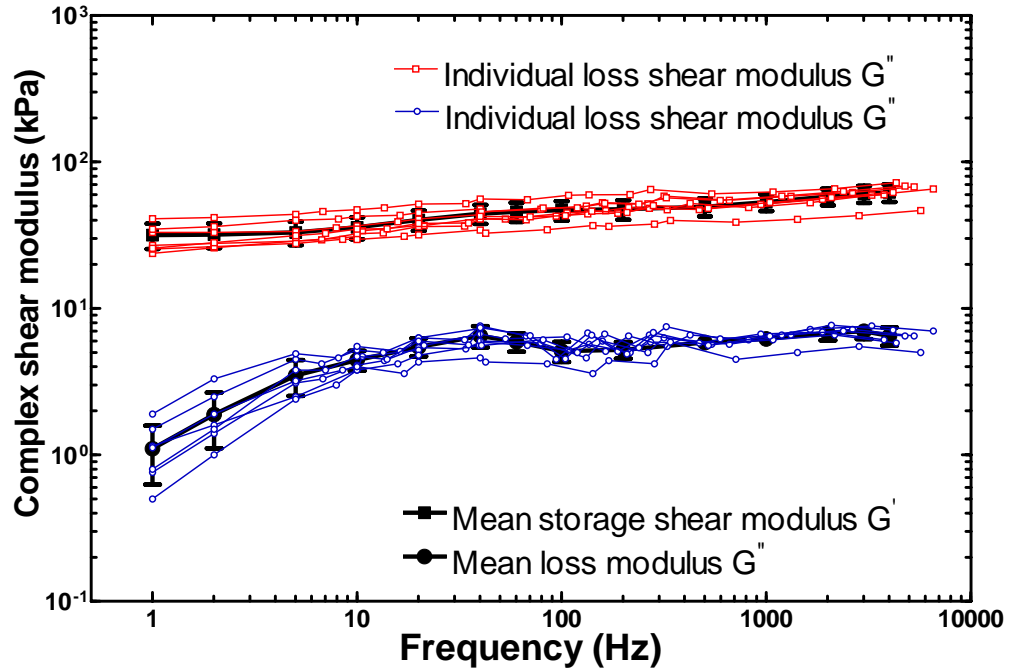


Figure 4.5 The master curves of the storage modulus and the loss modulus at 37°C from seven SAL samples and the mean master curves of the storage modulus and the loss modulus.

Table 4.3 The viscoelastic parameters of human SAL samples.

Specimen	SAL-1	SAL -2	SAL -3	SAL -4	SAL -5	SAL -6	SAL -7	Mean±S.D.
G_0 (kPa)	27.6	26.0	26.7	36.4	33.8	28.1	42.6	31.6±6.2
G_1 (kPa)	15.2	16.7	9.4	13.1	17.7	21.8	16.4	15.8±3.9
G_2 (kPa)	19.0	17.0	10.5	19.0	17.2	18.4	17.3	16.9±3.0
τ_1 (ms)	13.4	10.1	8.7	12.3	5.6	6.0	8.2	9.2±3.0
τ_2 (μ s)	174	181	100	134	92.8	69.7	64.5	117±47

The generalized linear solid model was used to describe the viscoelastic behavior of the SAL specimens. The experimental data of the storage shear modulus were used to fit the theoretical storage modulus-frequency relation (Eq.(4.6)) to determine the five parameters (G_0, G_1, G_2, τ_1 , and τ_2). The theoretical loss shear modulus was then calculated by substituting the values of the parameters into Eq. (4.7), and the results were compared with the experimental data. As an example, the

five parameters for SAL-1 were determined as $G_0=27.6$ kPa, $G_1=15.2$ kPa, $G_2=19.0$ kPa, $\tau_1=13.4$ ms and $\tau_2=174$ μ s, while for SAL-6, the five parameters were determined as $G_0=28.1$ kPa, $G_1=21.8$ kPa, $G_2=18.4$ kPa, $\tau_1=6.0$ ms and $\tau_2=69.7$ μ s. Table 2.5 lists the viscoelastic parameters determined from all seven SAL specimens with the mean values and S.D. Figure 4.6A shows the complex shear modulus of specimen SAL-1 derived from the generalized linear solid model in comparison with the experimental results and Fig. 4.6B shows that complex shear modulus curves for specimen SAL-6. The mean experimental complex modulus curves shown in Fig. 4.5 were also fitted by the generalized linear solid model with the five parameters determined as $G_0=31.8$ kPa, $G_1=15.4$ kPa, $G_2=16.0$ kPa, $\tau_1=8.9$ ms and $\tau_2=121$ μ s. The results are shown in Fig. 4.6C where the theoretical complex modulus curves were compared with the mean experimental data.

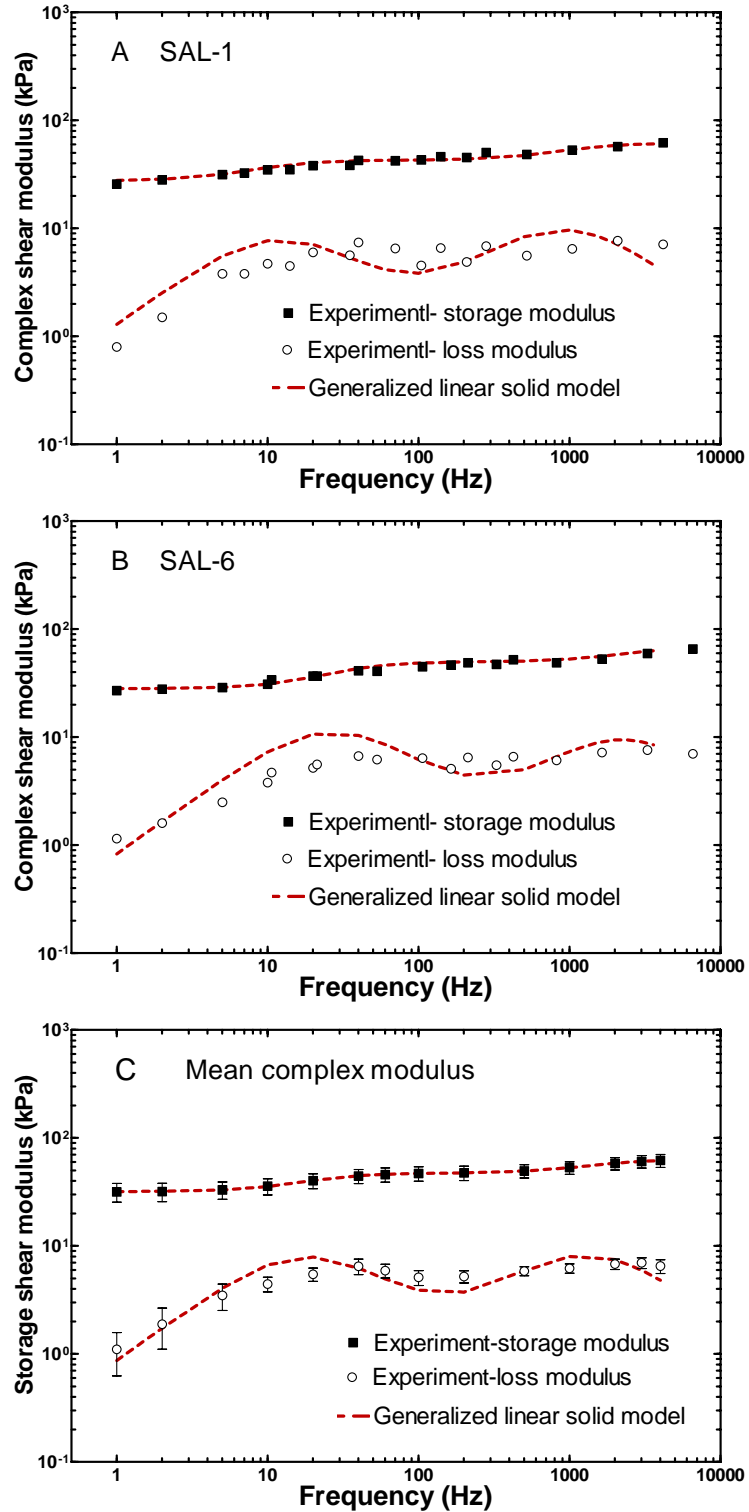


Figure 4.6 The theoretical fitting of generalized linear solid model to the experimental complex modulus for (A): sample TM-7 and (B) the mean experimental complex modulus.

4.6 Discussion

To date, there is no report about the dynamic properties of human SAL in the literature. The results reported in this study fill the gap in the biomechanics of middle ear tissues. However, the mechanical properties of human SAL under quasi-static conditions have been studied by Gan et al. (2011a) using pulling tests in MTS. Their study demonstrates that the human SAL is a typical viscoelastic material with hysteresis, and stress relaxation function. The human SAL shows nonlinear stress-strain relationship and the shear modulus changes from 3.6 to 220 kPa when the shear stress increases from 2 to 140 kPa. In this study, the complex shear modulus of the SAL specimens was obtained over the frequency range from 1 to 3760 Hz. The storage shear modulus at 1 Hz can be considered comparable to the shear modulus obtained from the quasi-static tests. The mean storage shear modulus of seven SAL specimens at 1 Hz was 31.7 kPa obtained from this study, which was among the range from 3.6 to 220 kPa, which was reported by Gan et al. As the SAL is a nonlinear material, whose shear modulus varies with the stress or strain level changing, we further compared the results from two studies at the same strain. Displacement amplitude of 0.1 mm was used in the dynamic tests of this study. Thus, the maximum shear strain is about 1.25 calculated by Eq. (4.2) with the thickness of 0.08 mm. Gan et al. reported the mean shear stress at 17.5 kPa, and mean shear modulus at 35.2 kPa when the shear strain was 1.25. The value of 35.2 kPa was close to the result (31.7 kPa) reported in this study. The difference between the results

from two studies may be probably caused either the individual variation of the human SAL specimens or the different experiment setup and testing conditions.

The complex shear modulus G' and G'' of the human SAL obtained in this study can be converted into the complex modulus E' and E'' and applied into the FE model of the human ear. There is very simple relation between the shear modulus and elastic modulus, which is expressed by the equation

$$E' = 2(1 + \nu)G' \quad E'' = 2(1 + \nu)G'' \quad (4.9)$$

where ν is the Poisson's ratio of SAL. The value of 0.3 was widely used for ν in the published FE models of ear (Gan et al., 2004, 2007; Zhao et al., 2009) and it is adopted in this study. Thus, the mean storage modulus E' was 82.4 kPa at 1 Hz and 160.9 kPa at 3760 Hz. The mean loss modulus E'' was 2.86 kPa at 1 Hz and 16.9 kPa at 3760 Hz. Similar as discussed in Chapter 2, Section 2.2.3, the application of the complex modulus of the SAL into the FE model of ear can avoid Rayleigh type damping, which may cause too high damping at higher frequencies, and help improve the accuracy of the model.

In most published FE model of human ear (Gan et al., 2004, 2007; Wada, et al., 1992; Zhao et al., 2009), the constant elastic modulus was used for the SAL and the large variations existed for the values from 0.065 to 5.5 MPa. In this study, the storage modulus E' ranged from 82.4 kPa to 160.9 kPa depending on the frequency. These values are in the range of the published data. In the recent FE model of ear reported by Zhang and Gan (2011a), frequency-dependent complex modulus was used for the middle tissues including SAL. The values of 2.0 MPa, 10.8 MPa and 25

μ s were used for the viscoelastic parameters E_0 , E_1 , and τ_1 , respectively. The complex modulus E' and E'' used in the model were much larger than those obtained in this study. The difference may be caused by the inaccurate reconstruction of the SAL geometry in those FE models.

4.7 Conclusion

This is the first study to report the dynamic properties of the human SAL specimens in the auditory frequency range (up to 3760 Hz). The dynamic tests were conducted at frequencies from 1 Hz to 40 Hz at three different temperatures: 5°, 25° and 37°C. The frequency- temperature superposition (FTS) was applied to expand the frequency range to a higher level. The generalized linear solid model was used to describe the viscoelastic behavior of the SAL samples. The storage shear modulus G' and the loss shear modulus G'' in the frequency domain was obtained from the seven SAL specimens. The mean storage shear modulus was 31.7 kPa at 1 Hz and 61.9 kPa at 3760 Hz. The mean loss shear modulus was 1.1 kPa at 1 Hz and 6.5 kPa at 3760 Hz. The data reported here contribute to the biomechanics of the middle ear tissues and may help improve the accuracy of the FE model for the human ear.

CHAPTER 5.

SUMMARY AND FUTURE STUDY

5.1 Summary

In this study, two new methods were developed to measure the dynamic properties of human middle ear soft tissues including TM, RWM and SAL in auditory frequency range. In the first method, the vibrations of the specimen in response to acoustic stimuli were measured by LDV over the frequency range of 200-8000 Hz. The dynamic experiments were simulated in FE models for acoustic-structure coupled analysis in ANSYS. The dynamic properties of the membrane specimens (TM and RWM) were derived by the inverse-problem solving method. In the second method using DMA based on the FTS principle, the dynamic tests were conducted for the TM and SAL specimens at the frequencies from 1 Hz to 40 Hz at three different temperatures: 5°, 25° and 37°C. The FTS principle was applied to expand the frequency range to higher frequencies. The dynamic properties of TM specimens were measured by both methods, which were presented in Chapter 2. The dynamic properties of RWM specimens were measured by first method using acoustic driving, which were presented in Chapter 3. The dynamic properties of SAL specimens were measured by the second method using DMA, which were presented in Chapter 4. The approach using acoustic driving and LDV can reach higher frequency compared with the second approach using DMA. However, it is only applicable for the membrane tissues like TM and RWM. The approach using

DMA is a direct measurement in frequency domain and does not need the assistance of FE modeling analysis and the inverse-problem solving method. . The experimental methods developed in this study may be used to measure other human soft tissues and have a impact on the experimental biomechanics.

The generalized linear solid model was used to describe the viscoelastic behaviors of these middle ear tissues. The complex modulus of TM, RWM, and SAL were obtained in the auditory frequency range (at least 3760 Hz) as the results. The results reported in this study add the data to research of middle ear biomechanics. The complex modulus and the loss factor obtained in the dynamic tests can be applied into the FE model of human ear instead of the classic elastic modulus and Rayleigh type damping and help to improve the accuracy of the FE model.

5.2 Future Study

Future studies on the mechanical properties of middle ear soft tissues and their applications may include:

- 1) To measure the dynamic properties of middle ear soft tissues in diseased conditions, such as otitis media, which is one of the most common middle ear diseases in children. Otitis media may significantly change the thickness of the TM and RWM. The morphological variations may also change their mechanical properties. To study the relationship between the morphological and mechanical changes in the diseased ears may help understand the mechanism of hearing loss

induced by otitis media.

2) To measure the dynamic properties of other middle ear tissues, such as IS joint, suspensory ligaments and muscle tendons, using the methods developed in this study.

3) To apply the dynamic properties of middle ear tissues into the FE model of the human ear. The application of the frequency dependent complex modulus may improve the accuracy of the FE model, especially at high frequency range.

4) To develop a nonlinear viscoelastic model for the middle ear soft tissues. It was reported that middle ear soft tissues show typical nonlinear behavior (Cheng et al., 2007; Cheng and Gan, 2007, 2008a, 2008b; Gan et al., 2011a; Zhang and Gan, 2011b). The nonlinear model is necessary in the analysis of the middle ear response under large static load (middle ear pressure) or dynamic load (blast wave). A nonlinear viscoelastic model will be developed and its parameters will be determined based on the experimental data.

REFERENCES

1. Aernouts, J., J.R. Aerts and J.J.J. Dirckx. 2012. Mechanical properties of human tympanic membrane in the quasi-static regime from in situ point indentation measurements. *Hear. Res.* 290:45-54.
2. Aernouts, J. and J.J.J. Dirckx. 2012. Static vs. dynamic gerbil tympanic membrane elasticity: derivation of the complex modulus. *Biomechanics and Modeling in Mechanobiology.* 11:829-840.
3. Aernouts, J. and J.J.J. Dirckx. 2012. Viscoelastic properties of gerbil tympanic membrane at very low frequencies. *Journal of Biomechanics.* 45: 919–924.
4. Bess, F.H. and L. Humes. 2008. *Audiology : the fundamentals.* Lippincott Williams & Wilkins, Philadelphia.
5. Bohnke, F. and W. Arnold. 1999. 3D-finite element model of the human cochlea including fluid-structure couplings. *Orl-Journal for Oto-Rhino-Laryngology and Its Related Specialties.* 61: 305-310.
6. Bolz, E.A. and D.J. Lim. 1972. Morphology of the stapediovestibular joint. *Acta Otolaryngol.* 73: 10-17.
7. Borg, E. and S.A. Counter. 1989. The Middle-Ear Muscles. *Scientific American* 261: 74–78.
8. Brunner, H. 1954. Attachment of the stapes to the oval window in man. *Archiv. Otolaryngol.* 59:18-29.
9. Büki B., P. Avan, J.J. Lemaire, M. Dordain, J. Chazal and O. Ribári. 1996. Otoacoustic emissions: a new tool for monitoring intracranial pressure changes through stapes displacements. *Hear Res.* 94: 125-139.
10. Büki B., A. Chomiccki, M. Dordain, J.J. Lemaire, H.P. Wit, J. Chazal and P. Avan. 2000. Middle-ear influence on otoacoustic emissions. II: contributions of posture and intracranial pressure. *Hear Res.* 140: 202-211.
11. Buunen, T.J.F. and M.S.M.G. Vlaming. 1981. Laser-Doppler Velocity Meter Applied to Tympanic Membrane Vibrations in Cat. *Journal of the Acoustical Society of America.* 69: 744-750.
12. Carpenter, A.M., D. Muchow and M.V. Goycoolea. 1989. Ultrastructural studies of the human round window membrane. *Arch. Otolaryngol. Head Neck Surg.* 115:585–590.

13. Causse J.B. and A. Lopez, L. Juberthie, J.C. Olivier. 1991. Stapedotomy: the JB Causse technique. *Ann Acad Med Singapore*. 20: 618-623
14. Chan, R.W. 2001. Estimation of viscoelastic shear properties of vocal-fold tissues based on time-temperature superposition. *J. Acoust. Soc. Am.* 110: 1548-1561.
15. Cheng, T., C. Dai and R.Z. Gan. 2007. Viscoelastic properties of human tympanic membrane. *Annals of Biomedical Engineering*. 35: 305-314.
16. Cheng, T., and R.Z. Gan. 2007. Mechanical properties of stapedial tendon in human middle ear. *Journal of Biomechanical Engineering*. 129: 913-918.
17. Cheng, T., and R.Z. Gan. 2008a. Experimental measurement and modeling analysis on mechanical properties of tensor tympani tendon. *Med Eng Phys*. 30: 358-366.
18. Cheng, T., and R.Z. Gan. 2008b Mechanical properties of anterior malleolar ligament from experimental measurement and material modeling analysis. *Biomechanics & Modeling in Mechanobiology*. 7: 387-394.
19. Chu, E.A. and R.K. Jackler. 2003. The Artificial Tympanic Membrane (1840-1910): From Brilliant Innovation to Quack Device. *Otology & Neurotology*. 24:507-518.
20. Dai, C., M.W. Wood and R.Z. Gan. 2007. Tympanometry and laser Doppler interferometry measurements on otitis media with effusion model in human temporal bones. *Otology & Neurotology*. 28: 551-558.
21. Daphalapurkar, N.P., C. Dai, R.Z. Gan and H. Lu. 2009. Characterization of the linearly viscoelastic behavior of human tympanic membrane by nanoindentation. *J Mech Behav Biomed Mater*. 2: 82-92.
22. Decraemer, W.F., S.M. Khanna and W.R. Funnell. 1989. Interferometric measurement of the amplitude and phase of tympanic membrane vibrations in cat. *Hear Res*. 38: 1-17.
23. Decraemer, W.F., M.A. Maes and V.J. Vanhuyse. 1980. An elastic stress-strain relation for soft biological tissues based on a structural model. *J Biomech*. 13: 463-8.
24. de Souza, C. and M.E. Glasscock. 2004. *Otosclerosis and Stapedectomy: diagnosis, management, and complication*. NY: Thieme, New York.
25. Faddis, B.T. 2008. Structural and functional anatomy of the outer and middle ear. In Clark, W., and K. Ohlemiller (Eds.): *Anatomy and physiology of hearing for audiologists*. Thomson Delmar Learning, Clifton Park, New York.

26. Fay, J., S. Puria, W.F. Decraemer and C. Steele. 2005. Three approaches for estimating the elastic modulus of the tympanic membrane. *J Biomech.* 38: 1807-1815.
27. Feng, B. and R.Z. Gan. 2004. Lumped parametric model of the human ear for sound transmission. *Biomechanics & Modeling in Mechanobiology.* 3: 33-47.
28. Ferry, J.D. 1950. Mechanical Properties of Substances of High Molecular Weight .6. Dispersion in Concentrated Polymer Solutions and Its Dependence on Temperature and Concentration. *J. Am. Chem. Soc.* 72: 3746-3752.
29. Ferry, J.D. 1980. *Viscoelastic Properties of Polymer* 3rd ed. Wiley, New York.
30. Fraga, A.N., V.A. Alvarez, A. Vazquez and O. De La Osa. 2003. Relationship between Dynamic Mechanical Properties and Water Absorption of Unsaturated Polyester and Vinyl Ester Glass Fiber Composites. *Journal of Composite Materials.* 37:1553-1574.
31. Fung, Y.C. 1993. *Biomechanics: Mechanical Properties of Living Tissues* 2nd ed. Springer, New York.
32. Gan, R.Z., R.K. Dyer, M.W. Wood and K.J. Dormer. 2001. Mass loading on the ossicles and middle ear function. *Annals of Otology, Rhinology & Laryngology.* 110: 478-485.
33. Gan, R.Z., B. Feng and Q. Sun. 2004. Three-dimensional finite element modeling of human ear for sound transmission. *Ann. Biomed. Eng.ering.* 32: 847-59.
34. Gan, R.Z., C. Dai and M.W. Wood. 2006a. Laser interferometry measurements of middle ear fluid and pressure effects on sound transmission. *J Acoust Soc Am.* 120:3799-3810.
35. Gan, R.Z., Q. Sun, B. Feng and M.W. Wood. 2006b. Acoustic-structural coupled finite element analysis for sound transmission in human ear--pressure distributions. *Medical Engineering & Physics.* 28: 395-404.
36. Gan, R.Z., B.P. Reeves and X. Wang. 2007. Modeling of sound transmission from ear canal to cochlea. *Annals of Biomedical Engineering.* 35: 2180-2195.
37. Gan, R.Z., F. Yang and X. Zhang and D. Nakmali. 2011a. Mechanical properties of stapedial annular ligament. *Medical Engineering & Physics.* 33: 330-339.
38. Gan, R.Z, X. Zhang, and X. Guan. 2011b. Modeling Analysis of Biomechanical Changes of Middle Ear and Cochlea in Otitis Media. *AIP Conference Proceedings.* 1403: 539-544.

39. Goycoolea, M.V. and L. Lundman. 1997. Round window membrane. Structure function and permeability: a review. *Microscopy Research & Technique*. 36: 201-211.
40. Gyo, K., H. Aritomo and R.L. Goode. 1987. Measurement of the ossicular vibration ratio in human temporal bones by use of a video measuring system. *Acta Oto-Laryngologica*. 103: 87-95.
41. Haberman, R.S. 2004. *Middle Ear and Mastoid Surgery*. Thieme Medical Pub, New York.
42. Hellstrom, S., P.O. Eriksson, Y.J. Yoon and U. Johansson. 1997. Interactions between the middle ear and the inner ear: Bacterial products. *Ann N Y Acad Sci*. 830: 110-119.
43. Huang, G., N.P. Daphalapurkar, R.Z. Gan and H. Lu. 2008. A method for measuring linearly viscoelastic properties of human tympanic membrane using nanoindentation. *Journal of Biomechanical Engineering*. 130: 014501.
44. Hüttenbrink, K.B. 2003. Biomechanics of stapesplasty: a review. *Otol Neurotol*. 24: 548-557.
45. Ihlenbury, F. 1998. *Finite Element Analysis of Acoustic Scattering*. Springer, New York,
46. Johnson, M., S.L. Walter, B.D. Flinn and G. Mayer. 2010. Influence of moisture on the mechanical behavior of a natural composite. *Acta Biomater*. 6:2181-2188.
47. Keefe, D.H., and M.P. Feeney. 2009. Principles of acoustic immittance and acoustic transfer functions. In J. Katz (Ed): *Handbook of Clinical Audiology*, 6th edition, Lippincott Williams and Wilkins, Baltimore. 125-156.
48. Kirikae, I. 1960. *The structure and function of the middle ear*. the University of Tokyo Press, Tokyo.
49. Kuyper, L.C., W.F. Decraemer and J.J.J. Dirckx. 2006. Thickness distribution of fresh and preserved human eardrums measured with confocal microscopy. *Otology & Neurotology*. 27: 256-264.
50. Hoffman, D.W., and R.P. Bobbin. 1986. *Neurobiology of Hearing: The Cochlea*. Raven Press, New York.
51. Li, P.M., H. Wang, C. Northrop, S.N. Merchant and J.B. Nadol. 2007. Anatomy of the round window and hook region of the cochlea with implications for cochlear implantation and other endocochlear surgical procedures. *Otology & Neurotology*. 28:641-648.

52. Lieberthal, A.S., A.E. Carroll, T. Chonmaitree, T.G. Ganiats, A. Hoberman, M.A. Jackson, M.D. Joffe, D.T. Miller, R.M. Rosenfeld, X.D. Sevilla, R.H. Schwartz, P.A. Thomas and D.E. Tunkel. 2013. The Diagnosis and Management of Acute Otitis Media. *Pediatrics*. DOI: 10.1542/peds.2012-3488.
53. Lim, D.J. 1970. Human tympanic membrane. An ultrastructural observation. *Acta Oto-Laryngologica*. 70: 176-186.
54. Lim, D.J. 1995. Structure and function of the tympanic membrane: a review. *Acta Oto-Rhino-Laryngologica Belgica*. 49: 101-115.
55. Lopez, A., L. Juberthie, J.C. Olivier, J.B. Causse and J. Robinson. 1992. Survival and evolution of vein grafts in otosclerosis surgery: structural and ultrastructural evidence. *Am J Otol*. 13: 173-184.
56. Luo, H., H. Lu, C. Dai and R.Z. Gan. 2009a. A comparison of Young's modulus for normal and diseased human eardrum at high strain rate. *Int. J. Experimental and Computational Biomechanic*. 1:1-22.
57. Luo, H., C. Dai, R.Z. Gan and H. Lu. 2009b. Measurement of Young's Modulus of Human Tympanic Membrane at High Strain Rates', *J. Biomech. Eng*. 131: 064501-1 -8.
58. Machiraju, C., A.V. Phan, A.W. Pearsall and S. Madanagopal. 2006. Viscoelastic studies of human subscapularis tendon: Relaxation test and a Wiechert model. *Computer Methods and Programs in Biomedicine*. 83: 29-33.
59. Mclaughlin, J., A. Thomas and J.R. Yoon. 2011. Basic Theory for Generalized Linear Solid Viscoelastic Models. In Bal, G., D. Finch, P. Kuchment, J. Schotland, P. Stefanov and G. Uhlmann. (eds): *AMS Contemporary Mathematics Volume: Tomography and Inverse Transport Theory*. 101-134.
60. Merchant, N., A. Incesulu and R.J. Glynn. 2001. Histologic studies of the posterior stapediovestibular joint in otosclerosis. *J Otol Neurotol*. 22:305-310.
61. Middlebrooks, J.C. and D.M. Green. 1991. Sound localization by human listeners. *Annu Rev Psychol*. 42: 135-59.
62. Murakami, S., K. Gyo and R.L. Goode. 1997. Effect of middle ear pressure change on middle ear mechanics. *Acta Otolaryngol*. 117:390-395.
63. Murakami, S., K. Gyo and R.L. Goode. 1998. Effect of increased inner ear pressure on middle ear mechanics. *Otolaryngol Head Neck Surg*. 118: 703-708.
64. Nicolle, S. and J.F. Paliarne. 2010. Dehydration effect on the mechanical behaviour of biological soft tissues: Observations on kidney tissues. *Journal of the Mechanical Behavior of Biomedical Materials*. 3: 630-635.

65. Nielsen, L.E. and R.F. Landel. 1994. *Mechanical Properties of Polymers and Composites* 2nd ed. Marcel Dekker, New York.
66. Nomura, Y. 1984. Otolological significance of round window membrane, *Adv Otorhinolaryngol.* 33: 1-162.
67. Ohashi, M., S. Ide, T. Kimitsuki, S. Komune and T. Sukanuma. 2006. Three-dimensional regular arrangement of the annular ligament of the rat stapediovestibular joint, *Hearing Research.* 213:11-16.
68. Olson, E.S., H. Duifhuis, and C.R. Steele. 2012. Von Békésy and cochlear mechanics. *Hear Res.* 293:31-43
69. Paparella, M.M., P.A. Schachernl and Y.B. Choo. 1983. The round window membrane: otological observations. *Annals of Otology, Rhinology & Laryngology.* 92: 629-634.
70. Peters, G.W., J.H. Meulman and A.A. Sauren. 1997. The applicability of the time/temperature superposition principle to brain tissue. *Biorheology.* 34: 127-138.
71. Radebaugh, G.W. and A.P. Simonelli. 1983. Temperature-frequency equivalence of the viscoelastic properties of anhydrous lanolin USP. *Journal of pharmaceutical sciences.*72: 422-425.
72. Sahni, R.S., M.M. Paparella, P.A. Schachern, M.V. Goycoolea and C.T. Le. 1987. Thickness of the human round window membrane in different forms of otitis media. *Arch Otolaryngol Head Neck Surg.* 113: 630-634.
73. Schnupp, J., I. Nelken , and A. King. 2011. *Auditory Neuroscience.* MIT Press, Cambridge, MA.
74. Schuknecht, H. and W. Barber. 1985. Histologic variants in otosclerosis. *Laryngoscope.* 95:1307–1307.
75. Shaw, E.A.G. 1974. The external ear. In Keidel, W.D. and W.D. Nef. (eds): *Handbook of sensory physiology*, vol. 1. Springer-Verlag, Berlin, Germany.
76. Souza, C.D. and M.E. Glasscock. 2004. *Otosclerosis and Stapedectomy: Diagnosis, Management and Complications.* Thieme Medical Publishers, New York.
77. Szilard, R. 1974. *Theory and Analysis of Plates: Classical and numerical methods.* Prentice-Hall, Englewood Cliffs, New Jersey.

78. Tajvidi, M., R.H. Falk and J.C. Hermanson. 2005. Time-temperature superposition principle applied to a kenaf-fiber/high-density polyethylene composite. *Journal of Applied Polymer Science*. 97: 1995-2004.
79. Torres, M., and F. Giráldez. 1998. The development of the vertebrate inner ear. *Mechanisms of Development* 71:5-21
80. To' th, M., A. Alpar, L. Patonay and I. Olah. 2006. Development and surgical anatomy of the round window niche. *Annals of Anatomy*. 188: 93-101.
81. Vollandri, G., F.D. Puccio, P. Forte, and C. Carmignani. 2011. Biomechanics of the tympanic membrane. *J Biomech*. 44:1219-1236
82. von Békésy, G. 1960. *Experiments in hearing*. McGraw-Hill Book Company, New York.
83. von Unge, M., W.F. Decraemer, D. Bagger-Sjoberg and J.J. Dirckx. 1993. Displacement of the gerbil tympanic membrane under static pressure variations measured with a real-time differential moiré interferometer. *Hear Res*. 70: 229-242.
84. Wang, X., T. Cheng and R.Z. Gan. 2007. Finite-element analysis of middle-ear pressure effects on static and dynamic behavior of human ear. *Journal of the Acoustical Society of America* 122: 906-917.
85. Ward, I. M. 1971. *Mechanical Properties of Solid Polymers*. Wiley, New York.
86. Wever, E.G., and M. Lawrence. 1982. *Physiological Acoustics*. Princeton University Press, Princeton, New Jersey.
87. Whyte, J.R., L. Gonzalez, A.I. Cisneros, C. Yus, A. Torres and R. Sarrat. 2002. Fetal development of the human tympanic ossicular chain articulations. *Cells Tissues Organs*. 171:241-249.
88. Williams, M.L., R.F. Landel and J.D. Ferry. 1955. Temperature Dependence of Relaxation Mechanisms in Amorphous Polymers and Other Glass-Forming Liquids. *Physical Review*. 98: 1549-1549.
89. Wolff, D, R. Bellucci. 1956. The human ossicular ligaments. *Ann. Otol. Rhinol. Laryngol*. 65: 895-909.
90. Zhang, X. and R.Z. Gan. 2010. Dynamic properties of human tympanic membrane-experimental measurement and modeling analysis. *International Journal of Experimental and Computational Biomechanics*. 1:252-270.

91. Zhang, X. and R.Z. Gan. 2011a. A comprehensive model of human ear for analysis of implantable hearing devices. *IEEE Trans Biomed Eng.* 58:3024-3027.
92. Zhang, X. and R.Z. Gan. 2011b. Experimental measurement and modeling analysis on mechanical properties of incudostapedial joint. *Biomech Model Mechanobiol.* 10(5): 713-726.
93. Zhang, X. and R.Z. Gan. 2013a. Dynamic Properties of Human Tympanic Membrane Based on Frequency-Temperature Superposition. *Ann. Biomed. Engi.* 41:205-214.
94. Zhang, X. and R.Z. Gan. 2013b. Dynamic Properties of Human Round Window Membrane in Auditory Frequencies. *Medical Engineering & Physics.* 35:310-318.
95. Zhang, X. and R.Z. Gan. 2013c. Finite Element Modeling of Energy Absorbance in normal and disordered Human Ear. *Hearing Research.* doi: 10.1016/j.heares.2012.12.005. [Epub ahead of print]
96. Zhao, F., T. Koike, J. Wang, H. Sienz and R. Meredith. 2009. Finite element analysis of the middle ear transfer functions and related pathologies. *Medical Engineering & Physics.* 31: 907-916.

APPENDIX

LIST OF ABBREVIATIONS

dB	Decibel (acoustic)
DMA	Dynamic mechanical analyzer
FE	Finite element
FTS	Frequency-temperature superposition
LDV	Laser Doppler vibrometer
MTS	Mechanical testing system
RWM	Round window membrane
SAL	Stapedial annular ligament
SHTB	Split Hopkinson tension bar
SPL	Sound pressure level
TB	Temporal bone
TM	Tympanic membrane